

AP-E 430624

(12)  
B-5

LEVEL III

AD

TECHNICAL REPORT ARBRL-TR-02300 ✓

IMPROVED ANALYTICAL SHAPED CHARGE CODE: BASC

AD A100275

John T. Harrison

March 1981

DTIC  
ELECTED  
JUN 16 1981  
S D  
B



US ARMY ARMAMENT RESEARCH AND DEVELOPMENT COMMAND  
BALLISTIC RESEARCH LABORATORY  
ABERDEEN PROVING GROUND, MARYLAND

Approved for public release; distribution unlimited.

DTIC FILE COPY

816 04035

Destroy this report when it is no longer needed.  
Do not return it to the originator.

Secondary distribution of this report by originating  
or sponsoring activity is prohibited.

Additional copies of this report may be obtained  
from the National Technical Information Service,  
U.S. Department of Commerce, Springfield, Virginia  
22161.

The findings in this report are not to be construed as  
an official Department of the Army position, unless  
so designated by other authorized documents.

The use of trade names or manufacturers' names in this report  
does not constitute endorsement of any commercial product.

## UNCLASSIFIED

SECURITY CLASSIFICATION OF THIS PAGE (When Data Entered)

REPORT DOCUMENTATION PAGE			READ INSTRUCTIONS BEFORE COMPLETING FORM
1. REPORT NUMBER  TECHNICAL REPORT ARBRL-TR-02300	2. GOV'T ACCESSION NO.  AD-A100275	3. RECIPIENT'S CATALOG NUMBER	
4. TITLE (and Subtitle)  IMPROVED ANALYTICAL SHAPED CHARGE CODE: BASC	5. TYPE OF REPORT & PERIOD COVERED  Final		
7. AUTHOR(s)  John T. Harrison	8. PERFORMING ORG. REPORT NUMBER(s)		
9. PERFORMING ORGANIZATION NAME AND ADDRESS  US Army Ballistic Research Laboratory ATTN: DRDAR-BLT Aberdeen Proving Ground, MD 21005	10. PROGRAM ELEMENT, PROJECT, TASK AREA & WORK UNIT NUMBERS  TL161102AH43		
11. CONTROLLING OFFICE NAME AND ADDRESS  US Army Armament Research and Development Command US Army Ballistic Research Laboratory (DRDAR-BL) Aberdeen Proving Ground, MD 21005	12. REPORT DATE  MARCH 1981		
14. MONITORING AGENCY NAME & ADDRESS (if different from Controlling Office)	13. NUMBER OF PAGES  100		
	15. SECURITY CLASS. (of this report)  UNCLASSIFIED		
	15a. DECLASSIFICATION/DOWNGRADING SCHEDULE		
16. DISTRIBUTION STATEMENT (of this Report)  Approved for public release, distribution unlimited.			
17. DISTRIBUTION STATEMENT (of the abstract entered in Block 20, if different from Report)			
18. SUPPLEMENTARY NOTES			
19. KEY WORDS (Continue on reverse side if necessary and identify by block number)  Liner acceleration and collapse Shaped Charge Jet Formation Theory Shaped Charge Penetration Explosive metal interaction			
20. ABSTRACT (Continue on reverse side if necessary and identify by block number) (ddg)  The work of many researchers has been combined to produce a simplified, analytical, computer code to address the shaped charge problem. This code named BASC (BRL Analytical Shaped Charge) is programmed in the FORTRAN language. BASC utilizes a modified version of the metal acceleration model of M. Defourneaux of France to account for both the final liner velocity and its acceleration history. The BASC code accurately predicts jet-tip velocity and treats the buildup of the massive lead pellet, for both heavy confined and unconfined charge geometries. Calculation of the massive lead pellet has traditionally			

UNCLASSIFIED

SECURITY CLASSIFICATION OF THIS PAGE(When Data Entered)

been difficult and is accomplished in BASC by including time dependent acceleration and material compressibility in the region of the liner near the apex of the conical liner. The BASC code includes the jet formation theory of Pugh, Eichelberger, and Rostoker; the shaped-charge penetration theory of DePersic, Simon and Merendino for penetration-standoff curves; and the piece wise penetration of Defourneaux for hole profiles. BASC enables parametric investigations of shaped charge problems with relatively small amounts of computer time since the code is basically analytic. Results from the BASC code are compared to experiments as well as to more sophisticated hydrodynamic computer codes. The report documents BASC, including the equations utilized, necessary empirical relations, FORTRAN listing of the program, selected problem examples and comparison with experiments.

UNCLASSIFIED

SECURITY CLASSIFICATION OF THIS PAGE(When Data Entered)

## TABLE OF CONTENTS

	Page
LIST OF ILLUSTRATIONS. . . . .	5
LIST OF TABLES . . . . .	7
I. INTRODUCTION . . . . .	9
II. GOVERNING EQUATIONS. . . . .	11
III. CALCULATIONAL SCHEME . . . . .	30
IV. COMPARISON OF BASC CODE RESULTS. . . . .	34
V. LIMITATIONS OF BASC. . . . .	44
VI. FUTURE MODIFICATIONS TO THE CODE . . . . .	44
VII. SUMMARY. . . . .	46
REFERENCES . . . . .	47
APPENDIX A - FLOWCHART OF COMPUTER PROGRAM . . . . .	49
APPENDIX B - FORTRAN IV COMPUTER PROGRAM LISTING, SAMPLE INPUT AND OUT. . . . .	59
DISTRIBUTION LIST. . . . .	97

Accession For	
NTIS GRA&I <input checked="" type="checkbox"/>	
DTIC TAB <input type="checkbox"/>	
Unannounced <input type="checkbox"/>	
Justification	
By _____	
Distribution/ _____	
Availability Codes	
Dist	Avail and/or Special
A	

3/4

## LIST OF ILLUSTRATIONS

Figure	Page
1. Projection of a Metal Plate by High Explosive. . . . .	12
2. $\phi_0$ and k are Functions of the Detonation Wave Angle. . . .	14
3. $1/\phi$ vs $\mu$ as Determined from Experiments. Data is taken from Reference 11. . . . .	15
4. Line Drawing Illustrating the Quantities Employed in the BASC Code for a Generalized Axisymmetric Collapse of a Shaped-Charge . . . . .	19
5. Illustration of the Relationship between Variables and the Collapse Process. . . . .	20
6. Illustration of the Resolved Variables in the Laboratory Coordinate System . . . . .	21
7. Illustration of the Variables Employed in the BASC Code to limit Jet Formation. The Jet Limiting Criteria for a Coherent Jet (A and B) is $M_K = V_f/c < 1.23$ . . . . .	23
8. Schematic Cross-Section of a Shaped-Charge Jet Penetrating a Target in Two States: (a) Continuous and Discontinuous, (b) Discontinuous . . . . .	28
9. Comparison between Experimental and BASC Code results of Jet and Collapse Velocities from the 105-mm, Unconfined, Shaped Charge. . . . .	36
10. Comparison of Calculations of Jet Mass vs Cone Mass between BASC Code and Experimental Results from the 105-mm, Unconfined, Shaped-Charge (Reference 13) . . . .	37
11. Comparison between BASC Code and Experimental Results for Scaled, Heavily-Confining, Shaped-Charge (Reference 10). Jet and Collapse Velocities vs % of the Distance from the Apex of the Cones are Shown. Solid Lines are BASC Code results. The Dashed Line is the Final, Computed, Compressed Jet Velocity Profile. The Jet Tip for both Experimental and BASC Results is Shown Compressed into a Position 48% from the Apex of the Cone . . . .	38

## LIST OF THE ILLUSTRATIONS

Figure	Page
12. Comparison of Calculations of the Flow Field between BASC Code and a 2-D, Hydrodynamic Code (BRLSC) (Reference 2). These Calculations are of the 105-mm, Unconfined, Shaped-Charge Shown at the Time Approximately 25 $\mu$ s after the initiation of the Explosive. The BRLSC Code Results are to the Left of the Axis of Symmetry and the BASC Code Results are to the Right. . . . .	42
13. Comparison of Calculated and Measured Jet Tip Velocities from Shaped-Charge Designs 1 through 4, shown on Table III. . . . .	43

## LIST OF TABLES

### Table

I. BASC Calculations and Measured, Experimental radio-graphic Data of Jet Velocity, Mass, and Kinetic Energy for the 3.2-in. (81.3-mm), BRL, Precision Shaped Charge . . .	39
II. Summary of Results from the Small-Caliber, Shaped Charge Study for the 38.1-mm (1½-in.), Base Diameter Design . . . . .	39
III. Computational Matrix and Summary of Results . . . . .	40

7/8

## I. INTRODUCTION

The Ballistic Research Laboratory (BRL) of the U.S. Army Armament Research and Development Command (ARRADCOM) has a wide interest in the shaped-charge problems, ranging from detailed studies of the flow characteristics of the collapsing liner, to designing practical devices for future warhead applications. For these efforts several experimental and theoretical techniques are employed. Often, it is necessary to determine parametric relationships in the design application. Since it is more feasible to utilize theoretical calculations that are economically sound for parametric studies, the BRL has several finite-difference, hydrodynamic, computer codes that have been applied to shaped-charge problems.<sup>1,2</sup> Although these codes are adaptable to various geometrical considerations, they require operator experience and a seasoned analyst to insure proper application. Further, large, high-speed computers, and long calculational times are necessary. Quite often, it is desirable to have a simplified procedure for addressing parametric design studies quickly and economically. The BRL computer code named BASC (BRL Analytical Shaped Charge)<sup>3</sup> was formulated from analytic expressions to provide such capability. Although several advantages occur with the original BASC approach, several areas of difficulty were experienced, particularly those relating to accurate calculation of jet tip or lead pellet behavior and confined charges. Extensive semi-empirical functions, regarding liner acceleration and confinement effects, have been included to provide more accurate representations. This improved, simplified procedure, hereinafter referred to as the BASC code also, together with additional refinements are presented and discussed in this report.

---

<sup>1</sup>J. T. Harrison and R. R. Karpp, "Terminal Ballistic Applications of Hydrodynamic Computer Code Calculations," BRLR 1984, April 1977. (AD A041065)

<sup>2</sup>J. T. Harrison, "A Comparison Between the Eulerian, Hydrodynamic Computer Code (BRLSC) and Experimental Collapse of a Shaped Charge Liner," ARBRL-MR-0284!, June 1978 (AD A059711)

<sup>3</sup>J. Harrison, R. DiPersio, R. Karpp and R. Jameson, "A Simplified Shaped Charge Computer Code: BASC," DEA-AF-F/G-7304 Technical Meeting: Physics of Explosives, Vol II, April-May 1974, Paper 13 presented at the Naval Ordnance Laboratory, Silver Spring, MD.

The BASC code is an assembly of various theoretical and empirical techniques. Central to the procedure utilized in BASC is the Defourneaux model<sup>4</sup> for final plate velocity resulting from the shock of an adjacent detonating explosive. This assumption is adequate for portions of the liner which are initially removed (remote) from the collapse (jet formation) region or cone axis. In actuality, several shock reverberations are required to achieve a final liner metal velocity. Material near to the apex of the cone can enter the collapse process long before the liner is accelerated fully and, hence, does not achieve its ultimate velocity. This leads to the well known phenomena referred to as "the inverse velocity gradient" which forms the massive jet tip. This phenomena has been observed<sup>5</sup> and calculated earlier.<sup>1,2,6</sup> The author has modified the Defourneaux model to account for the time-dependent acceleration of the liner resulting in a gradual build-up to the ultimate collapse velocity. Since liner elements near the apex region of a cone will not achieve this ultimate velocity, the first element of the jet will move more slowly than the following elements of the jet. The faster elements collide and are compressed into the massive lead pellet. The final jet-tip velocity will become the mass-weighted average of these inverse velocity elements. This is the jet-tip velocity, which will be used in jet penetration theory. BASC uses a combination of the shaped-charge penetration of DiPersio, Simon and Merendino (DSM)<sup>7</sup> and the piece wise penetration of Defourneaux<sup>4</sup>. The DSM model is used to calculate total penetration-standoff curves and the piecewise penetration model is used to calculate whole profiles.

In addition to the inverse velocity gradient, flow into the stagnation region during the collapse process from particles near the apex of a conical liner may be supersonic and fail to form a jet or form a so-called incoherent jet. This is the jet-no-jet criteria. The criteria used in BASC is a modified version of the supersonic limitations of Chou, et. al.<sup>8</sup> The final theoretical technique used in BASC is the

---

<sup>4</sup>M. Defourneaux, "Hydrodynamic Theory of Shaped Charges and of Jet Penetration," Memorial DeL'art Ille'rie Francasise-T, 44, 1970.

<sup>5</sup>R. DiPersio, C. W. Whiteford, and J. Simon, "An Experimental Method of Obtaining Collapse Velocities of the Liner Walls of a Linear Shaped-Charge Liner," BRL-MR-1696, September 1965. (AD #478326)

<sup>6</sup>A. Kiwan and H. Wisniewski, "Theory and Computations of Collapse and Jet Velocities of Metallic Shaped Charge Liners," BRLR-1620, November 1972. (AD #907161)

<sup>7</sup>R. DiPersio, J. Simon, and A. Merendino, "Penetration of Shaped-Charge Jets Into Metallic Targets," BRLR 1296, September 1965. (AD #476717)

<sup>8</sup>P. Chou, J. Carleone, R. Karpp, "Criteria for Jet Formation from Impinging Shells and Plates," J. Appl. Physics, Vol. 47, No. 7, July 1976.

Pugh, Eichelberger, and Rostoker (PER) theory of jet formation.<sup>9</sup>

This report includes a description of analytical equations, the procedures for their application and a FORTRAN listing of BASC. Experimental results for selected shaped charge problems are presented in a comparison to the calculations. The range of useful applications is discussed as well as the limitations of the approach.

BASC is a "living code" which has provided insights to the jet-formation process and is a very good tool for parametric design for a selected class of problems.

A simplified flow chart and the FORTRAN code listing is presented in Appendices A and B, respectively.

## II. GOVERNING EQUATIONS

The initial equation used in the liner acceleration portion of the BASC code determines the angle of liner bending,  $\phi$ , produced by a detonation wave traveling with a velocity, D, and inclined to the liner wall at an angle, i (the angle of incidence). This relationship is illustrated in Figure 1. The author has modified the original platepush relationship of Defourneaux to be

$$\frac{1}{\phi} = \frac{1}{\phi_0} + K \frac{\rho e}{eB}, \quad (1)$$

$$B = 1 + A/\rho_c e_c,$$

where  $\rho$  and  $e$  are the density and thickness of the liner wall, and  $e$  is the explosive thickness. Added are  $\rho_c$ ,  $e_c$ , and  $A$  which are, respectively, density, thickness, and a constant, which is determined from the experimental data for the confinement casing around the charge<sup>10</sup>. The constant, A, when set to zero, represents an unconfined explosive charge and the Defourneaux relationship, as illustrated in Figure 1.  $\phi_0$  and K are functions of the angle of incidence, i, and

<sup>9</sup>E. M. Pugh, R. J. Eichelberger and N. Rostoker, "Theory of Jet Formation by Charges with Lined Conical Cavities," *J. Appl. Physics*, Vol. 23, No. 5, May 1952.

<sup>10</sup>R. DiPersio, J. Simon, and T. Martin, "A Study of Jets From Scaled Conical Shaped-Charge Liners," BRLMR-1298, August 1960. (AD #246352)

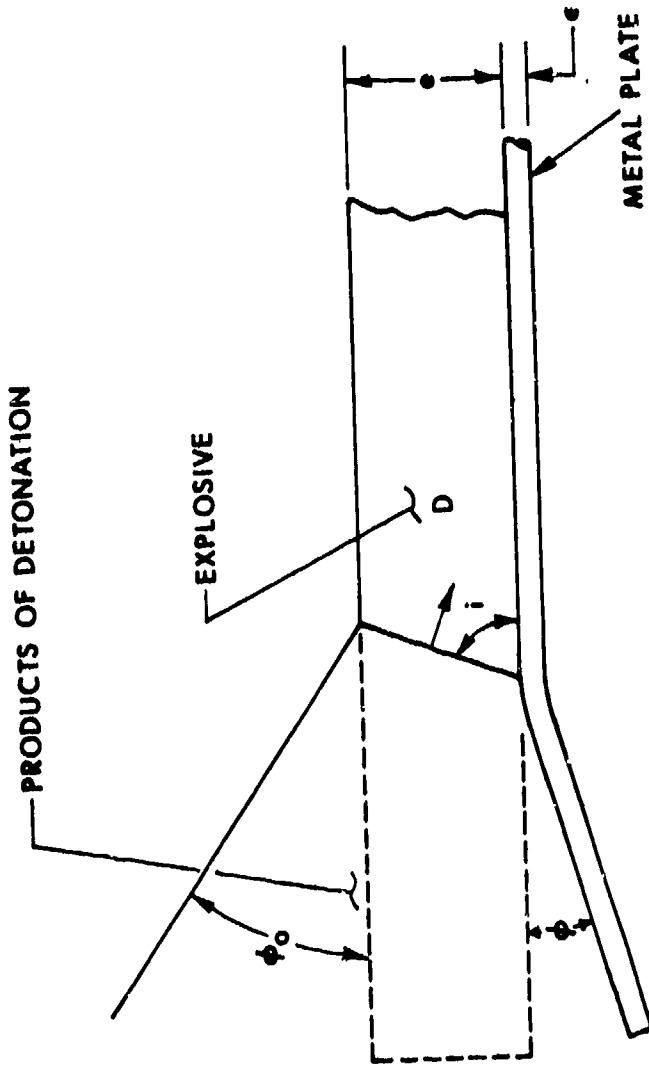


Figure 1. Projection of a Metal Plate by High Explosive

are determined for certain types of explosives.<sup>11</sup> Figure 2 illustrates the functional relationship between  $\phi_0$ , K, and i. K is a constant over the range of i considered for typical shaped-charge designs, i.e. a conical liner contained in a cylinder of explosive. Figure 3 illustrates the linear relationship, Equation 1, that  $1/\phi$  has with the ratio of liner mass per unit volume to explosive mass per unit volume, given as

$$\mu = \frac{\rho_e}{\rho_{H.E.}} e ,$$

where  $\rho_{H.E.}$  is the density of the explosive. The values of  $1/\phi_0$  and K used in Equation 1 are the Y-intercept and the ratio of the slope of the line to the density of explosive respectively. Equation 1 along with the Taylor formula,

$$v_0 = 2D \sin \frac{\phi}{2} ,$$

where D is the explosive detonation rate, will result in collapse velocities,  $v_0$ , obtained by Gurney.<sup>12</sup> Two types of explosive compositions are shown in Figure 3 (data taken from reference 11) which represent the linear function at a constant grazing (parallel) incidence, i, of the detonation from the normal to the metal surface (see Figure 1).

From the theory of Defourneaux, as the detonation wave sweeps toward the base of a typical shaped charge,  $\phi$  decreases due to the decrease in the explosive thickness, e, shown in Figure 3. This assumption that  $\phi$  decreased monotonically with a decrease in e is justified for most of the liner collapse since there is sufficient time for the liner to undergo several shock reverberations and achieve a bending angle close to its maximum before entering the flow of jet formation. However, the region near the apex of the cone

---

<sup>11</sup>M. DeFourneaux and L. Jacques, "Explosive Deflection of a Liner as a Diagnostic of Detonation Flows," Proceedings Fifth Symposium (International) on Detonation, ACR-184 Office of Naval Research-Department of Navy, pp. 457-466, Pasadena, California, August 18-21, 1979.

<sup>12</sup>R. W. Gurney, "The Initial Velocity of Fragments from Bombs, Shells, and Grenades," BRL Report No. 405, Sept. 1943. (AD #ATI36218)

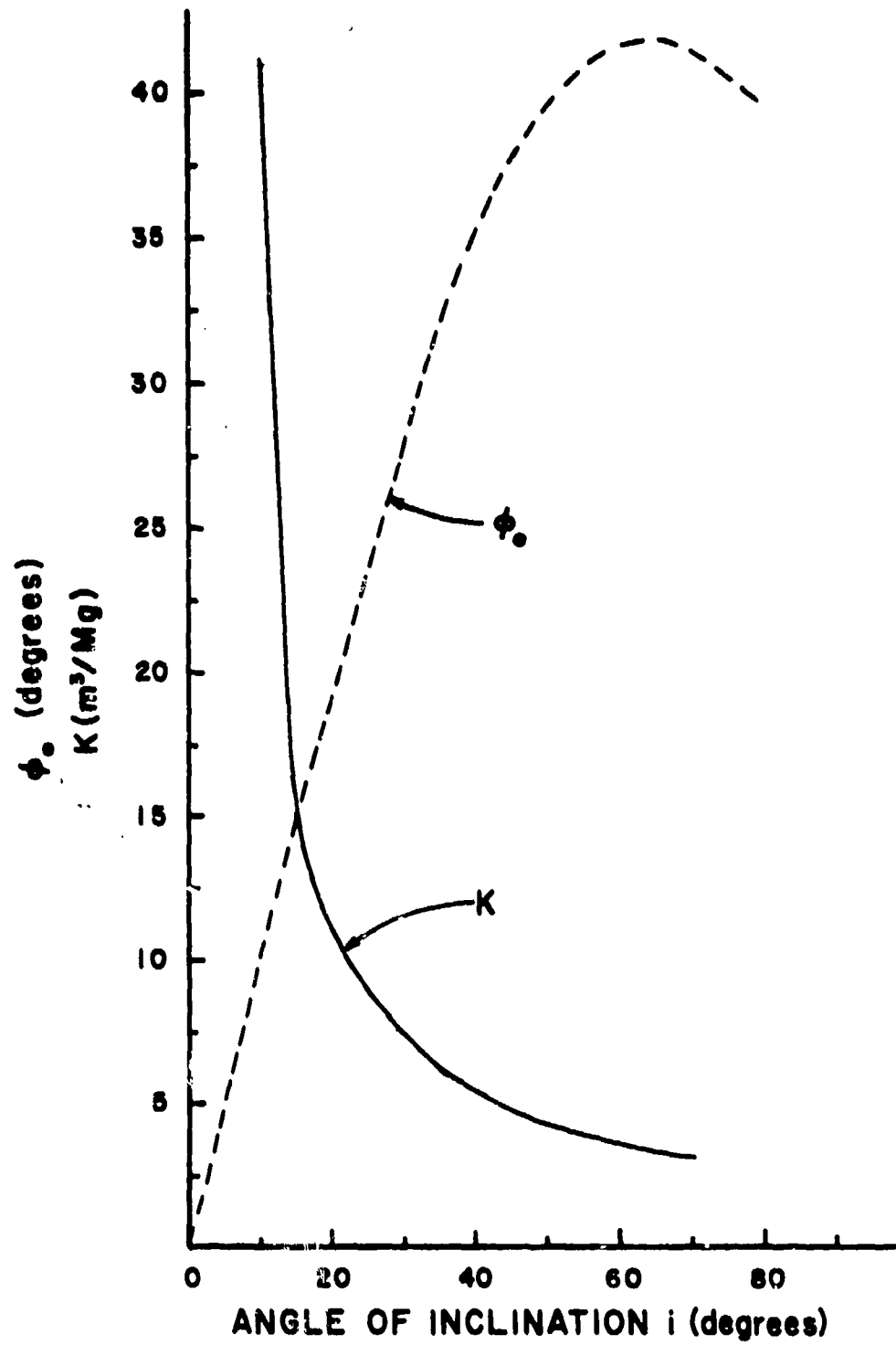


Figure 2.  $\phi_0$  and  $K$  are functions of the detonation wave angle to the liner.

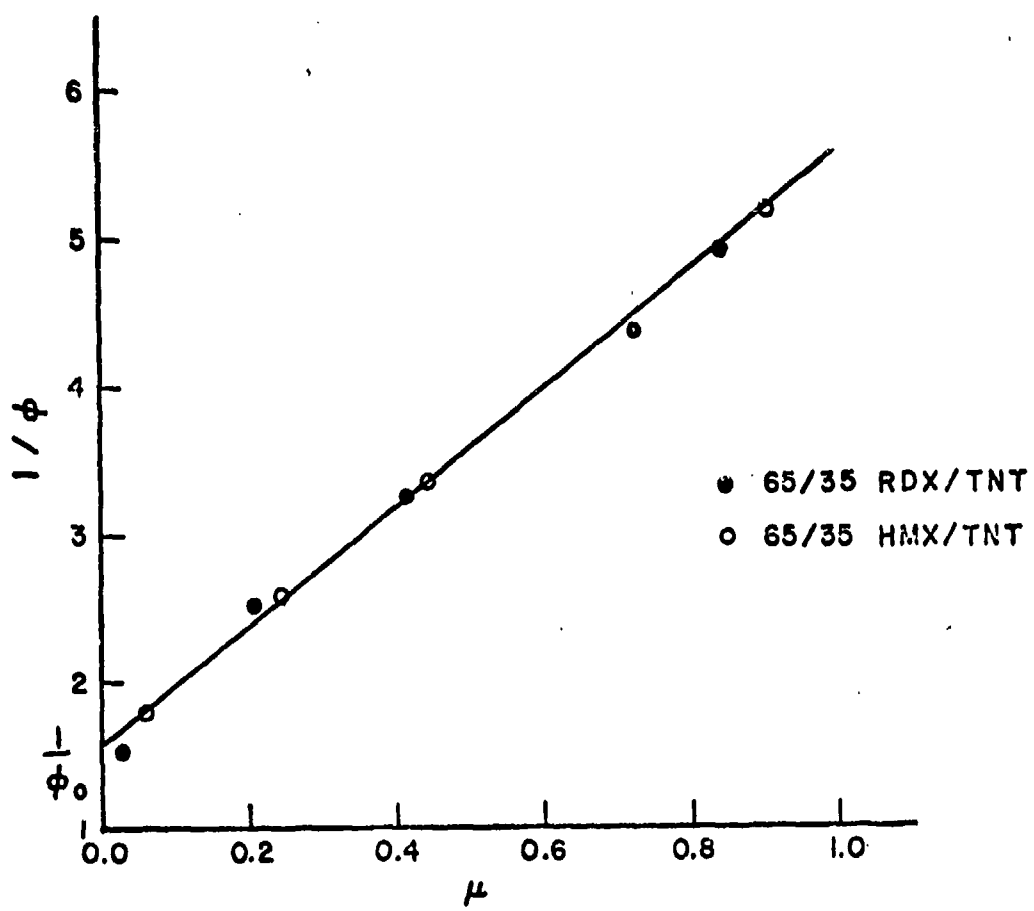


Figure 3.  $1/\phi$  vs  $\mu$  as determined from experiments. Data is taken from Reference 11.

enters the flow shortly after its initial acceleration and hence does not achieve its ultimate bending angle. Therefore, for material close to the liner's apex,  $\phi$  will increase to a maximum. This maximum will be located near liner elements that originate from a position approximately 40% of the liner height measured from the apex of the cone. After this point,  $\phi$  will decrease according to theory. We call this "the inverse collapse process." Associated with this process is the total time that a liner element takes to reach the axis. The equation for the collapse time is

$$\tau = (r \sin i) / (D(\sin(a+\phi) - \sin a)), \quad (2)$$

where several new variables are introduced.  $r$  is the instantaneous distance of a liner element from the axis before its collapse.  $a$  is the half angle of the cone of a conical liner or, in the general case, the instantaneous angle with the axis made by a tangent line to the liner.  $\tau$  will be affected by the inverse collapse process. Material close to the liner apex enters the flow of jet formation sooner than would be predicted by the collapse of Defourneaux.<sup>4</sup>

In order to calculate the inverse collapse process, a new equation for the bending angle,  $\phi$  and an iterative scheme were added to the code. The new equation for  $\phi$  is

$$\phi_N = \phi e^{\sqrt{\frac{b}{\tau}}}, \quad (3)$$

where  $b = C_1 \left[ \frac{k\rho e}{eB} \right],$

$C_1$ , is a constant determined from shape-charge collapse data.<sup>13</sup> The iterative scheme, between Equations (2) and (3), continues until the criteria of  $\phi_N$  approaching  $\phi$  within an epsilon is satisfied.

Having determined  $\phi$  and  $\tau$ , we can proceed with the collapse process.

---

<sup>13</sup>F.E. Allison and R. Vitali, "An Application of Jet Formation Theory to the 105-mm Shaped-Charge," BRLR-1165, March 1962. (AD #277458)

The velocity of collapse of the liner walls,  $v_o$ , toward the charge axis to form the jet is given by

$$v_o = 2D(\sin(\phi/2)) / (\sin i) \quad (4)$$

The apparent explosive detonation velocity, with respect to liner wall is given by

$$Da = D / \sin i \quad (5)$$

The substitution of Equation 5 into Equation 4 yields

$$v_o = 2Da \sin(\phi/2). \quad (6)$$

This is the so-called Taylor formula utilized in the code. The angle between the collapse direction and the charge axis is given by

$$\gamma = (\pi/2) - (\alpha + (\phi/2)). \quad (7)$$

The liner element first hits the axis at a distance,  $\bar{s}_p$ , from the liner apex, given by

$$\bar{s}_p = (z \sin \phi) / (\cos \alpha (\sin(\alpha+\phi) - \sin \alpha)), \quad (8)$$

where  $z$  is the axial component of the liner element position before its collapse.

While the liner is collapsing, the angle formed by a tangent to the collapsed portion on the axis and the axis itself (called the collapse angle) is computed from

$$\tan(\beta - \alpha) = \frac{\Delta z [\sin(\alpha + \phi) - \sin \alpha] \tan \phi + r \Delta \phi \cos \alpha}{\Delta z [\sin(\alpha + \phi) - \sin \alpha] - r \Delta \phi \cos \alpha \tan \phi}, \quad (9)$$

where  $\Delta z$  is the axial increment chosen in the computational scheme, and  $\Delta \phi$  is the incremental change in  $\phi$  between adjacent liner elements. The cartesian coordinates of a liner element (which originates at position  $z, r$ ) during collapse are given by the pair of equations:

$$\begin{aligned} x(z, t) &= z + v_o n \Delta t \sin(\alpha + (\phi/2)) \\ y(z, t) &= r - v_o n \Delta t \cos(\alpha + (\phi/2)), \end{aligned} \quad (10)$$

where  $\Delta t$  is the time interval taken by the detonation wave between successive liner elements and  $n$  is a positive integer. These equations apply in the time interval given by

$$0 < n\Delta t \leq \tau.$$

Figure 4 is an illustration of the relationship of the variables employed in the BASC code of a generalized axisymmetric collapse of a typical shaped charge. Shown on Figure 5 are drawings giving a detailed description of the collapse process. Figure 5A shows the velocity vectors of an element at point, P, on the collapsing liner. The element is projected toward the axis of symmetry with a collapse velocity,  $v_o$ , and a bending angle,  $\phi$ . When the detonation wave with velocity,  $D$ , has progressed a distance,  $P'$ , (i.e. from point P to point Q) during the time interval,  $\tau$ , then the element initially at point P will collide with the cone axis, producing the geometrical relations at the collision or stagnation point,  $sp$ ; shown in Figure 5B. This relationship at the stagnation point is with respect to a coordinate system moving at the stagnation point velocity,  $v_{sp}$ . The velocity of the liner wall flowing into the stagnation point is  $v_f$  and the angle between it and the cone axis is the collapse angle,  $\beta$ . Figure 5C shows a cross-section of the collapsing liner depicting the variables employed. Applying Bernoulli's equations at the stagnation point, we find that the flow velocity,  $v_f$ , separates into two equal but directionally opposite velocities. One is called the jet velocity,  $v_j$ , and the other is called the slug velocity,  $v_N$ . This relationship is shown on Figure 6. Resolving the flow velocity,  $v_f$ , at the stagnation point in the laboratory coordinate system (Figure 6A), the following set of equations are obtained:

$$v_j = v_f + v_{sp}, \quad (11)$$

$$v_N = v_{sp} - v_f. \quad (12)$$

In accordance with the laws of conservation of mass and momentum, when the liner material reaches the cone axis after its collapse, it proceeds either as a fast-moving jet or as the more massive but slower-moving slug (Figure 6A). The jet velocity equation that results is

$$v_j = v_o \cos(\alpha + (\phi/2) - (\beta/2)) / \sin(\beta/2), \quad (13)$$

and the equation for the slug velocity is

$$v_N = v_o \sin(\alpha + (\phi/2) - (\beta/2)) / \cos(\beta/2). \quad (14)$$

The relative distribution of mass (Figure 6B) that results in jet and

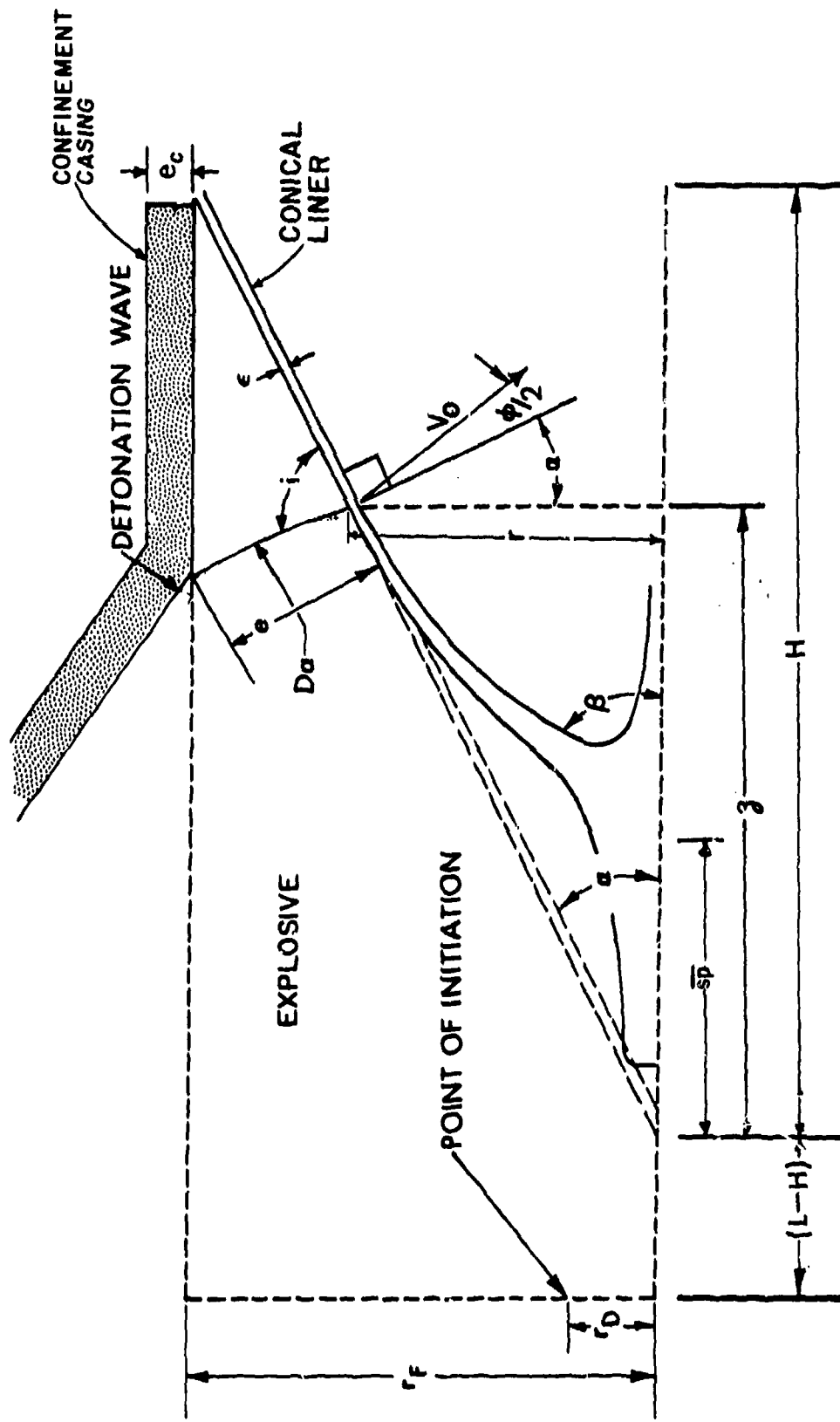
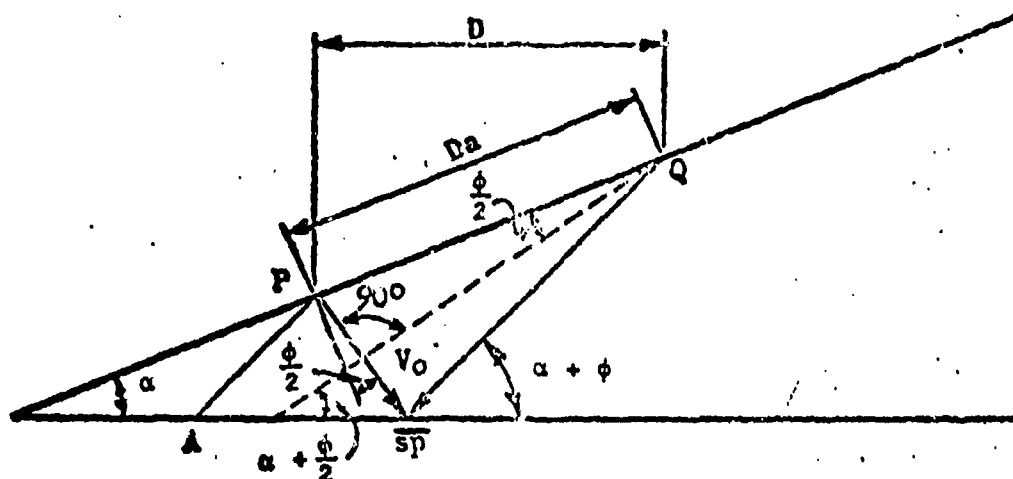
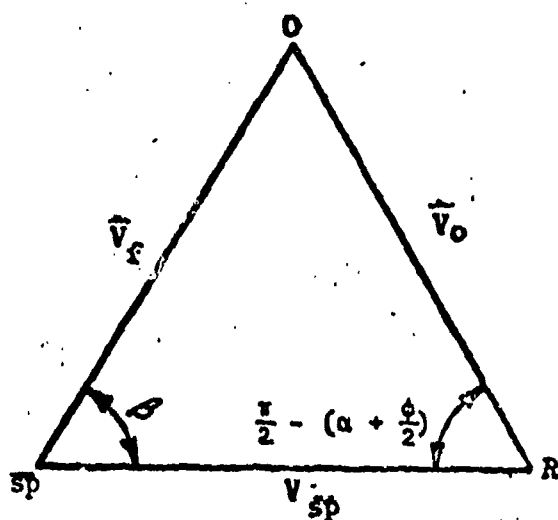


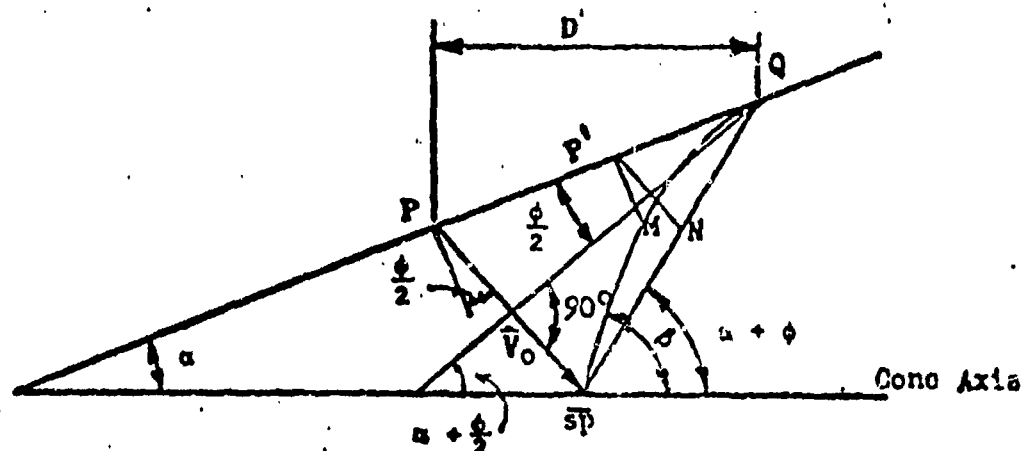
Figure 4. Line drawing illustrating the quantities employed in the BASC code of a generalized axisymmetric collapse of a shaped-charge.



A. Velocity vectors of an element of the collapsing liner.

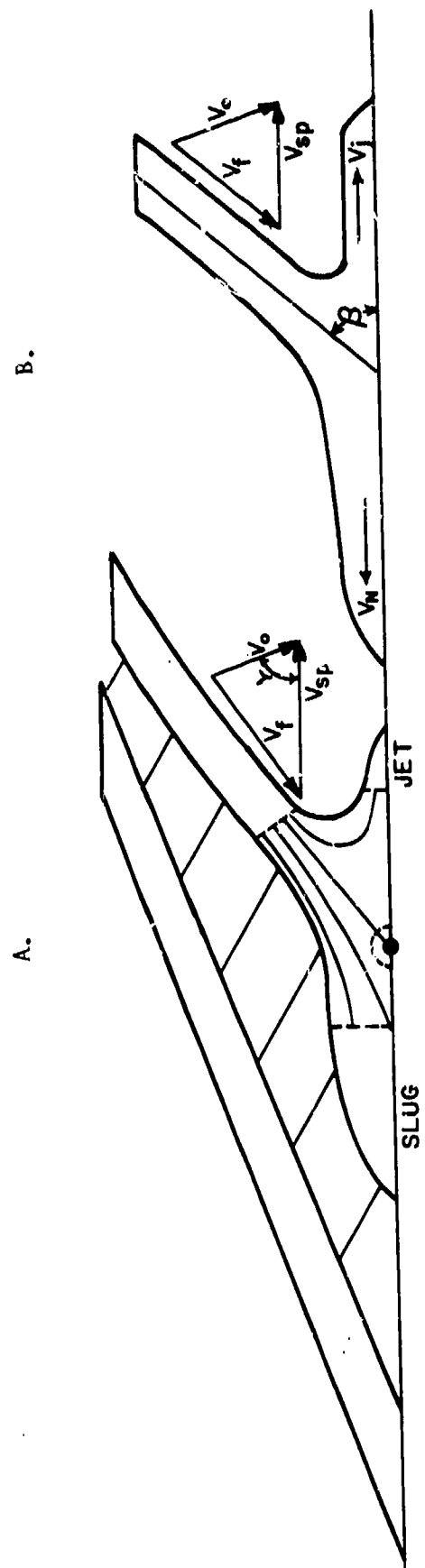


B. Geometrical relations at the stagnation point.



C. Cross-section of collapsing liner.

Figure 5. Illustration of the relationship between variables and the collapse process.



$$M_i = M_L \sin^2(\beta/2)$$

$$V_j = V_f + V_{sp}$$

$$V_w = V_{sp} - V_f$$

Figure 6. Illustration of the resolved variables in the laboratory coordinate system.

slug material are calculated, respectively, by

$$\frac{dm_j}{dm_L} = \sin^2(\beta/2) \quad (15)$$

and

$$\frac{dm_N}{dm_L} = \cos^2(\beta/2) .$$

Also, the relative distribution of the kinetic energy for the jet and slug, respectively, are

$$\frac{dE_j}{dE_L} = \cos^2(\alpha + (\phi/2) - (\beta/2)) \quad (16)$$

and

$$\frac{dE_N}{dE_L} = \sin^2(\alpha + (\phi/2) - (\beta/2)) .$$

The variables  $dm_L$  and  $dE_L$  are the incremental change in the liner's mass and kinetic energy, respectively.

The impinging flow velocity,  $v_f$ , has been considered by shaped-charge researchers such as Walsh, et. al.<sup>14</sup>; Cowan, et. al.<sup>15</sup>; and Chou, et. al.<sup>8</sup> to be critical in the jet-formation theory. As illustrated in Figure 7, when  $v_f$  is less than the material sound speed,  $c$ , the jet formed is coherent or a good jet (Figure 7A). Even when  $v_f$  is slightly greater than  $c$ , this too forms a coherent jet (Figure 7B). But, when  $v_f$  is sufficiently greater than  $c$ , the jet will be incoherent or bifurcated. We call it a no-jet condition (Figure 7C). From equations 11 and 12, solving for  $v_f$  yields

$$v_f = .5(v_j - v_N) . \quad (17)$$

We then use the following relationship as the jet limiting criteria for a coherent jet:

$$M_R = v_f/c < 1.23 . \quad (18)$$

<sup>14</sup>J. M. Walsh, R. G. Shreffler, and F. J. Willig, "Limiting Velocity Conditions for Jet Formation in High Velocity Collisions," *Journal of Applied Physics*, Vol. 24, No. 3, pp. 349-359, March 1957.

<sup>15</sup>G. R. Cowan and A. H. Holtzman, "Flow Configurations in Colliding Plates: Explosive Bonding," *Journal of Applied Physics*, Vol. 34, No. 4, pp. 928-939, April 1963.

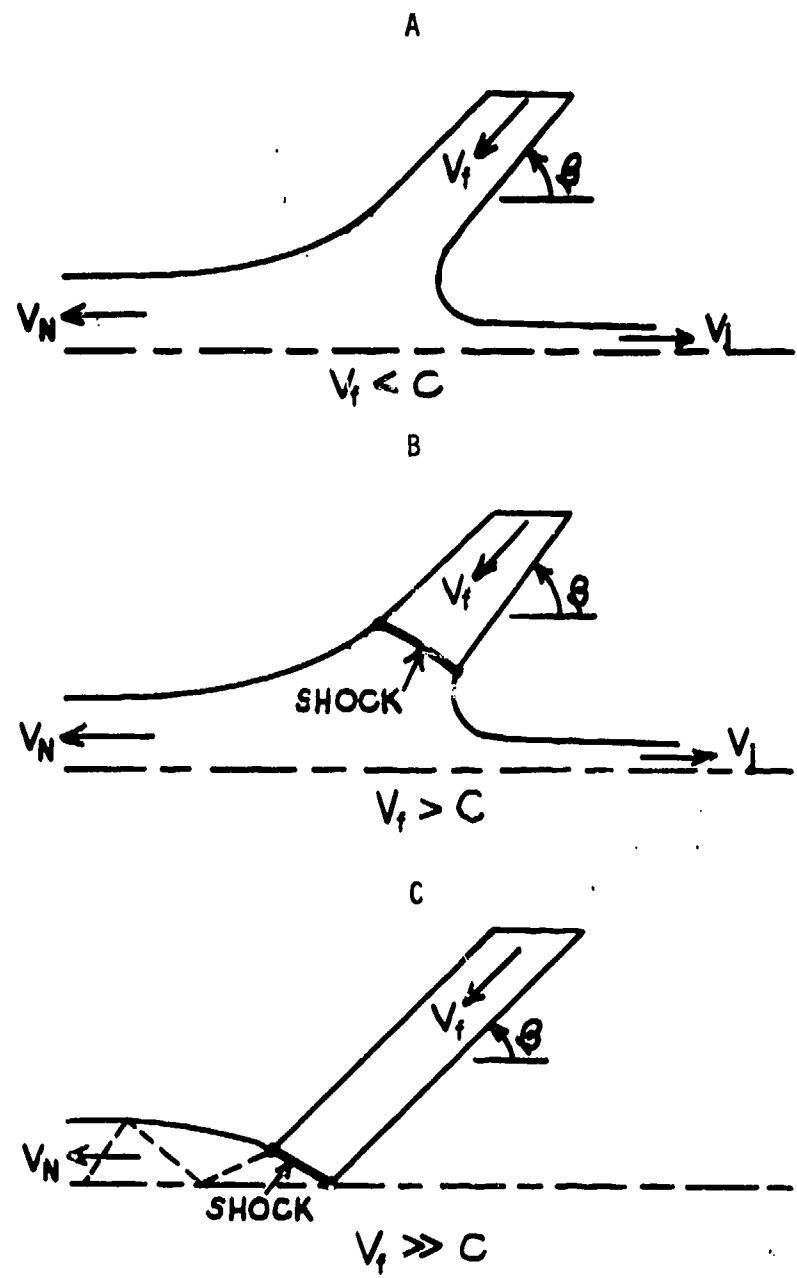


Figure 7. Illustration of the variables employed in the BASC code to limit jet formation. The jet limiting criteria for a coherent jet (A and B) is  $M_R = v_f/c < 1.23$ .

The threshold factor for a coherent jet,  $M_t = 1.23$ , is determined by comparing radiographic, jet-particle data measured<sup>16</sup> from experiments<sup>17</sup> with BASC results. The threshold factor holds for several materials considered in BASC calculations.

In order to determine the jet-tip velocity and the mass of the lead pellet to be used in the shaped-charge penetration theory, the inverse velocity gradient has to be equilibrated and the jet mass in this region to be compressed into a single zonal element, LP. This zone will then contain the so-called steady-state, lead pellet. The equilibrated jet-tip velocity,  $v_{jo}$ , is obtained by the following process:

$$v_j^{i+1} = \frac{v_j^{i+1} \left[ \frac{dm_j}{dm_L} \right]^{i+1} dm_L^{i+1} + v_j^i \left[ \frac{dm_j}{dm_L} \right]^i dm_L^i}{\left[ \frac{dm_j}{dm_L} \right]^{i+1} dm_L^{i+1} + \left[ \frac{dm_j}{dm_L} \right]^i dm_L^i}$$

for  $v_j^{i+1} > v_j^i$  and  $1 \leq i \leq LP$ , where  $i$  is the  $i^{\text{th}}$  zonal element. The equilibrated jet-tip velocity is

$$v_{jo} = v_j^{\text{LP}} \quad (18)$$

The steady-state, lead pellet mass is

$$dm_{jo} = \sum_{i=1}^{\text{LP}} \left[ \frac{dm_j}{dm_L} \right]^i dm_L^i \quad (19)$$

In the theory of shaped-charge jet penetration into a target used in BASC, an important parameter is the time that a given liner element, which enters into the jet, arrives at the bottom of the target hole when penetration is in progress. Time is usually started from the moment the detonation wave reaches the apex of the liner. A time parameter,  $\theta$ , is defined by

$$\theta = t_z + \tau \quad , \quad (20)$$

---

<sup>16</sup>Private Communication from J. Blische at BRL.

<sup>17</sup>R. DiPersio, W.H. Jones, A.B. Merendino, and J. Simon, "Characteristics of Jets from Small Caliber Shaped Charges with Copper and Aluminum Liners," BRLMR No. 1866, September 1967. (AD #823839)

where  $t_0$  is the time at which the detonation wave reaches the liner element at an initial axial distance,  $z_0$ , from the apex and  $\tau$  is the time taken by this element to collapse onto the charge axis. The sum of standoff distance from the liner base to the initial surface of the target,  $h$ , and the liner height,  $H$ , defines  $Z_0$ :

$$Z_0 = h + H. \quad (21)$$

The time for the tip of the jet to reach the target surface is

$$T_0 = Z_0 / v_{j0} \quad (22)$$

It is assumed that the jet tip originates from the zonal element, LP, and contains the highest velocity of the jet,  $v_{j0}$ . An element from the liner between LP and base results in a jet velocity,  $v_j$ , which is less than  $v_{j0}$  and is a function of its initial axial distance,  $z$ . A parameter,  $\mu$  is defined by

$$\mu = v_{j0} / v_j \quad (23)$$

The time for the portion of jet formed from a given element of the liner to reach the bottom of the target hole is

$$T = \mu^{(1+k)} [T_0 + (1+k) \sum_0^i \mu^{-k} (\Delta f)_i] \quad (24)$$

where  $(\Delta f)_i = f_i - f_{i-1}$  and denotes the  $i^{\text{th}}$  zonal element. In

this equation,  $k = \sqrt{\rho_j / \rho_c}$ , where  $\rho_j$  is the jet density (assumed equal to the liner density), and  $\rho_c$  is the target density.  $f$  is a time parameter given by

$$f = ((\theta/\mu) - (\bar{s}p/v_{j0})) , \quad (25)$$

where  $\bar{s}p$  was previously defined by Equation 8, and  $v_{j0}$ ,  $\theta$ , and  $\mu$  were defined by Equations 18, 20, and 23. The value of  $\mu$  to be used outside the bracket in Equation 24 is that which applies to the original elemental liner position.  $\Delta f$  is the difference in  $f$  values between adjacent elemental positions, and the summation applies to all adjacent elemental positions up to the point in question on the liner.

While the jet is still continuous in nature, it stretches due to its velocity gradient and, therefore, decreases in diameter with increase in time. The equation for calculating the jet radius,  $r_j$ , is

$$r_j^2 = \frac{2 r \epsilon D \sin^2(\beta/2)}{\frac{\Delta z}{\Delta t_z} |_T \sin i} \quad (26)$$

In this equation,  $r$  is the initial radial position of the liner element from the charge axis,  $\epsilon$  is the liner thickness at this position, and  $\beta$  is the collapse angle that is formed when this element reaches the charge axis. The factor,  $\frac{\Delta z}{\Delta t_z} |_T$ , is given by

$$\frac{\Delta z}{\Delta t_z} |_T = (T - t_z) \frac{\Delta v_j}{\Delta t_z} - v_j + \frac{\Delta(z - r \cot(\beta/2))}{\Delta t_z} \quad (27)$$

In this equation,  $t_z$  is defined following Equation 20 and  $\Delta t$  is the incremental time interval between arrival of the detonation wave between successive liner elements (a constant). The value computed by Equation 27 is a function of time,  $T$ , which starts at zero when the detonation wave first reaches the liner apex. It is a negative value which increases in absolute value as  $T$  increases. Therefore, it can be seen from Equation 26 that the jet radius, which originates from material at any point on the liner, decreases with an increase in  $T$ . The minus sign in Equation 26 is necessary to make  $r_j^2$  a positive quantity.

When the jet cannot sustain any further stretching, it breaks up into individual axial particles. It is assumed that this occurs throughout the whole jet at the same time. The breakup time for the jet is designated as  $T_b$  and, at present, must be obtained from experimental observations. At times greater than the jet breakup time, the individual jet particles do not stretch in length or decrease in diameter. The constant jet particle radius that one obtains for material originating from a given element of the liner

is calculated by Equation 26 in which the factor  $\frac{\Delta z}{\Delta t_z} |_T$  is calculated

at the breakup time,  $T_b$ , in Equation 27. However, radii of different particles are different due to the variability of the initial liner element position in Equations 26 and 27.

The equations that are used for jet penetration theory are dependent upon the standoff distance between the charge and the target. If the target is placed close enough to the charge so that the jet tip reaches the target before the time of jet breakup, one set of equations are used. On the other hand, if the jet particulates before reaching the target surface, a different set of equations must be used. In the former case, even though the jet

starts penetrating in the continuous state, it becomes discontinuous before the end of penetration and different equations are required after time  $T_1$ . The variables and the two states of penetration are illustrated in Figure 8.

The jet penetrates the target in both the continuous and discontinuous state whenever the following criteria is satisfied:

$$z_o < v_{jo} T_1 \quad . \quad (28)$$

The depth of penetration into the target,  $p$ , for any  $T$ , such that  $T_0 \leq T \leq T_1$ ,

$$p = z_o \left[ \left( \frac{T}{T_0} \right)^{\frac{1}{k/(k+1)}} - 1 \right] \quad , \quad (29)$$

where all factors have been previously defined. For times greater than  $T_1$ , the equation used is

$$p = z_o \left[ (k+1) \left( \frac{T_1}{T_0} \right)^{\frac{1}{k/(k+1)}} \frac{T}{T_1 + kT_1} - 1 \right] \quad . \quad (30)$$

The total penetration depth into the target is calculated by

$$P_T = (k+1) (v_{jo} T_1)^{\frac{k}{k+1}} z_o^{\frac{k+1}{k}} - \sqrt{k(k+1) U^{\min} T_1} (v_{jo} T_1)^{\frac{k}{k+1}} z_o^{\frac{k+1}{k}} - z_o \quad . \quad (31)$$

The only hitherto undefined term in Equation 31 is the factor  $U^{\min}$ . This is called the minimum penetration velocity. According to theory, the velocity of penetration into the target monotonically decreases with increase in penetration depth until it reaches the

value  $U^{\min}$ . When  $U^{\min}$  is reached, penetration stops and all remaining jet material just piles up at the bottom of the target

hole.  $U^{\min}$  is an empirical constant whose value depends upon the target material and its hardness. It is invariant with standoff distance. With a given charge, target, and standoff distance, the computer calculates the constant total penetration depth from Equation 31. This value is used by the computer as a signal to stop calculating  $p$  in Equation 30 and also to determine the time at the end of the penetration process. The radius of the hole in the target before the time of jet breakup is given by

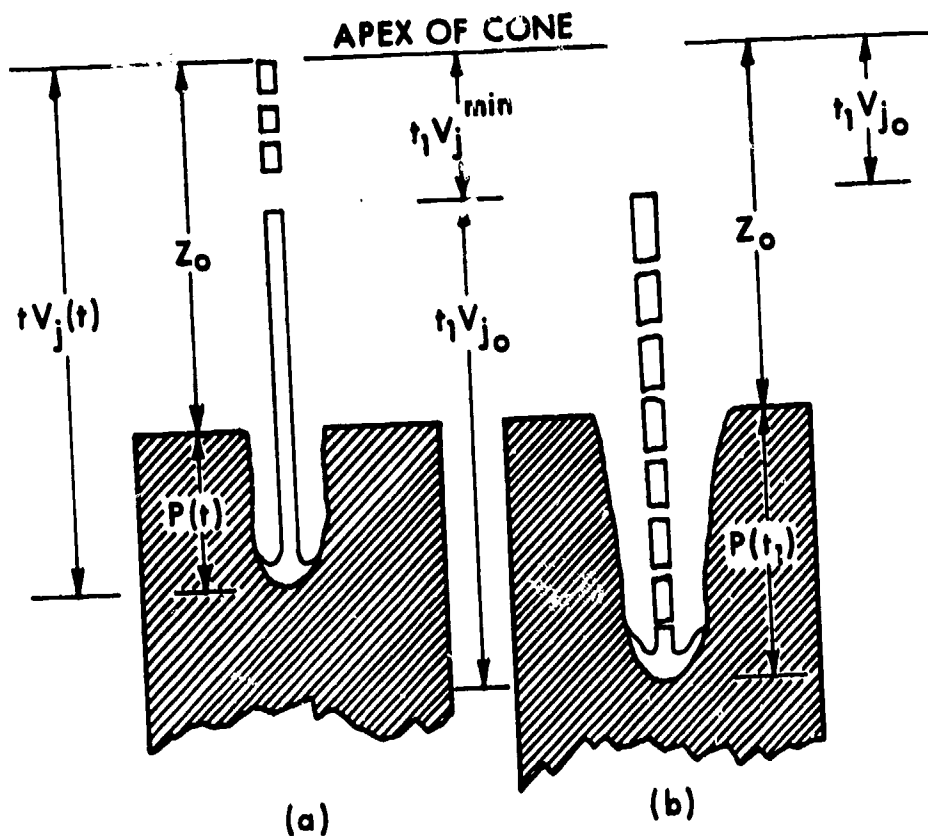


Figure 8. Schematic cross section of a shaped-charged jet penetrating a target in two states:  
 (a) Continuous and discontinuous,  
 (b) Discontinuous.

$$r_c = \sqrt{\frac{\rho_j}{2kc_k}} \sqrt{\frac{T_1}{T_0}} \left( \frac{z_o}{z_o + p} \right)^{\frac{3+k}{2k}} v_{jo} r_j . \quad (32)$$

This equation contains one last empirical constant of the target,  $c_k$ . This is the jet kinetic energy needed to produce a unit of hole volume in the target. Its value depends upon the target used and its hardness. The value of  $r_j$  in Equation 32 is obtained by Equations 26 and 27. After the breakup time,  $T_1$ , the hole radius is obtained by

$$r_c = \sqrt{\frac{\rho_j}{2kc_k}} \frac{1}{k} \left[ (k+1) \left( \frac{z_o}{v_{jo} T_1} \right)^{\frac{1}{k+1}} - \frac{z_o + p}{v_{jo} T_1} \right] v_{jo} r_j , \quad (33)$$

where  $r_j$  is now obtained by Equations 26 and 27 with the restriction that the factor  $\frac{\Delta Z}{\Delta t_z}|_T$  must be evaluated at  $T = T_1$ . The hole profile, as computed by Equation 33, is terminated when the penetration depth,  $p$ , reaches the value  $P_T$  as calculated by Equation 31.

The last set of penetration equations is used when the standoff distance between charge and target is so large that the following condition is satisfied:

$$z_o > v_{jo} T_1 . \quad (34)$$

In this case, all penetration is accomplished by the jet while it is particulated in nature. The equation for penetration depth is then

$$p = v_{jo} (T - T_0) T_1 / (T_1 + (T/k)) \quad (35)$$

where the time factor,  $T$ , varies between the time of first target impact,  $T_0$ , and the time of last jet penetration,  $T_p$ . The total penetration depth is given by

$$P_T = [v_{jo} T_1 - \sqrt{U^{\min} T_1 (v_{jo} T_1 + (z_o/k))}] k . \quad (36)$$

The radius of the hole produced in the target as a function of its depth is given by

$$r_c = v_{jo} r_j (1 - (p/k v_{jo} T_1)) \sqrt{\rho_j / 2k c_k}, \quad (37)$$

where the jet radius,  $r_j$ , is obtained by Equations 26 and 27 with the restriction that the factor  $\frac{\Delta Z}{\Delta t_z} |_{T_1}$  is evaluated at  $T = T_1$ .

The variation of total penetration depth with standoff distance is computed by means of Equations 31 and 36. The factor  $Z_0$  is the only variable in these equations. Equation 31 is used first until  $Z_0$  increases to the value  $v_{jo} T_1$ , then Equation 36 is used.

### III. CALCULATIONAL SCHEME

The BASC code enables one to perform parametric studies for designing warheads. The variables employed in the code of the generalized, axisymmetric collapse of a shaped charge were illustrated previously in Figure 4. The parameters which can vary include the following:

$\alpha$	(ALPHA)	The half angle of the liner (degrees)
$K$	(CON)	The empirical constant for the detonation products. Value known for Composition B explosive.
$\epsilon$	(EPS)	The thickness of the liner (cm)
$\rho_j$	(RHOJ)	The density of the liner (gm/cm <sup>3</sup> )
$\rho_c$	(RHOC)	The density of the target (gm/cm <sup>3</sup> )
$r_F$	(RF)	Radius of the base of target (cm).
$H$	(H)	Height of the liner (cm). If $H$ is zero, $H$ will be calculated by $H = \frac{r_F}{\tan \alpha}$ .

D	(D)	Detonation velocity (cm/ $\mu$ s)
S0	(S0)	Standoff distance between base of liner and target, (cm)
C <sub>K</sub>	(CK)	Constant for determining hole volume
T <sub>1</sub>	(T1)	Jet breakup time ( $\mu$ s)
U <sup>MIN</sup>	(UMIN)	Velocity cutoff for the penetration of jet into a target (cm/ $\mu$ s)
L	(DPOINT)	Initially the total length of the charge (cm) but is converted to be the initiation point of the explosive (i.e. DPOINT = L-H).
RDPT	(RDPT)	Radius above axis where explosive is initiated (cm).
JOHN	(JOHNI)	If JOHNI greater than zero, $\phi$ will vary; if not, $\phi_0$ will be a calculated constant.
N	(N)	The number of zones into which the grid is subdivided. If N is zero, default is seventy zones.

The code will set up the grid based upon Figure 4 and the equation for increment in Z is

$$DZ = H/N \quad (38)$$

and from this the time increment is

$$DTZ = DZ/D \quad (39)$$

Therefore, at each increment in Z we have also the corresponding time increment.

The code then marches sequentially through the governing equations (1-19), calculating and storing jet formation information to be printed and plotted at the end of the iteration. Those variables include:

i	I	i <sup>th</sup> zone
$\alpha$	ALPHA(I)	Tangent angle of liner wall to the axis (degrees)
z	Z(I)	z distance from apex to base of liner

$t_z$	TZ(I)	Time at the $i^{\text{th}}$ zone
$\gamma$	GAMMA(I)	Angle (degrees)
$E$	E(I)	Thickness of explosive above $i^{\text{th}}$ zone
$\phi$	PHI(I)	Angle (degrees)
$\beta$	BETA(I)	Angle (degrees)
$\Delta\phi$	DPHI(I)	Increment of angle $\phi$
$\frac{1}{\phi}$	RPHI(I)	Reciprocal of angle $\phi$
$v_o$	V(I)	Collapse velocity (cm/ $\mu$ s)
$r$	R(I)	Radius of the $i^{\text{th}}$ zone (cm)
$\tau$	TAU(I)	Time to collapse $i^{\text{th}}$ zone ( $\mu$ s)
$\overline{sp}$	C(I)	Distance from the apex of the liner where $i^{\text{th}}$ zone will hit the axis (cm)
$v_j$	VJ(I)	Velocity of the jet in (cm/ $\mu$ s)
$v_N$	VN(I)	Velocity of the slug in (cm/ $\mu$ s)
$\frac{dm_j}{dm_L}$	DMJ(I)	Relative mass of the jet, dimensionless
$\frac{dm_N}{dm_L}$	DMN(I)	Relative mass of the slug, dimensionless
$\frac{dE_j}{dE_L}$	DEJ(I)	Relative energy of the jet, dimensionless
$\frac{dE_N}{dE_L}$	DEN(I)	Relative energy of the slug, dimensionless
$v_f$	RV(I)	Relative velocity between the jet and slug

In the penetration portion of BASC, the constants listed below must be calculated:

$$VJO = \text{jet tip velocity from Equation 18} \quad (40)$$

$$ZO = H + SO \quad (41)$$

$$TO = \frac{ZO}{VJO} \quad (42)$$

$$AKAY = \sqrt{\frac{\rho_j}{\rho_c}} \quad (43)$$

$$PT = \text{Total penetration (cm) from Equation 31 or 36} \quad (44)$$

The next set of outputs are for the penetration of the jet into the target. The code also marches through the governing Equations 20-37, calculating and storing penetration information to be printed and plotted at the end of the iteration. The variables calculated and stored are listed below:

i	I	$i^{\text{th}}$ zone
$\mu$	AMU(I)	Relative velocity between the jet tip velocity and jet velocity of the $i^{\text{th}}$ zone
$\theta$	THETA(I)	Time parameter in microseconds
f	F(I)	Time parameter in microseconds
$\Delta f$	DF(I)	Time increment of f in microseconds.
T	T(I)	Time that the $i^{\text{th}}$ element reaches the bottom of the target hole in microseconds.
$\Delta t$	DT(I)	Time increment of T
r	RSQ(I)	is $\sqrt{r_j^2}$ which is the radius of the $i^{\text{th}}$ element of the jet.
A	A(I)	is equal to $z - r \cot \beta/2$ .
$\Delta A$	DELA(I)	is the increment of A(I).
$\Delta v_j$	DVJ(I)	is the increment of jet velocity.

$\frac{\Delta z}{\Delta t_z}$	DZODT(I)	Equation 27 in governing equations
$r_c$	RC(I)	Radius of the hole in target of the $i^{\text{th}}$ zone in centimeters
p	p(I)	Depth of penetration in centimeters

After these parameters have been printed and plotted, the code then returns to start and begins another case. This is continued until the end of file (i.e. next problem) is encountered causing the run to terminate.

#### IV. COMPARISON OF BASC CODE RESULTS

The performance of the BASC code is best illustrated by presenting results of a calculation and comparing these results, where possible, with experimental data or with results from other numerical techniques. The first set of comparisons will be with experimental results from the following:

- a. 105-mm, unconfined,  $42^{\circ}$ , copper-lined shaped charge with a Composition B explosive fill tested by Allison and Vitali.<sup>13</sup>
- b. A study of jets from scaled,  $42^{\circ}$ , copper-lined, conical shaped charges filled with Composition B explosive (test by DiPersio, et. al.<sup>10</sup>).
- c. 3.2-inch, BRL precision, shaped charge with a copper liner  $42^{\circ}$  apex angle, and Composition B explosive fill, having its jet characteristics measured<sup>16</sup> from radiographic data recorded at the BRL.
- d. A study of jet characteristics from small-caliber shaped charges with copper and aluminum liners and variation in apex angle from  $20^{\circ}$  to  $90^{\circ}$ . All charges were filled with Composition B explosive. The tests conducted at the BRL by DiPersio, et. al.<sup>17</sup>

The second set of comparisons will be another numerical technique. The other technique is the two-dimensional, hydrodynamic computer program based upon the Eulerian numerical scheme called the BRLSC (Ballistic Research Laboratory Shaped Charge) code.<sup>18</sup> The BRLSC

---

<sup>18</sup>M.L. Gittings, "BRLSC: An Advanced Eulerian Code for Predicting Shaped Charges," Vol. I, BRL CR 279, Prepared by System, Science and Software, December 1976. (AD #A023962)

code is a modified version of the HELP (Hydrodynamic Elastic-Plastic) code<sup>19</sup> developed by System, Science and Software.

Figure 9 and 10 are experimental comparisons for the 105-mm, unconfined, shaped charge. Collapse velocity,  $v_c$ , and jet velocity,  $v_j$ , as a function of the relative distance from the apex of the cone are shown on Figure 9. The dashed line is the jet velocity after jet compression and illustrates exact agreement with both the jet tip velocity and position on the axis between BASC and experiment. This illustrates that jet tip is compressed into one element at a position which is approximately 40% of the distance from the apex of the cone. The collapse velocity is slightly higher than that calculated by Allison and Vitali, but the overall agreement is good. Figure 10 shows a comparison of the predictions of jet mass versus cone mass between the BASC code and Allison and Vitali. Those two predictions are in slight disagreement with one another because Allison and Vitali were unable to recover 100% of all the slug material. They used essentially the same theory as the BASC code to predict jet mass, and all of the material is required to accurately predict the true conservation laws.

Figure 11 is the second experimental comparison of the scaled, shaped charge with a heavy confinement casing. This figure shows collapse velocity,  $v_c$ , and jet velocity,  $v_j$ , as a function of the relative distance from the apex of the cone. The dashed line is the compressed jet velocity distribution. This again illustrates exact agreement for both jet tip velocity and its position on the axis between BASC and experiment. The open squares at approximately the 48% position from the apex of the cone shows the spread in the experimental data from the experimental scaled rounds. The BASC code results are identical for the same scaled rounds (see Reference 10). Shown at the base of the cone, for values greater than 80% of the distance from the apex of the cone, is a change in the slope of the jet velocity curve. This is due to gas leakage or breaking of the confinement casing. This phenomenon is modeled in BASC as a gradual change in the confinement factor, A in Equation 1, until it reaches zero, i.e. unconfined. This comparison shows very good agreement with the experimental results.

Table I is a tabulation of a comparison between measured, radiographic experimental data and BASC code results from the 3.2-inch, BRL, precision shaped charge. The jet tip velocity and mass at jet particle number one are in agreement, but the accumulated total jet mass from jet particle number one to jet particle number

<sup>19</sup> J. Hageman and J.M. Walsh, "HELP, A Multi-Material Eulerian Program For Compressible Fluid and Elastic-Plastic Flows in Two Space Dimensions and Time," BRL CR 39, Prepared by System, Science and Software, May 1971. (AD Nos. 726459 and 726460)

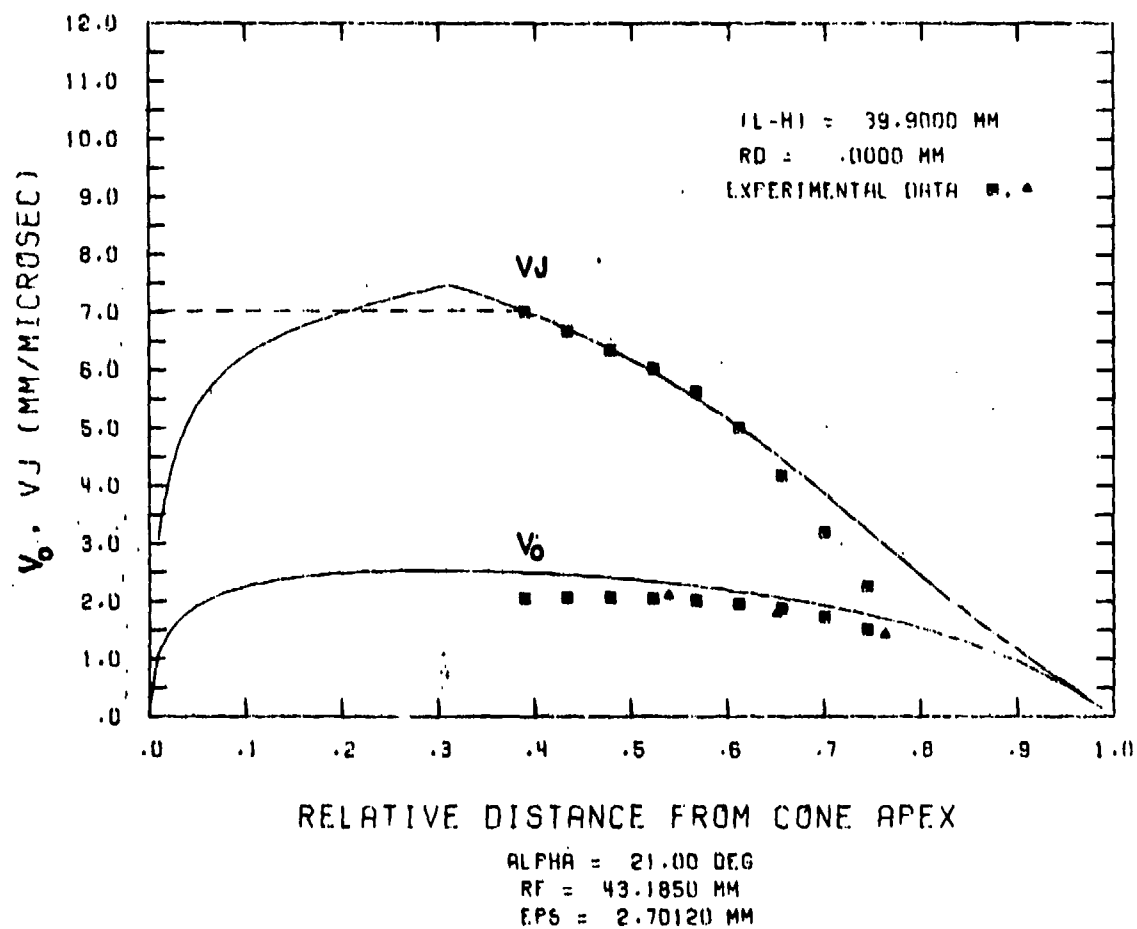


Figure 9. Comparison between experimental and BASC Code results of jet and collapse velocities from the 105-mm, unconfined, shaped charge.

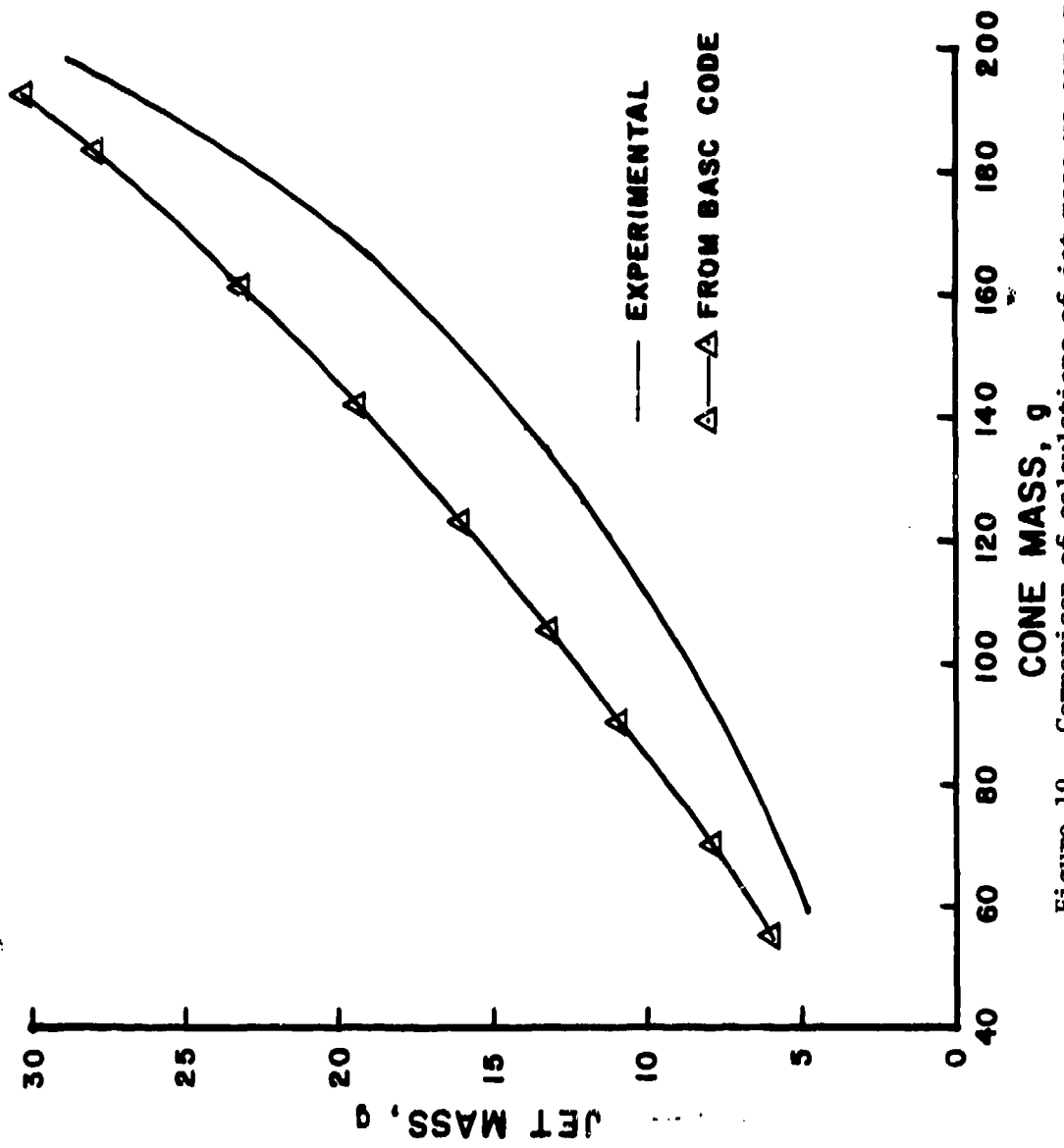


Figure 10. Comparison of calculations of jet mass vs cone mass between BASC code and experimental results from the 105-mm, unconfined, shaped-charge (Reference 13).

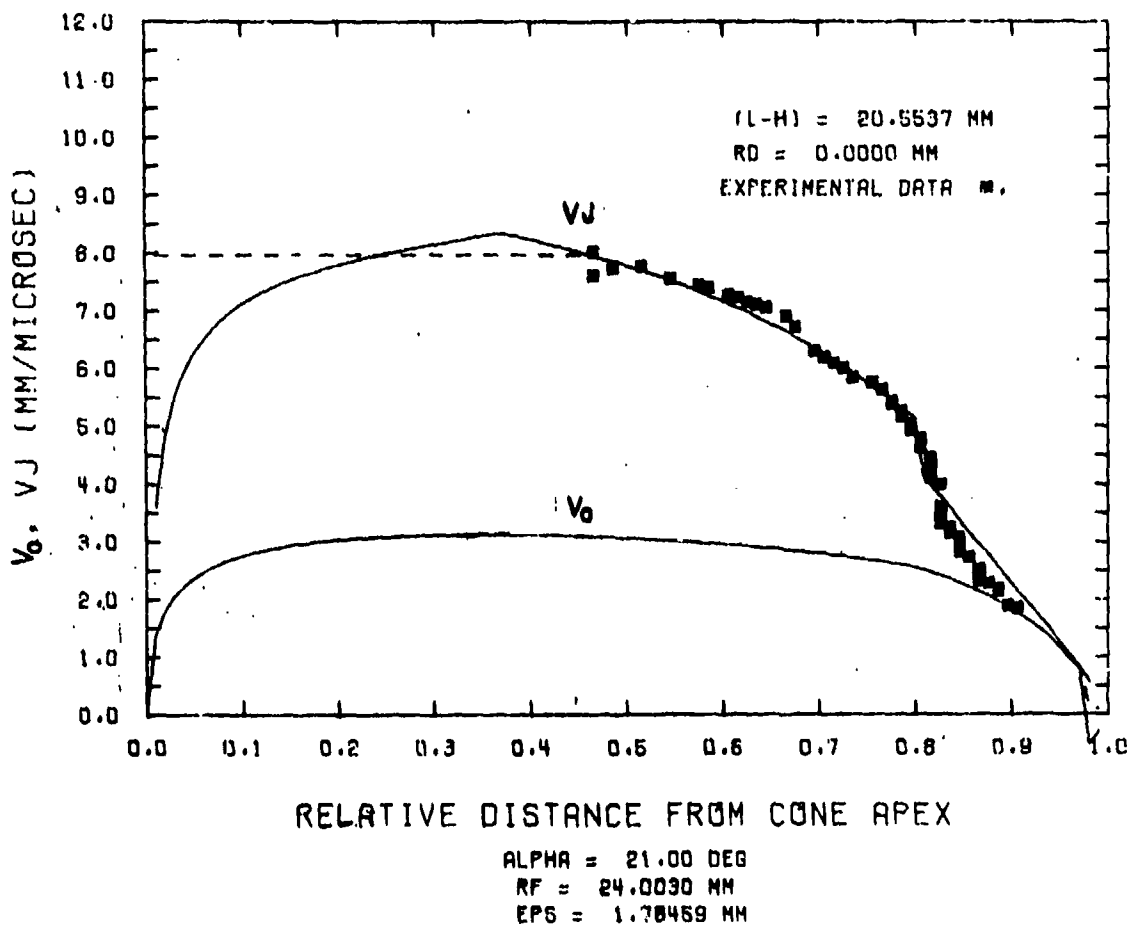


Figure 11. Comparison between BASC code and experimental results for scaled, heavily-confined, shaped charges (Reference 10). Jet and collapse velocities vs % of the distance from the apex of the cones are shown. Solid lines are BASC code results. The dashed line is the final, computed, compressed jet velocity profile. The jet tip for both experimental and BASC results is shown compressed into a position 48% from the apex of the cone.

forty-three is 10 grams heavier in the BASC code results. Also, the code results show 46% more total accumulated kinetic energy from the first forty-three jet particles than that obtained from experiment. Overall, this comparison is reasonable considering the material loss from such physical effects as erosion and possible errors in the data reduction measurements and calculations of the experimental results.

Table I. BASC Calculations and Measured, Experimental Radiographic Data<sup>16</sup> of Jet Velocity, Mass, and Kinetic Energy for the 3.2-in. (81.3-mm), BRL, Precision, Shaped Charge

Jet Particle No.	Velocity (km/s)		Accumulated Mass (g)		Kinetic Energy (kJ)	
	Measured	BASC	Measured	BASC	Measured	BASC
1	7.74	7.74	3.7	4.3	110.	128.
43	2.90	2.98	22.6	32.6	348.	507.

The last experimental comparison will be the characteristics of jets from small caliber shaped charges with copper and aluminum liners. In this study, only the liner designs referred to as 1½-inch (38.1-mm) liner base diameter charges in Reference 17 will be considered. The apex angle will include 20°, 40°, 60° and 90° cones for both the copper and aluminum liners. These are all confined with a steel casing around the charge. The pertinent dimensions for the shaped-charge designs considered can be found in Reference 17 on pages 9 and 10. The results from the BASC code calculations and the experiments are summarized on Table II. All of the results of the BASC code are within a 5% error boundary except the liner type with a 90° apex angle and aluminum cone which is 10%. The results of the calculations are slightly higher than the experiments for all of the aluminum liner types.

Table II. Summary of Results From the Small-Caliber, Shaped-Charge Study for the 38.1-mm (1½-in.), Base Diameter Design

Liner Type	Jet Tip Velocity, $V_{j0}$ (km/s)	
	Experiment	Predicted (BASC)
20° apex angle, Cu Cone	9.9	9.80
40° apex angle, Cu Cone	8.2	8.00
60° apex angle, Cu Cone	6.7	6.64
90° apex angle, Cu Cone	5.5	5.48

<u>Liner Type</u>	<u>Experiment</u>	<u>Predicted (BASC)</u>
20° apex angle, Al Cone	11.2	11.80
40° apex angle, Al Cone	9.3	9.75
60° apex angle, Al Cone	8.1	8.54
90° apex angle, Al Cone	6.8	7.50

The final two sets of comparisons involve the two numerical techniques: BASC and BRLSC. First, Figure 12, is a comparison of the calculated flow field for the 105-mm, unconfined shaped charge reported<sup>20</sup> for the BRLSC code and the BASC code at 25  $\mu$ sec after initiation of the explosive. The radius of the jet and slug are in excellant agreement, but the tip of the jet is slightly behind in the BASC calculation. This is due to the fact that the BASC code takes very large time steps which will not allow the inverse velocity gradient to be equilibrated at this snap shot in time. The second set of comparisons between BASC and BRLSC codes is shown on Table III. The results shown are from an improved version of the BRLSC Code.<sup>20</sup> Table III is a tabulation of six calculated results from BASC and BRLSC as well as four experimental results, which can be used as a guide in this comparison. All of the calculations and experiments in this study involved identical copper liners (21°, 81.3-mm base diameter, 1.9-mm thickness). Calculations 1 through 4 employed TNT, Comp B, Octol and PBX, respectively as explosive filler.

Table III. Computational Matrix and Summary of Results

Calculation Number	HE Fill	Confinement	Total Jet Mass (g)		Jet Kinetic Energy (kJ)	
			BRLSC	BASC	BRLSC	BASC
1	TNT	Light	19.66	28.42	196.	385.
2	Comp B	Light	22.56	30.73	287.	507.
3	Octol	Light	27.40	32.03	349.	570.
4	PBX	Light	27.97	33.49	381.	614.
5	Comp B	Heavy	33.63	60.41	475.	1262.
6	Octol	Heavy	35.17	60.16	360.	1406.

<sup>20</sup>R.T. Sedgwick, L.J. Walsh and M.S. Chawla, "Effects of High Explosive Parameters and Degree of Confinement on Jets from Lined Shaped Charges," BRL CR 245, Prepared by System, Science and Software, July 1975. (AD #B006987L)

Calculation Number	Predicted Final Jet Tip Velocity (km/s)		Measured Jet Tip Velocity (km/s)
	BRLSC	BASC	
1	5.95	6.79	6.8
2	7.15	7.74	7.7
3	7.40	8.17	8.1
4	7.80	8.44	8.3
5	7.44	8.86	---
6	7.78	9.36	---

In these four calculations, the charge was confined in an aluminum casing (treated as being unconfined in the BASC code). Calculations 5 and 6 employed Comp B and Octol as explosive fills which were confined in a steel casing; with a thickness of 10mm. The calculational matrix is shown in Table III with the degree of confinement provided by the aluminum and steel casing is referred to as light and heavy, respectively. The summary of the results of both codes (BASC and BRLSC) as well as the results of the jet tip velocities measured from experiments<sup>21</sup> are also shown in Table III. The quantities summarized represent the total jet which is composed of jet material having a velocity greater than or equal to a velocity of 2.8 km/s. The results indicate the ratio of predicted total jet mass of BRLSC code to the BASC code is approximately 65% for all calculations.

The comparison of jet tip velocity data is illustrated on Figure 13. The theoretically predicted values for calculations 1 through 4 from both the BASC and BRLSC codes are compared with the experimental determined jet tip velocity data. Figure 13 is a plot of calculated jet velocities versus the measured jet tip velocities. The open triangles are the final jet tip velocities as predicted by the BRLSC code<sup>20</sup> and the open squares are those predicted by the BASC code. There is very good agreement between the BASC code and the observed results for those rounds considered and the BRLSC code's agreement is less than 10% except for TNT which is 12.5%.

In summary, we have demonstrated in these comparisons the predictive ability of the BASC code. In addition, several of its salient features has been shown. These features include the predictive characteristics of BASC with respect to variations in casing confinement, variations in cone apex angle, variations in liner density and thickness, variations in explosive fill, and the effects of scaling. We have, also, demonstrated its predictive ability with respect to other sophisticated numerical schemes.

---

<sup>21</sup>J. Simon, "The Effect of Explosive Detonation Characteristics on Shaped-Charge Performance," BRLMR-2414, August 1979. (AD #B000337L)

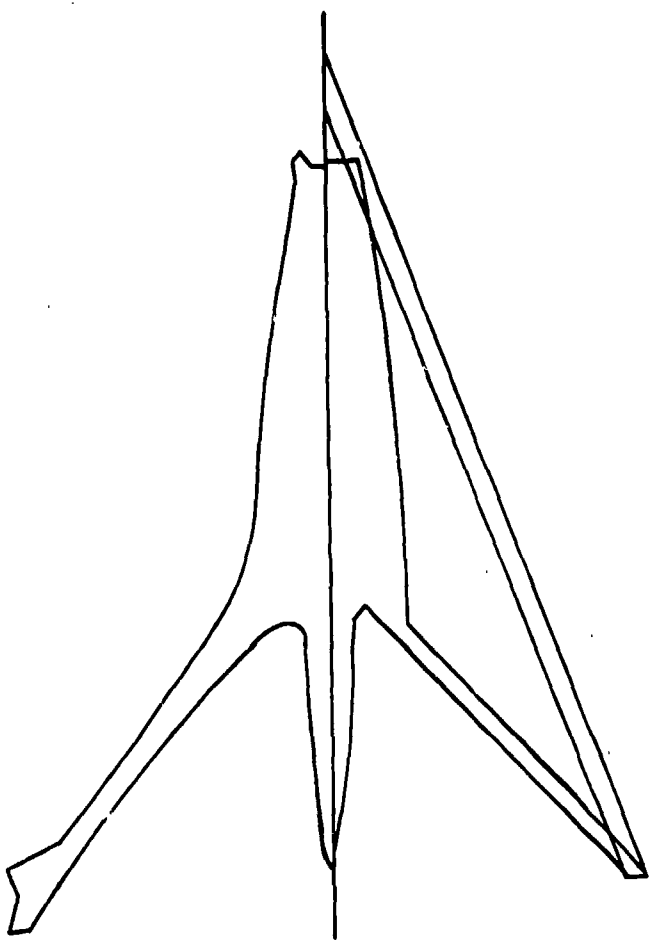


Figure 12. Comparison of calculations of the flow field between BASC code and a 2-D, Hydrodynamic Code (BRLSC) (Reference 2). These calculations are of the 105-mm, unconfined, shaped-charge shown at the time approximately 25 $\mu$ s after the initiation of the explosive. The BRLSC Code results are to the left of the axis of symmetry and the BASC code results are to the right.

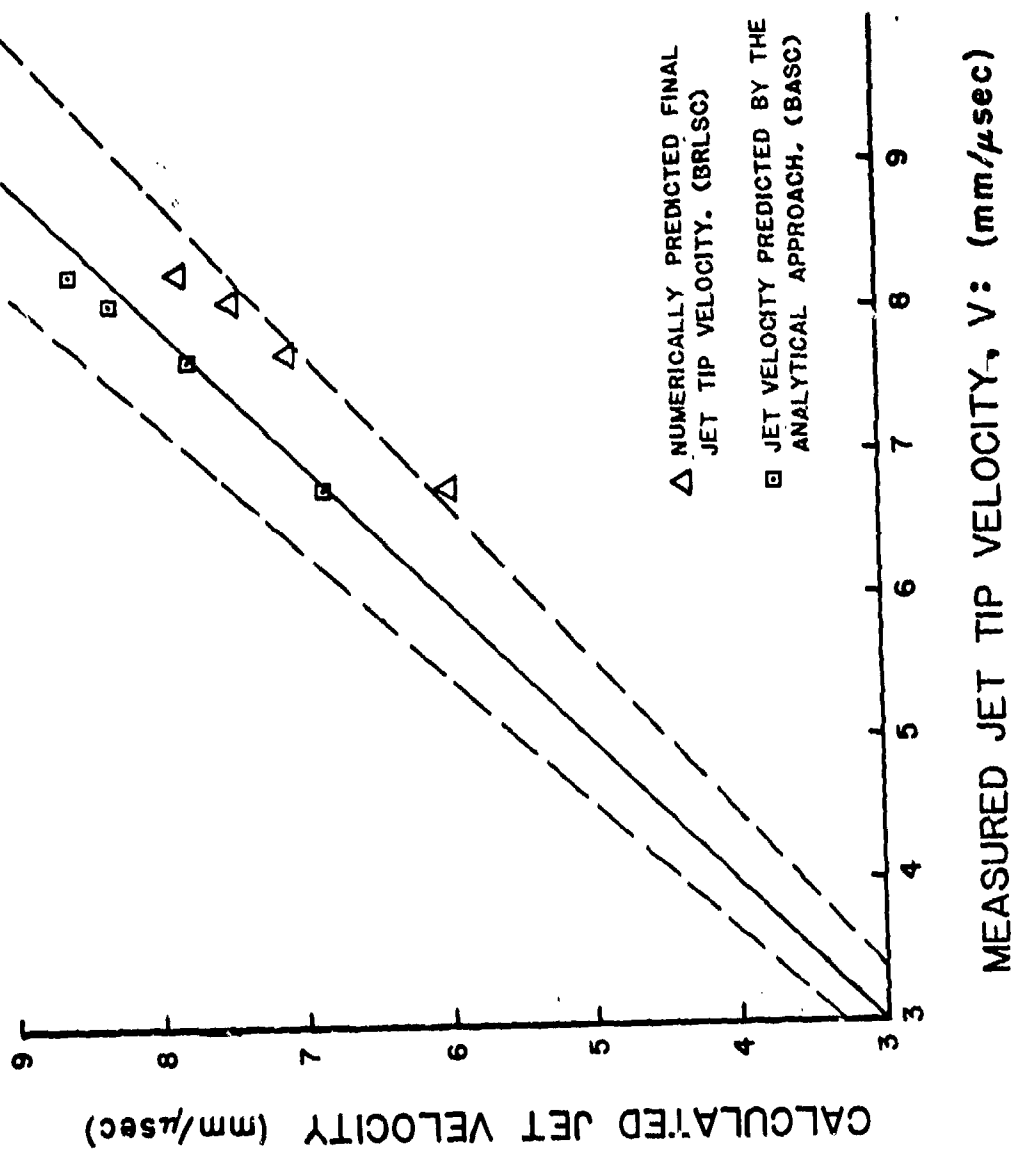


Figure 13. Comparison of Calculated and Measured Jet Tip Velocities from Shaped-Charge Designs 1 through 4, Shown on Table III.

Based upon these comparisons, it is concluded that, for many conical shaped-charge designs, the BASC code is a useful, predictive model for jet characteristics. Since it requires only fractions of a minute to do several shaped-charge design calculations on most computing systems (large or small), this calculational scheme is an economical approach for warhead design and analysis.

#### V. LIMITATIONS OF BASC

The current version of BASC requires several empirically determined constants. The collapse model requires the determination of  $\phi$  and  $k$ ; their relationship to the angle of incidence,  $i$ ; the constant  $A$  for a confined casing; and finally,  $C_1$ , a constant calibrated to the 105-mm, unconfined, shaped charge for the time of collapse near the apex of the cone. Penetration requires a cutoff velocity,  $U_{min}$ , and a breakup time,  $T_1$ .

Breakup time, as used in the theory of DiPersio, et. al.<sup>7</sup>, is a quantity determined from a radiograph of the jet. It is treated as a constant, but only approximates that value for conical liners with uniform wall thicknesses. Work by Simon<sup>21</sup> shows that breakup time for a given geometry remains a constant over changes in the Chapman-Jouguet pressure of 186-380 kbars. The codes, as used, requires a predetermined value for  $T_1$  for a given shaped-charge geometry. The value of  $T_1$  scales with cone diameter. All of these limitations stem from the empirical nature of the equations of the code.

Geometrical considerations for conical collapse may or may not be a limitation to the BASC code. Research will have to be conducted in order to determine this fact. Since the initial cone half-angle varies as a function of distance along the axis,  $z$ , and since each zonal element has no interaction with other elements, all geometrical considerations should be solvable.

Current limitations will be corrected by future changes to the code. These changes are explained in the next section.

#### VI. FUTURE MODIFICATIONS

There are several tasks intended to improve BASC. The major areas of research are the following: (1) modeling the jet formation for

several different materials and geometrical consideration, (2) modeling the viscous effects, as suggested by Walters,<sup>22</sup> in a nature compatible with BASC, (3) modeling the breakup of the jet with reference to a maximum strain to break, (4) modeling the threshold for a jet-no-jet criteria for many more materials.

As explained earlier, elements in the apex region of a conical liner reach the jet formation region before these elements are accelerated to their maximum attainable velocity. To account for this characteristic of conical, liner apex flow, which is so important in determining exact jet-tip velocities, transient acceleration is being modeled by an empirical constant determined from normalized, copper liner data<sup>13</sup>. This constant accounts for the number of shock reverberations that occur in the copper liner before it enters the flow of jet formation. We can improve upon this constant by obtaining experimental collapse data for a number of different materials.

Research conducted by Simon indicates that the breakup of the shaped-charge jet may be related to a maximum strain, which is a function of strain rate. These observations were made for copper liners with many different explosive fillers ranging from TNT (C-J pressure 186 kbars) to a high HMX explosive (C-J pressure 380 kbars), but with only one charge and liner geometry. Work is continuing by Chou, et. al.,<sup>23,24</sup> to define the critical condition for breakup models based on these results and will be added to the code where piecewise strains and strain rates will be calculated. We will continue to calculate penetration velocity, U, and will terminate penetration according to a minimum value of U as demonstrated by DiPersio, et. al.; but we will explore the use of  $v_{J\min}$  as the penetration cut-off criteria. Finite-difference codes may be applied either directly or in a simplified form to generate a library of parameters by computational experiments. This will assist in the research of some of these critical parameters utilized in the BASC code.

As certain elements of the shaped-charge collapse problem are accurately modelled, that section of the BASC code will be modified. The code is considered a "living" code, constantly being updated but applied within its limitations at all stages of its development.

<sup>22</sup>W. Walters, "Influence of Material Viscosity on the Theory of Shaped-Charge Penetration," ARBRL-MR-02041, August 1979. (AD #B041485L)

<sup>23</sup>P.C. Chou and J. Carleone, "Calculations of Shaped-Charge Jet Strain, Radius and Breakup Time," BRLCR-246, July 1976. (AD #B007240L)

<sup>24</sup>J. Carleone, P.C. Chou, and R. Ciccarelli, "Shaped-Charge Jet Stability and Penetration Calculations," BRLCR-351, September 1977. (AD #A050117)

## VII. SUMMARY

BASC is a simple, well-documented, shaped-charge code that may be applied to many problems to predict trends and gross effects. Difficulties in predicting the jet-tip characteristics still exist for some materials, but future modifications should correct this deficiency. The code is so structured that it can grow and become more widely applicable as modeling improvements are available.

## ACKNOWLEDGEMENT

The author is grateful to Robert DiPersio, now retired, and Robert R. Karpp, now of Los Alamos Scientific Laboratory, for their many contributions in the formulation of the BASC code.

The author is grateful to Mary Scarborough of the BRL for her artistic work in the preparation of the illustrations used in this report.

## REFERENCES

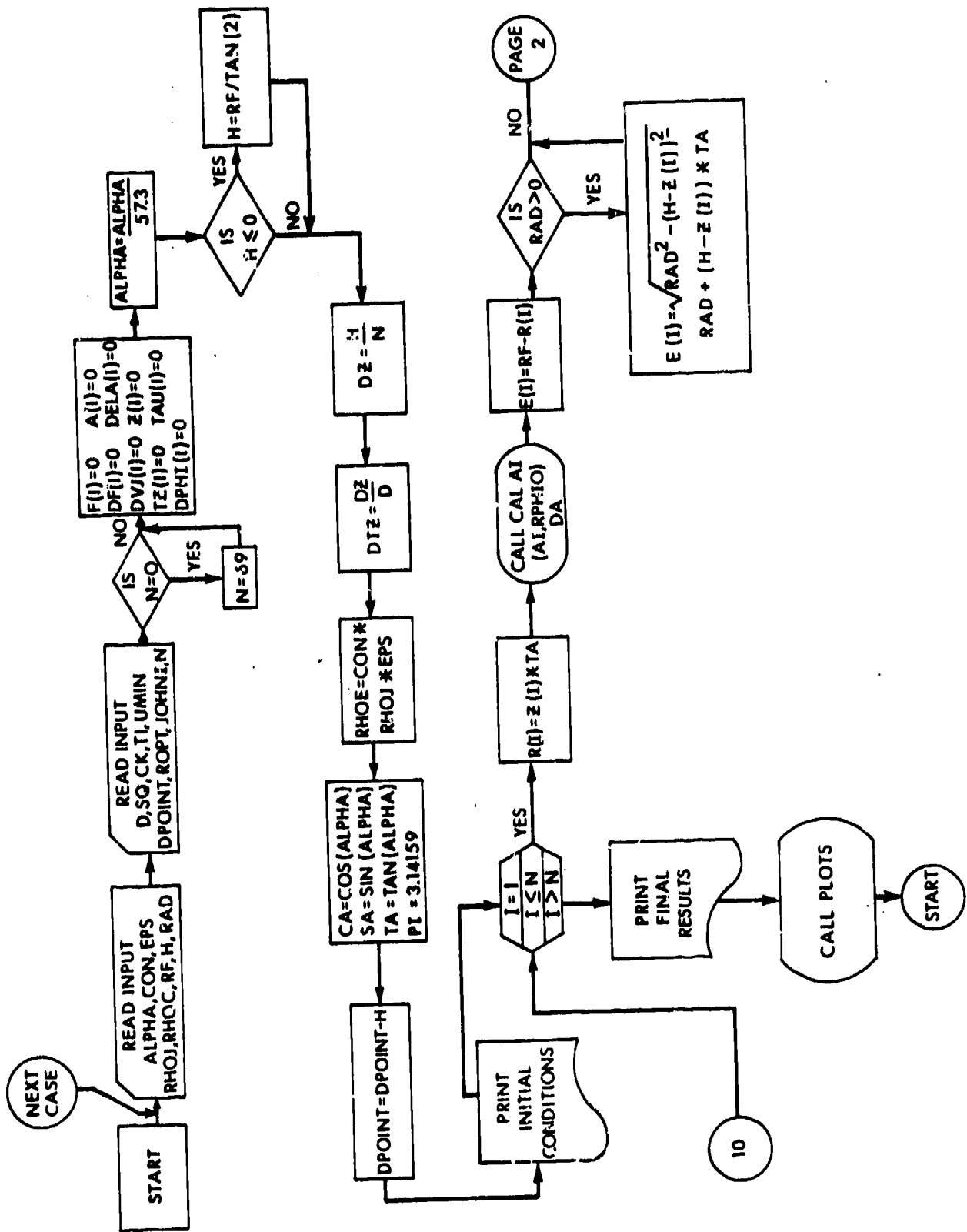
1. J.T. Harrison and R.R. Karpp, "Terminal Ballistic Applications of Hydrodynamic Computer Code Calculations," BRLR 1984, April 1977. (AD #A041065)
2. J.T. Harrison, "A Comparison between the Eulerian, Hydrodynamic Computer Code (BRLSC) and Experimental Collapse of a Shaped Charge Liner," ARBRL-MR-02841, June 1978. (AD A059711)
3. J. Harrison, R. DiPersio, R. Karpp and R. Jameson, "A Simplified Shaped Charge Computer Code: BASC," DEA-AF-F/G-7304 Technical Meeting: Physics of Explosives, Vol II, April-May 1974, Paper 13 presented at the Naval Ordnance Laboratory; Silver Spring, MD.
4. M. Defourneaux, "Hydrodynamic Theory of Shaped Charges and of Jet Penetration," Memorial DeL'art Ille'rie Francasise-T, 44, 1970.
5. R. DiPersio, C.W. Whiteford, and J. Simon, "An Experimental Method of Obtaining Collapse Velocities of the Liner Walls of a Linear Shaped-Charge Liner," BRL-MR-1696, September 1965. (AD #478326)
6. A. Kiwan and H. Wisniewski, "Theory and Computations of Collapse and Jet Velocities of Metallic Shaped Charge Liners," BRLR-1620, November 1972. (AD #907161)
7. R. DiPersio, J. Simon, and A. Merendino, "Penetration of Shaped-Charge Jets into Metallic Targets," BRLR 1296, September 1965. (AD #476717)
8. P. Chou, J. Carleone, R. Karpp, "Criteria for Jet Formation from Impinging Shells and Plates," J. Appl. Physics, Vol. 47, No. 7, July 1976.
9. E.M. Pugh, R.J. Eichelberger and N. Rostoker, "Theory of Jet Formation by Charges with Lined Conical Cavities," J. Appl. Physics, Vol. 23, No. 5, May 1952.
10. R. DiPersio, J. Simon, and T. Martin, "A Study of Jets From Scaled Conical Shaped-Charge Liners," BRLMR-1298, August 1960. (AD #246352)
11. M. Defourneaux and L. Jacques, "Explosive Deflection of a Liner as a Diagnostic of Detonation Flows," Proceedings Fifth Symposium (International) on Detonation, ACR-184 Office of Naval Research-Department of Navy, pp. 457-466, Pasadena, California, August 18-21, 1970.

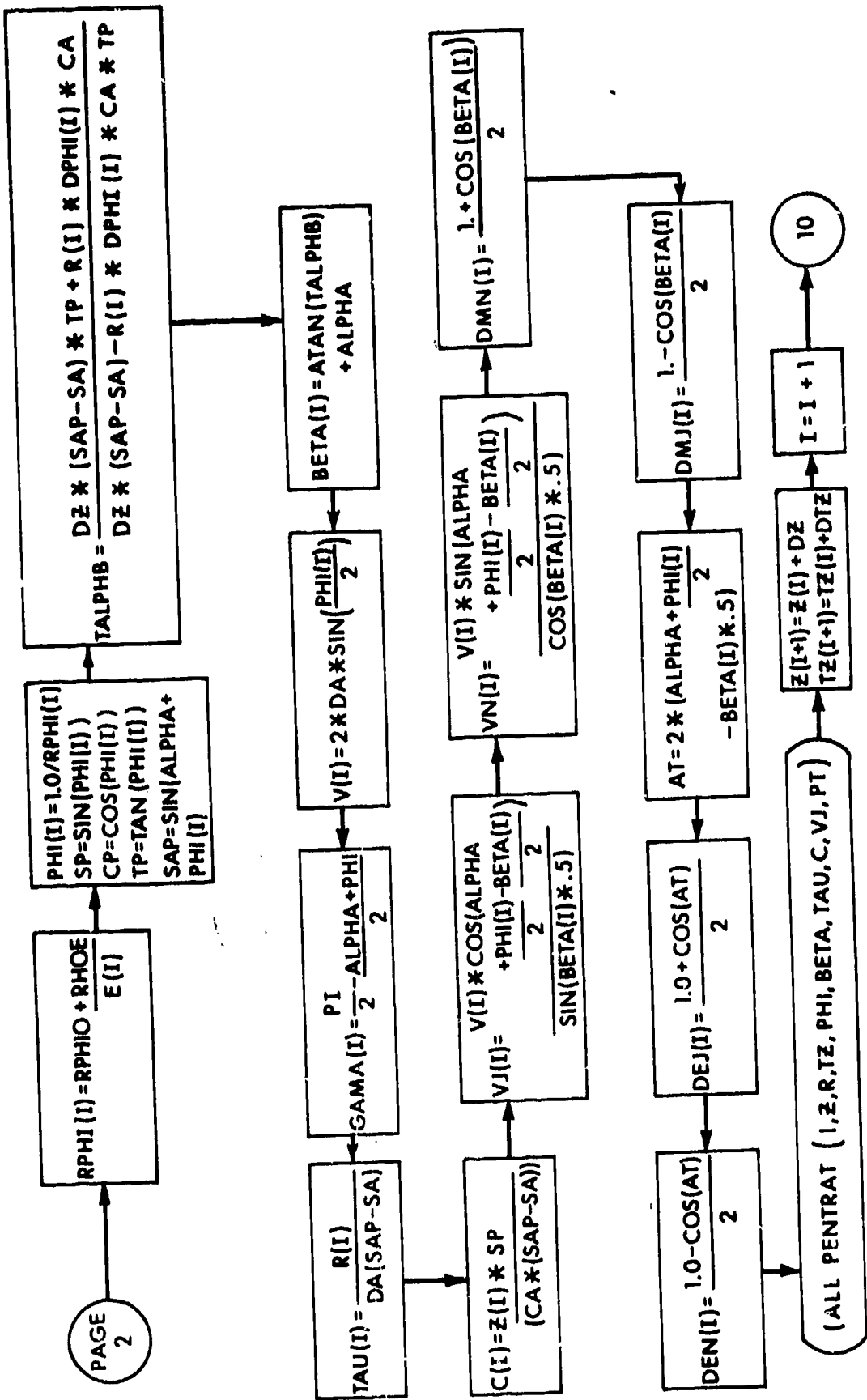
#### REFERENCES (Cont'd)

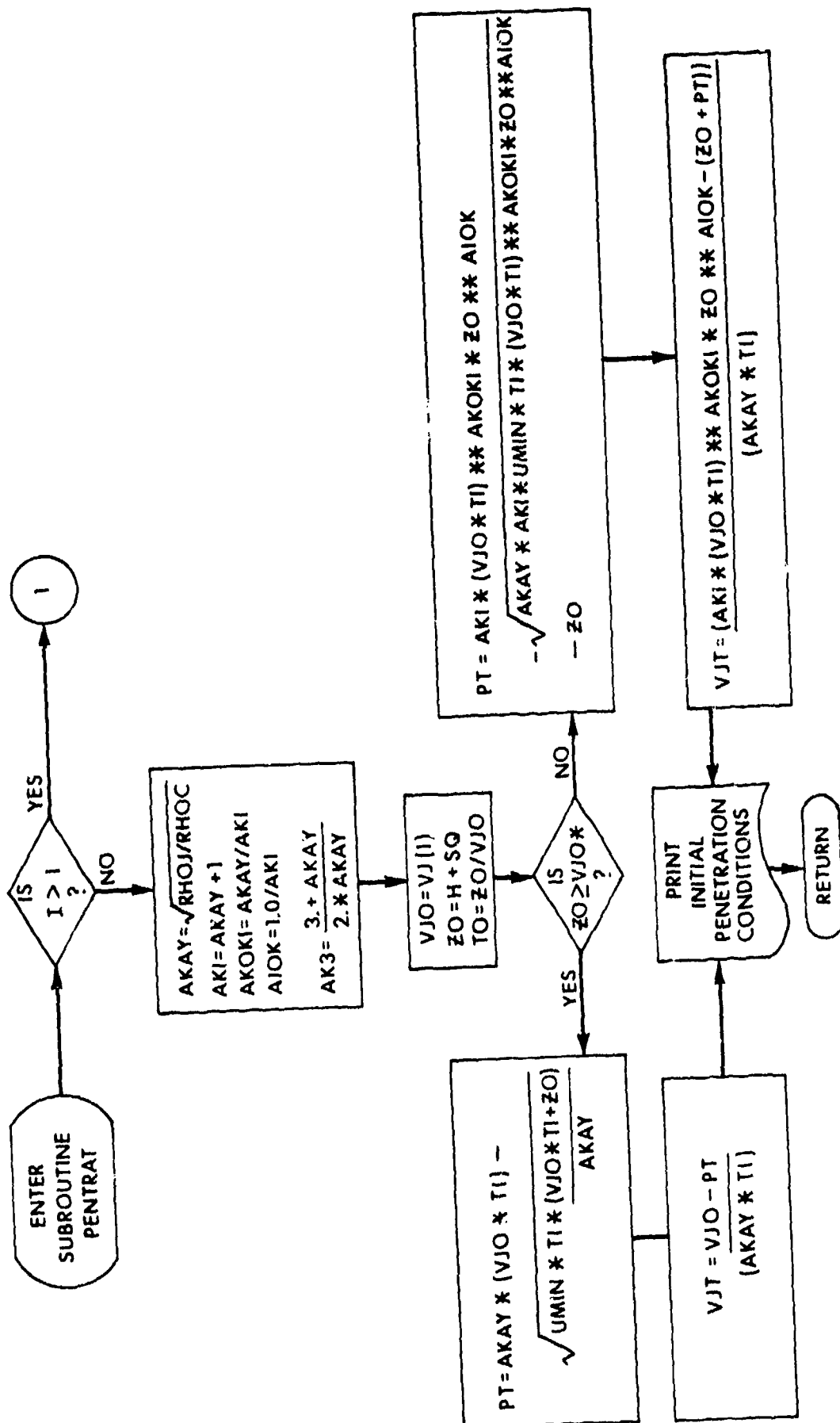
12. R.W. Gurney, "The Initial Velocity of Fragments from Bombs, Shells, and Grenades," BRL Report No. 405, Sept. 1943. (AD #ATI36218)
13. F.E. Allison and R. Vitali, "An Application of Jet Formation Theory to the 105-mm Shaped Charge," BRLR-1165, March 1962. (AD #277458)
14. J.M. Walsh, R.G. Shreffler, and F.J. Willig, "Limiting Velocity Conditions for Jet Formation in High Velocity Collisions," Journal of Applied Physics, Vol. 24, No. 3, pp. 349-359, March 1957.
15. G.R. Cowan and A.H. Holtzman, "Flow Configurations in Colliding Plates: Explosive Bonding," Journal of Applied Physics, Vol. 34, No. 4, pp. 928-939, April 1963.
16. Private Communication from J. Blische at BRL.
17. R. DiPersio, W.H. Jones, A.B. Morendino, and J. Simon, "Characteristics of Jets from Small Caliber Shaped Charges with Copper and Aluminum Liners," DRLMR No. 1866, September 1967. (AD #823839)
18. M.L. Gittings, "BRLSC: An Advanced Eulerian Code for Predicting Shaped Charges," Vol. I, BRL CR 279, Prepared by System, Science and Software, December 1975. (AD #A023962)
19. L.J. Hageman and J.M. Walsh, "HELP, A Multi-Material Eulerian Program For Compressible Fluid and Elastic-Plastic Flows in Two Space Dimensions and Time," BRL CR 39, Prepared by System, Science and Software, May 1971. (AD Nos. 726459 and 726460)
20. R.T. Sedgwick, L.J. Walsh and M.S. Chawla, "Effects of High Explosive Parameters and Degree of Confinement on Jets from Lined Shaped Charges," BRL CR 245, Prepared by System, Science and Software, July 1975. (AD #B006987L)
21. J. Simon, "The Effect of Explosive Detonation Characteristics on Shaped Charge Performance," BRLMR-2414, September 1974. (AD #B000337L)
22. W. Walters, "Influence of Material Viscosity on the Theory of Shaped-Charge Penetration," ARBRL-MR-02941, August 1979. (AD #B041485L)
23. P.C. Chou and J. Carleone, "Calculations of Shaped-Charge Jet Strain, Radius and Breakup Time," BRLCR-246, July 1975. (AD #B007240L)
24. J. Carleone, P.C. Chou, and R. Ciccarelli, "Shaped-Charge Jet Stability and Penetration Calculations," BRLCR-351, September 1977. (AD #A050117)

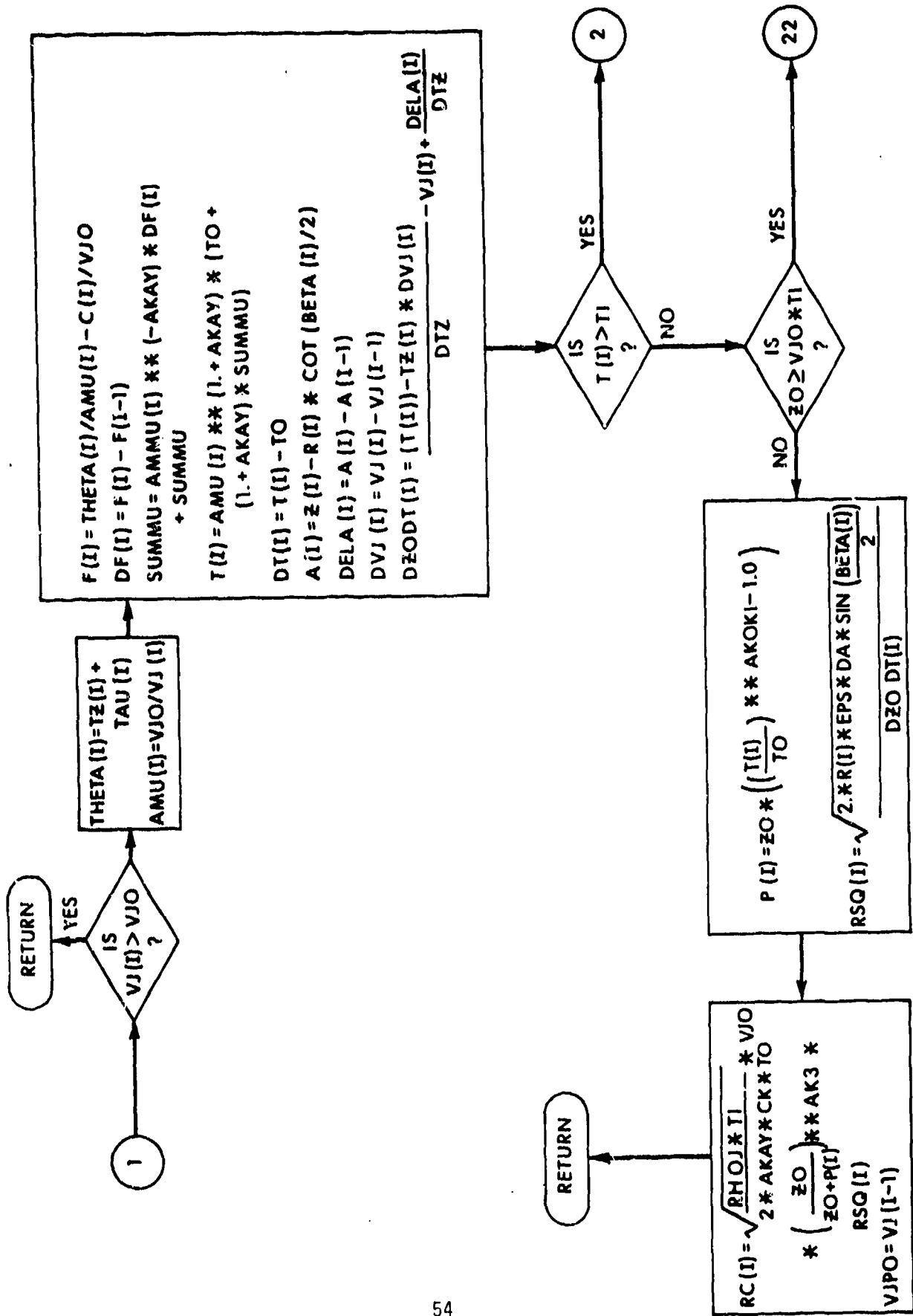
APPENDIX A  
FLOWCHART OF COMPUTER PROGRAM

49 / 50









RETURN

$$P(I) = \frac{VJO * (T(I) - TO * TI)}{TI + T(I) - AKAY}$$

$$VJP = VJO * (TI + \frac{TO}{AKAY})$$
$$\frac{TI + T(I)}{AKAY}$$

$$DVJP = VJP - VJPO$$

$$VJPO = VJP$$

$$DZODT(I) = (TI - T(I)) * DVJP - VJP + DELA(I)$$

$$RSQ(I) = \sqrt{2 * R(I) * EPS * DA * \sin\left(\frac{\text{BETA}(I)}{2}\right) ** 2}$$
$$/ DZODT(I)$$

$$RC(I) = \sqrt{\frac{RHOJ}{2 * AKAY * CK} * RSQ(I) * VJO}$$

22

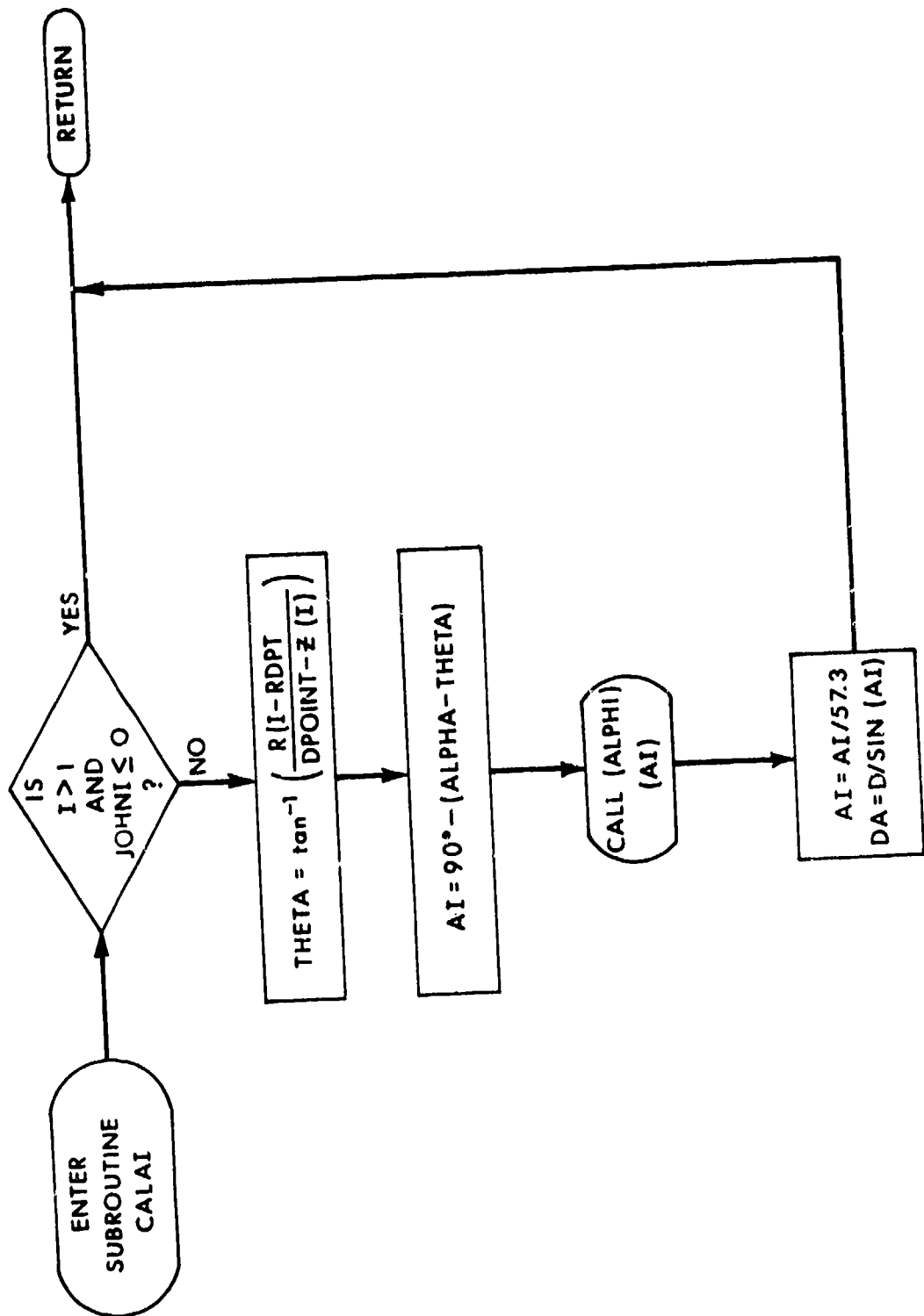


$$P(I) = \left( \frac{AKI * \left( \frac{T_I}{T_0} \right) ** AKOK * T(I)}{T(I) + AKAY * T_I} - 1.0 \right) * ZO$$

$$RSQ(I) = \sqrt{2 * R(I) * EPS * DA * \sin\left(\frac{\text{BETA}}{2}\right) ** 2} / DEODT(I)$$

$$RC(I) = \sqrt{\frac{RHOJ}{2 * AKAY * CK}} * \frac{VJO}{AKAY} * (AKI *$$

$$\left( \frac{ZO}{VJO * T_I} \right) ** AIOK - \frac{(ZO + P(I))}{VJO * T_I} \right) * RSQ(I)$$



GIVEN AI,  
ANGLE OF INCIDENCE  
IN DEGREES, INTERPOLATE  
INTO TABLE PHIO ( $\phi_o$ )

RPHIO = 1.0 / PHIO  
RPHIO = RPHIO \* 57.3

ENTER  
SUBROUTINE  
CALPHI

RETURN

APPENDIX B  
FORTRAN IV  
COMPUTER PROGRAM LISTING, SAMPLE INPUT AND OUTPUT

PROGRAM RASC(INPUT,OUTPUT,TAPES=INPUT,TAPEA=OUTPUT)  
 BRL ANALYTICAL SHAPED CHARGE (RASC) CODE  
 PROGRAMMED BY JOHN T. HARRISON  
 BRL ANALYTICAL SHAPED CHARGE CODE  
 WRITTEN IN STANDARD FORTRAN IV  
 SEMI-EMPIRICAL CODE BASED ON THE FORMULA-

$$1/\Phi = 1/\Phi_{H0} + K * \rho_{H0} * \epsilon / E$$

UNITS FOR THIS CODE ARE CENTAMETERS, GRAMS, AND MICROSECONDS.  
 THE CODE WILL CALCULATE COLLAPSE VELOCITY OF THE LINER AND  
 VELOCITIES, MASSES, AND ENERGIES OF BOTH THE JET AND SLUG.  
 THIS CODE WILL PREDICT PENETRATION AND HOLE PROFILE AND GIVE  
 PENETRATION-STANDOFF CURVES AND TABLES.

LIST OF VARIABLES

ALRAD	=	ALPHA IN RADIANS	MAIN 3
CON	=	DETTONATION PRODUCTS CONSTANT (K).	MAIN 4
DZ	=	DELTA Z DISTANCE ALONG THE LENGTH OF THE LINER	MAIN 5
DT7	=	TIME THE DETONATION WAVE ARRIVES AT EACH Z POINT	MAIN 6
AI	=	ANGLE OF INCIDENCE	MAIN 7
Z(I)	=	DISTANCE ALONG LINER	MAIN 8
TZ(I)	=	TIME AT EACH POINT ON LINER	MAIN 9
GAMA(I)	=	ANGLE BETWEEN AXIS AND COLLAPSE DIRECTION.	MAIN 10
BETA(I)	=	COLLAPSE ANGLE	MAIN 11
V(I)	=	COLLAPSE VELOCITY	MAIN 12
TAU(I)	=	TIME FOR EACH ELEMENT TO REACH THE AXIS	MAIN 13
PHI(I)	=	ANGLE OF LINER BENDING.	MAIN 14
PHIO	=	ANGLE OF EXPLOSIVE BENDING.	MAIN 15
RPHIN	=	1/PHIO	MAIN 16
RPHI	=	1/PHI	MAIN 17
C(I)	=	POINT ON THE AXIS WHERE EACH PARTICLE WILL HIT	MAIN 18
VJ(I)	=	VELOCITY OF THE JET	MAIN 19
VN(I)	=	VELOCITY OF THE SLUG	MAIN 20
CO	=	SOUND SPEED OF LINER MATERIAL ( COPPER CO=.395 CM/MSEC)	MAIN 21
RV(I)	=	FLOW VELOCITY (VF). DIRECTED INTO STAGNATION POINT.	MAIN 22
DFJ(I)	=	DELTA ENERGY IN EACH JET SEGMENT	MAIN 23
DEN(I)	=	DELTA ENERGY IN EACH SLUG SEGMENT	MAIN 24
R(I)	=	RADIUS OF THE CONE AT EACH DELTA Z DISTANCE	MAIN 25
DA	=	APPARENT DETONATION RATE.	MAIN 26
DML(I)	=	DELTA MASS OF THE LINER	MAIN 27
E(I)	=	AMOUNT OF EXPLOSIVE ABOVE EACH POSITION ON THE LINER	MAIN 28
DPOINT	=	INITIALLY IS THE TOTAL HEIGHT OF THE CHARGE. THEN BECOMES THE INITIATION POINT ON THE Z DIRECTION.	MAIN 29
NRAD	=	RADIUS OF CURVATURE OF THE CONFINEMENT. IF NRAD=0.-THEN THERE WILL BE A LINEAR THICKNESS OF EXPLGHM	MAIN 30

```

C C C CARD NUMBER 1
C C C IJOHN = 1, A PARAMETRIC STUDY. 2, A NEW CASE.
C C C HEAD = A HEADING CARD.

C C C CARD NUMBER 2
C C C
C C C ALPHA = HALF ANGLE OF THE CONE IN DEGREES. MAIN 57
C C C EPS = THICKNESS OF THE LINER,(0 IF UNKNOWN OR VARIABLE) MAIN 56
C C C RHOJ = DENSITY OF THE LINER MAIN 59
C C C RF = FINAL RADIUS OF THE CONE MAIN 60
C C C H = HEIGHT OF THE CONE. IF H=0., THEN H WILL BE COMPUTED. MAIN 61
C C C COF = CONFINEMENT FACTOR(0 FOR UNCONFINED, IF CONFINED = THICKN) MAIN 62
C C C RHOCON = DENSITY OF THE CONFINEMENT MAIN 63
C C C NPLT = NUMBER OF PLOTS. 0=SKIP, 1=ALL, 2=VEL. + PENETRATION MAIN 64
C C C NPOS = NUMBER OF (R,Z) POSITIONS TO BE READ IN. MAIN 65
C C C IF NPOS IS 0 DO NOT READ IN (R,Z) COORDINATES. MAIN 66
C C C CARD NUMBER 3 MAIN 67
C C C
C C C RHOC = DENSITY OF THE TARGET MAIN 68
C C C SO = STAND OFF DISTANCE MAIN 69
C C C IF SO= 0, PENETRATION STANOFF CURVES WILL BE PLOTTED. MAIN 70
C C C CK = CONSTANT FOR DETERMINING HOLE VOLUME MAIN 71
C C C IF (CK =0.) CK WILL BE CALCULATED AND UMIN WILL THEN MAIN 72
C C C BECOME THE BHM TO BE READ IN. MAIN 73
C C C UMIN = VELOCITY MIN. USED IN THE PENETRATION THEORY MAIN 74
C C C IF (CK =0.) UMIN WILL BE THE BHM. MAIN 75
C C C T1 = BREAKUP TIME OF THE JET MAIN 76
C C C IF ( T1 = 0.) T1 WILL BE CALCULATED. MAIN 77
C C C DPOINT = INITIALLY IS THE TOTAL HEIGHT OF THE CHARGE MAIN 78
C C C RDPT = RADIUS ABOVE AXIS WHERE EXPLOSIVE IS INITIATED. MAIN 79
C C C NEXPL = EQUATION OF STATE NUMBER FOR THE EXPLOSIVE. MAIN 80
C C C NEXPL    EXPLOSIVE      DENSITY      DETONATION RATE MAIN 81
C C C     1        COMP B       1.72          .8 MAIN 82
C C C     2        OCTOL       1.82          .85 MAIN 83
C C C     3        LX          1.84          .8774 MAIN 84
C C C N = THE NUMBER OF ZONES Z-AXIS IS TO SUBDIVIDED. IF N=0 THE MAIN 85
C C C DEFAULT VALUE IS N=69. MAIN 86
C C C
C C C DIMENSION EXPLO(6), RHOHE(6), DV(6) MAIN 87
C C C DIMENSION RI(100), IMAT(100) MAIN 88
C C C DIMENSION EPSI(100), DAI(100) MAIN 89
C C C DIMENSION RP(300), PLOT(3) MAIN 90
C C C DIMENSION PSO(50), PPT(50) MAIN 91
C C C DIMENSION CONF(4) MAIN 92
C C C DIMENSION UJK(200), DMJK(200) MAIN 93
C C C DIMENSION HEAD(6) MAIN 94
C C C DIMENSION DML(100), RV(100), DEL(100) MAIN 95
C C C DIMENSION Z(100), T2(100), TAU(100), E(100), PHI(100), DPHI(100), MAIN 96
C C C 1 BETA(100), GAMMA(100), R(100), C(100), VJ(100), VN(100), DMJ(100) MAIN 97
C C C 2 , DMN(100), DEJ(100), DEN(100), RPHI(100), V(100) MAIN 98

```

```

C      COMMON                               MAIN114
C      COMMON                               MAIN115
C      COMMON                               MAIN116
C      COMMON ALRAD, EPS, RHOJ, RHOC, RF, RPHI0, DTZ, SU, CK, DA, H, U, MAIN117
1 PT, DEGTOR                                MAIN118
COMMON AMU(100), THETA(100), F(100), DF(100), T(100), DT(100), MAIN119
1 G(100), P(100), A(100), DELA(100), DVJ(100), DZDT(100), MAIN120
2 RSO(100), RC(100), T1, UMIN                MAIN121
COMMON /PLLOT/ Z, TZ, TAU, E, PHI, DPHI, BETA, GAMMA, R, C, VU, VN,MAIN122
1 DMJ, DMN, DEJ, DEN, RPHI, V                 MAIN123
C
DATA HEAD(8) /1H>/
DATA CONF(1), CONF(2) /10HUNCONFINED, 1H>/
DATA CONF(3), CONF(4) /10HCONFINED , 1H>/
DATA PLOT(1), PLOT(2), PLOT(3)/4HSKIP,3HALL,9HVEL + FEN/
DATA EXPLO(1) /6HCOMP R/ + EXPLO(2) /5HOCOTOL/
DATA EXPLO(3) /4H TNT/,EXPLO(4)/8HPEX=9404/,EXPLO(5)/4HLX14/
DATA EXPLO(6)/4H0280/
DATA RHOHE(1), RHOHE(2) /1.72, 1.82/          MAIN131D
DATA RHOHE(3) /1.63/, RHOHE(4)/1.84/,RHOHE(5)/1.81/,RHOHE(6)/1.74/MAIN132D
DATA DV(1), DV(2), DV(3), DV(4) /.798, .848, .690, .880/   MAIN133D
DATA DV(5), DV(6) /.8749, .8477/              MAIN134D
******** READ IN HEADING ONE TIME FOR EACH PARAMETRIC STUDY*MAIN135
C      READ IN HEADING ONE TIME FOR EACH PARAMETRIC STUDY
C
1 CONTINUE
HEAD (5,37) IJOHN+HEAD
IF(EOF(5)) 98765*2
2 WRITE (6,36) IJOHN+HEAD
C      BEGIN LOOP FOR A PARAMETRIC STUDY
C
C      READ IN INPUT ( 2 CARDS. BOTH WITH 7E10.3,215 FORMAT.)
C
C      READ IN LINER AND CONFINEMENT INPUTS
C
C      READ (5,36) ALPHA, EPS, RHOJ, RF, H, COF, RHOC, NPLT, NF, S
C
C      READ IN TARGET AND EXPLOSIVE INPUTS
C
READ (5,36) RHOC, SU, CK, UMIN, T1, DPOINT, RDPT, NEXPL, N
SH=H
CO=.395
TMJJ=0.
JOHN=1
TECUT1=0.
TECUT2=0.
TECUT3=0.
TECUT4=0.
TECUT5=0.
TMJCUT=0.
TMCL1=0.
TMCL1=0.
TMCL1=0.
TMCL1=0.

```

```

TMCUTS=0.
RVMAX=0.
NRAD=0
NNDV(NEXPL)
ICOF=1
IF (COF.GT.0.) ICOF=3
CON=.78
IS=2
IF (IN.EQ.0) N=69
IERROR=0
RAD=FLOAT(NRAD)
VJ0=0.
TMLL=0.
TMJ=0
TEJ=0.
TKF=0.
TMN=0.
TML=0.
SUMVJ=0.
VJMAX=0.
UJKMAX=0.
TMASS=0.0
DMASS=0.
DMUTE=0.
DC 3 J=1,1400
2(J)=0.
3 AMU(J)=0.

C CONVERT ANGLE ALPHA FROM DEGREES TO RADIANS.
C
C PI=3.14159265389793
C DEGTOR=57.2957795131
C ALRAD=ALPHA/DEGTR
C TRRF=YAN(.5*ALRAD)
C COMPUTE THE HEIGHT OF THE LINER IF NO GIVEN IN INPUT.
C
C IF (H.LE.0.) H=RF/TAN(ALRAD)
C
C DZ=H/FLOAT(N)
C DTZ=DZ/D
C SET UP CONSTANTS TO BE IN LATER EQUATIONS.
C RHOE=CON*RHOJ*EPS
C SA=SIN(ALRAD)
C CA=COS(ALRAD)
C TA=TAN(ALRAD)
C IF (PF.LE.0.) RF=TA*H
C PIPS=PI/3,
C PIP =2.0*PI
C SIGMA=RHOJ*EPS
C
C DETONATION POINT IS THE HEIGHT OF THE CHARGE - HEIGHT OF THE CONE.
C DPOINT=DPC*NT-H
C IF (DPOINT. E.0.) DPOINT=2.*RF
C IF (COF.GT.0.) CONFTR=COF
C DELCOF=CONFTR/20.

MAIN157A
MAIN157L
MAIN158
MAIN159
MAIN160
MAIN161
MAIN162
MAIN163
MAIN164
MAIN165
MAIN166
MAIN167
MAIN167A
MAIN168
MAIN169
MAIN170
MAIN171
MAIN172
MAIN173
MAIN174
MAIN175
MAIN176
MAIN177
MAIN178
MAIN179
MAIN180
MAIN181
MAIN182
MAIN183
MAIN184
MAIN185
MAIN186
MAIN187
MAIN187A
MAIN188
MAIN189
MAIN190
MAIN191
MAIN192
MAIN193
MAIN194
MAIN195
MAIN196
MAIN197
MAIN198
MAIN199
MAIN200
MAIN200A
MAIN201
MAIN202
MAIN203
MAIN204
MAIN205
MAIN205A
MAIN206
MAIN207
MAIN208

```

```

C      COF = CONFINEMENT FACTOR (INCREASE IN EXPLOSIVE THICKNESS).      MAIN204
C      COF=1.+(.64*RHOCON*CONFTH*8.9*.177R/(7.8*.60198*RHOJ*EPS)*2.4003*HFMMAIN211
C      1 / (DPCINT*2.0553);                                              MAIN210
C      WRITE (6,28) ALPHA,CON,EPS,RHOJ,CONF(ICOF),CONFTH,RHOCON,COF,H,RF,MAIN213b
C      1 DZ,DTZ*N                                              MAIN212
C      WRITE (6,29) EXPLO(NEXPL),D,RHOHE(NEXPL),DPOINT,HDPT,RHUC,SD,      MAIN214W
C      1 ('MIN,PLOT(NPL,T+1)                                              MAIN215W
C      RRF=PF                                              MAIN216W
C      PHI(?)=3.0/DEGTOW                                              MAIN217
C      INITIAL TIME OF COLLAPSE      TW=TAU.                                MAIN218
C      TW=.
C      CONTANT FOR THE ACCELERATION ROUTINE.                            MAIN219
C      C1=2.*CO*EPS*RHOJ/(.392*.269*8.9)                                MAIN220
C      FTERM=,.00001                                              MAIN221
C
C      SETUP ROUTINE                                              MAIN222
C
C      SETUP INITIAL POSITIONS (R,Z)                                MAIN223
C
C      RI= INSIDE RADIUS OF THE CONE.      R = OUTSIDE RADIUS OF THE CONE.  MAIN224
C
C      X=EPS/CA                                              MAIN225
C
C      THIS IS A SETUP ROUTINE FOR A SHAPED CHAGE LINER WITH CONSTANT EPSMAIN232
C
C      IF (NPOS.EQ.0) NPOS=1                                              MAIN233
C      NPOS=NPOS+1                                              MAIN234
C      WRITE (6,27)                                              MAIN235
C      IF (NPOS.GE.N) GO TO 5                                              MAIN236W
C      DO 4 J=NPOS,N                                              MAIN237
C      Z(J)=Z(J-1)+DZ                                              MAIN238 +
C      IMAT(J)=1                                              MAIN239
C      R(J)=Z(J)*TA                                              MAIN239A
C      HI(J)=R(J)-X                                              MAIN240
C      IF (RI(J).LE.0.) RI(J)=0.                                              MAIN241
C      IF (RI(J).LE.0.) IS=J+1                                              MAIN242
C      IF(AEIS(RI(J))-0.0).LE..0001) HI(J)=0.0                                MAIN242A
C
C      4 CONTINUE                                              MAIN243
C
C      5 CONTINUE                                              MAIN244
C      WRITE (6,31)                                              MAIN245W
C      WPITE (6,34) (I,Z(I),I=1,N)                                              MAIN246W
C      WRITE (6,32)                                              MAIN247W
C      WRITE (6,34) (I,R(I),I=1,N)                                              MAIN248W
C      WRITE (6,33)                                              MAIN249W
C      WPITE (6,34) (I,RI(I),I=1,N)                                              MAIN250W
C
C      E D OF SETUP ROUTINE                                              MAIN251
C
C      TZ(1)=DPOINT/D                                              MAIN252
C      FPSI(1)=EPS                                              MAIN253
C
C      START SPACE + TIME ITERATION.                                MAIN254
C
C      DO 10 I=2,N                                              MAIN255
C      V(I)=0.                                              MAIN256
C
C

```

```

VN(I)=0.  

VJ(I)=0.  

UJK(I)=0.  

C FIND HALF APEX ANGLE-ALPHA  

DZ=Z(I)-Z(I-1)  

DR=R(I)-R(I-1)  

ALRAD=ATAN2(DR,DZ)  

SA=SIN(ALRAD)  

CA=COS(ALRAD)  

TA=TAN(ALRAD)  

IF (IMAT(I).EQ.1) CO=.392  

IF (IMAT(I).EQ.1) RHOJ=8.9  

EPS=(R(I)-RI(I))*CA  

C  

C GO TO SUBROUTINE CALAI TO CALCULATE INCLINATION ANGLE (AI),  

C (DA)-DETONATION COMPONENT TO VELOCITY, AND (RPHI0)=1./PHI0.  

C  

CALL CALAI (I,Z,R,DPOINT,DPNT,JOHN,I,AI)  

DAJ(I)=DA  

C  

C COF IS FACTOR FOR CONFINEMENT.  

C  

C IF RAD IS GIVEN NO EQ. 0, CLACULATE CURVED THICKNESS OF EXPLOSIVE.  

C  

C IF (RAD.GT.0.) E(I)=SQRT(ABS(RAD**2-(H-Z(I))**2))-RAD*(H-Z(I))*TA  

C  

C CALCULATE EXPLOSIVE THICKNESS  

E(I)=COF*(RF=R(I))*(COF=1.)*RHOCON*CONFTK/7.8  

C CALCULATE 1./PHI  

C  

TZ(I)=Z(I)/(DA*CA)  

TZ(I)=TZ(I)+TZ(I)  

THE90=.5*PI-AI  

THE=ALRAD-THE90  

EPSI(I)=EPS/COS(THE90)  

E(I)=E(I)/COS(THE)  

RHOE=CON*RHOJ*EPSI(I)  

CONE=RHOE*C1  

RPHI(I)=RPHI0*RHOE/E(I)  

C  

C SUBROUTINE TO CALCULATE THE ACCELERATION OF THE LINER.  

C  

C ROUTINE WILL ITEHATE ON TAU AND PHI.  

C  

DO 6 J=1,300  

CT=EXP((SQR(CONE/(E(I)*TW))))  

RP(J)=RPHI(I)*CT  

TW=P(I)/(DA*(SIN(ALRAD+1.0/RP(J))-SA))  

IF (J.EQ.1) GO TO 6  

IF (ABS(RP(J)-RP(J-1)).LE.ETERM) GO TO 7  

6 CONTINUE  

C  

C END ITERATIVE PROCESS  

C  

J=J-1  

7 CONTINUE

```

MAIN261  
MAIN262  
MAIN263  
MAIN266  
MAIN267  
MAIN268  
MAIN269  
MAIN270  
MAIN271  
MAIN272  
MAIN273  
MAIN273A  
MAIN274  
MAIN275  
MAIN276  
MAIN277  
MAIN278  
MAIN279  
MAIN280  
MAIN281  
MAIN282  
MAIN283  
MAIN284  
MAIN285  
MAIN286  
MAIN287  
MAIN288  
MAIN289  
MAIN290  
MAIN291  
MAIN292  
MAIN293  
MAIN294  
MAIN295  
MAIN296  
MAIN297  
MAIN298  
MAIN299  
MAIN300  
MAIN301  
MAIN302  
MAIN303  
MAIN304  
MAIN305  
MAIN306  
MAIN307  
MAIN308  
MAIN309  
MAIN310  
MAIN311  
MAIN312  
MAIN315  
MAIN316  
MAIN317  
MAIN318  
MAIN319  
MAIN320

```

C THE END OF THE INVERSE VELOCITY GRADIENT SUBROUTINE.          MAIN321
C                                                               MAIN322
C                                                               MAIN323
C                                                               MAIN324
C                                                               MAIN325
C                                                               MAIN326
C                                                               MAIN327
C                                                               MAIN328
C                                                               MAIN329
C                                                               MAIN330
C                                                               MAIN331
C                                                               MAIN332
C                                                               MAIN333
C                                                               MAIN334
C                                                               MAIN335
C                                                               MAIN336
C                                                               MAIN337
C                                                               MAIN338
C                                                               MAIN339
C                                                               MAIN340
C                                                               MAIN341
C                                                               MAIN342
C                                                               MAIN343
C                                                               MAIN344
C                                                               MAIN345
C                                                               MAIN346
C                                                               MAIN347
C                                                               MAIN348
C                                                               MAIN349
C                                                               MAIN349b
C                                                               MAIN350
C                                                               MAIN351
C                                                               MAIN352
C                                                               MAIN353
C                                                               MAIN354
C                                                               MAIN355
C                                                               MAIN356
C                                                               MAIN357
C                                                               MAIN358
C                                                               MAIN358A
C                                                               MAIN359
C                                                               MAIN360
C                                                               MAIN361
C                                                               MAIN361A
C                                                               MAIN361B
C                                                               MAIN361C
C                                                               MAIN361D
C                                                               MAIN362
C                                                               MAIN363
C                                                               MAIN364
C                                                               MAIN365
C                                                               MAIN366
C                                                               MAIN367
C                                                               MAIN368
C                                                               MAIN369
C
C TAU(I)=TW
C RPHI(I)=RP(J)
C
C PHI(I)=1.0/RPHI(I)
C DPHI(I)=ABS(PHI(I-1)-PHI(I))
C IF(PI(I).LE.0.0) GO TO 10
C SP=SIN(PHI(I))
C TP=TAN(PHI(I))
C SAP=SIN(ALRAD+PHI(I))
C CALCULATE TAN(BETA-ALPHA)
C
C TALPHAB=(DZ*(SAP-SA)*TP+H(I)*DPHI(I))/CA/(DZ*(SAP-SA)-R(I)*DPHI(I))    MAIN334
C *CA*TP)                                         MAIN335
C
C SOLVE FOR THE ANGLE BETA IN RADIANS.                         MAIN336
C
C BETA(I)=ATAN(TALPHAB)+ALRAD                                MAIN337
C IF (I.EQ.1) BETA(I)=ALRAD+PHI(I)                                MAIN338
C
C SOLVE FOR THE POINT OF COLLAPSE ON THE AXIS, STAGNATION POINT +SH.   MAIN339
C C(I)=Z(I)*SP/(CA*(SAP-SA))                                     MAIN340
C
C SOLVE FOR COLLAPSE VELOCITY                                     MAIN341
C V(I)=2.0*DA*SIN(PHI(I)*.5)                                     MAIN342
C GAMMA(I)=.5*PI-(ALRAD+.5*PHI(I))                                MAIN343
C VJ(I)=V(I)*COS(ALRAD+.5*PHI(I)-.5*BETA(I))/SIN(.5*BETA(I))      MAIN344
C VN(I)=V(I)*SIN(ALRAD+.5*PHI(I)-.5*BETA(I))/COS(.5*BETA(I))      MAIN345
C DML(I)=PIP*EPS*R(I)*DZ/CA                                       MAIN346
C DML(I)=DML(I)*RHOJ                                              MAIN347
C DMMASS=DML(I)                                                 MAIN348
C DMN(I)=.5*(1.+COS(BETA(I)))                                     MAIN349
C DMJ(I)=.5*(1.-COS(BETA(I)))                                     MAIN350
C AT=2.* (ALRAD+.5*PHI(I)-.5*BETA(I))                            MAIN351
C DEJ(I)=.5*(1.+COS(AT))                                         MAIN352
C DEN(I)=.5*(1.-COS(AT))                                         MAIN353
C
C COMPUTE THE RELATIVE VELOCITY OF THE JET AND SLUG.             MAIN354
C THIS IS THE FLOW VELOCITY. (VF).                               MAIN355
C RV(I)=.5*(VJ(I)-VN(I))                                         MAIN356
C IF(RV(I).GT.RVMAX) RVMAX=RV(I)                                 MAIN357
C
C TML=TML+DML(I)                                              MAIN358
C TMJ=TMJ+DMJ(I)*DML(I)                                         MAIN359
C
C IF THE FLOW VELOCITY IS GREATER THAN 1.23*CO, REMOVE MASS FROM JET    MAIN360
C IF(RV(I)/CO.GT.1.23) TMJ=0.                                         MAIN361
C ALSO REMOVE KINETIC ENERGY FOR JET.                           MAIN361A
C IF(RV(I)/CO.GT.1.23) TEJ=0.                                         MAIN361B
C TMN=TMN+DMN(I)*DML(I)                                         MAIN361C
C DMJK(I)=DMJ(I)*DML(I)                                         MAIN362
C DEL(I)=.5*DML(I)*V(I)**2                                         MAIN363
C TKE=TKE+DEL(I)                                              MAIN364
C TEJ=TEJ+DEJ(I)*DEL(I)                                         MAIN365
C UJK(I)=VJ(I)                                                 MAIN366
C IF (VJ(I)).LE.VJMAX) GO TO 9                                  MAIN367
C VJMAX=VJ(I)                                                 MAIN368
C

```

```

      OMJTE=DMJTE+DMJK(I)
      SUMVJ=SUMVJ+VJ(I)*DMJK(I)
      VJTE=SUMVJ/DMJTE
      MN=I
      9 CONTINUE
      10 CONTINUE
      END OF TIME AND SPACE INCREMENT ALONG THE HEIGHT OF THE LINER.
      CALL SUBROUTINE TO COMPRESS THE JET AND CALCULATE NEW JET VELOCITYMAIN379
      CALL VELGR (N,UJK,DMJK,IS1
      TFJCUT=0.
      DO 12 I=IS,N
      IF(UJK(I).GE..5) TMCUT1=TMCUT1+DMJK(I)
      IF(UJK(I).GE..4) TMCUT2=TMCUT2+DMJK(I)
      IF(UJK(I).GE..3) TMCUT3=TMCUT3+DMJK(I)
      IF(UJK(I).GE..2) TMCUT4=TMCUT4+DMJK(I)
      IF(UJK(I).GE..1) TMCUT5=TMCUT5+DMJK(I)
      IF(UJK(I).GE..25) TMJCUT=TMJCUT+DMJK(I)
      IF(UJK(I).GE..25) TEJCUT=TEJCUT+DEJ(I)*DEL(I)
      IF(UJK(I).GE..5) TECUT1=TECUT1+DEJ(I)*DEL(I)
      IF(UJK(I).GE..4) TECUT2=TECUT2+DEJ(I)*DEL(I)
      IF(UJK(I).GE..3) TECUT3=TECUT3+DEJ(I)*DEL(I)
      IF(UJK(I).GE..2) TECUT4=TECUT4+DEJ(I)*DEL(I)
      IF(UJK(I).GE..1) TECUT5=TECUT5+DEJ(I)*DEL(I)
      IF(UJK(I).LE.UJKMAX) GO TO 11
      IF(RV(I)/CO.GT.1.23) TEJCUT=0.
      IF(RV(I)/CO.GT.1.23) TMJCUT=0.
      IF(RV(I)/CO.GT.1.23) TECUT1=0.
      IF(RV(I)/CO.GT.1.23) TECUT2=0.
      IF(RV(I)/CO.GT.1.23) TFCUT3=0.
      IF(RV(I)/CO.GT.1.23) TECUT4=0.
      IF(RV(I)/CO.GT.1.23) TECUT5=0.
      IF(RV(I)/CO.GT.1.23) TMCUT3=0.
      IF(RV(I)/CO.GT.1.23) TMCUT4=0.
      IF(RV(I)/CO.GT.1.23) TMJCUT3=0.
      IF(RV(I)/CO.GT.1.23) TMJCUT2=0.
      IF(RV(I)/CO.GT.1.23) TMJCUT1=0.
      TMASS=TMASS+DMJK(I)
      UJKMAX=UJK(I)
      MN=I
      11 CONTINUE
      IF(RV(I)/CO.GT.1.23) TMASS=DMJK(I+1)
      IF(RV(I)/CO.GT.1.23) UJKMAX=UJK(I+1)
      IF(RV(I)/CO.GT.1.23) MN=I+1
      12 CONTINUE
      N1=1
      N2=N
      IF (N.GE.57) N2=57
      13 CONTINUE
      WRITE (6,23)
      WRITE (6,24)
      DO 14 I=N1,N2
      PHI(I)=PHI(I)*DEGTOR
      BETA(I)=BETA(I)*DEGTOR
      GAMMA(I)=GAMMA(I)*DEGTOR
      MAIN370
      MAIN371
      MAIN372
      MAIN373
      MAIN374
      MAIN375
      MAIN376
      MAIN377
      MAIN378
      MAIN379
      MAIN380
      MAIN381
      MAIN382
      MAIN383
      MAIN383A
      MAIN383B
      MAIN383C
      MAIN383D
      MAIN383E
      MAIN383F
      MAIN384
      MAIN384A
      MAIN384B
      MAIN384C
      MAIN384D
      MAIN384E
      MAIN385
      MAIN385A
      MAIN385B
      MAIN385C
      MAIN385D
      MAIN385E
      MAIN385F
      MAIN385G
      MAIN385H
      MAIN385I
      MAIN385J
      MAIN385K
      MAIN385L
      MAIN386
      MAIN387
      MAIN388
      MAIN389
      MAIN389A
      MAIN389B
      MAIN389C
      MAIN390
      MAIN391
      MAIN392
      MAIN393
      MAIN394
      MAIN395W
      MAIN396W
      MAIN397
      MAIN398
      MAIN399
      MAIN400

```

```

DPHI(I)=DPHI(I)*DEGTOR          MAIN401
Z(I)=Z(I)/H                      MAIN402
WRITE (6,23) I,Z(I),TZ(I),EPSI(I),E(I),PHI(I),BETA(I),DPHI(I),   MAIN403W
1,RPHI(I),V(I),R(I),TAU(I),C(I)  MAIN404W
BETA(I)=BETA(I)/DEGTOR          MAIN405
14 CONTINUE                       MAIN406
IF (N.LE.N2) GO TO 15            MAIN407
N1=N2+1                          MAIN408
N2=N                           MAIN409
GO TO 13                         MAIN410
15 CONTINUE                       MAIN411
TMJ=0.0                           MAIN411A
N1=1                            MAIN412
N2=N                           MAIN413
IF (N.GE.57) N2=57                MAIN414
16 CONTINUE                       MAIN415
WRITE (6,23)                      MAIN416W
WRITE (6,25)                      MAIN417W
DO 17 I=N1,N2                   MAIN418
TMJ=TMJ+DMJK(I)                  MAIN418A
IF (RV(I)/CO.GT.1.23) TMJ=0.      MAIN418B
WRITE (6,23) I,Z(I),VJ(I),VN(I),RV(I),DMJ(I),DMN(I),DEL(I),DML(I),MAIN419W
1,DMJK(I);TMJ                     MAIN420W
C
Z(I)=Z(I)*H                      MAIN421
17 CONTINUE                       MAIN422
IF (N.LE.N2) GO TO 18            MAIN423
N1=N2+1                          MAIN424
N2=N                           MAIN425
GO TO 16                         MAIN426
18 CONTINUE                       MAIN427
IF (IERROR.EQ.1) GO TO 20        MAIN428
IF (RHOC.EQ.0.0) GO TO 20        MAIN429
CALL PENETRATION SUBROUTINE CALCULATES JET RADIUS,DEPTH OF
  PENETRATION, HOLE RADIUS.,AND ALSO PENETRATION STANDOFF CURVES. MAIN430
C
CALL PENTRAT (N,Z,R,TZ,DMJ,BETA,TAU,C,UJK,RV,VJO,DMASS,MN,HEAD,PSOMAIN432
1,PPT,NCD,EPSI,DAI)              MAIN433
C
C
DO 19 I=1,N                      MAIN434
CONVERT VELOCITIES TO (MM/MICROSEC) FOR PLOTTING AND REPORTS. MAIN435
C
C
ALSO CONVERT DISTANCES TO MM.      MAIN436
C
BETA(I)=BETA(I)*DEGTOR          MAIN440
VJ(I)=VJ(I)*10.                  MAIN441
V(I)=V(I)*10.                    MAIN442
C(I)=C(I)*10.                    MAIN443
UJK(I)=10.*UJK(I)                MAIN444
Z(I)=Z(I)/H                      MAIN444A
19 CONTINUE                       MAIN445
IF (NPLOT.EQ.0) GO TO 20         MAIN446
CALL PLOTS (N,UJK,DPOINT,RPDT,HEAD,PSO,PPT,NCD,NPLT,IS)    MAIN447
20 CONTINUE                       MAIN448
UJKMAX=UJKMAX*10.                MAIN449
C
PFINT SUMMARY OF RESULTS        MAIN450
C
                                         MAIN451

```

```

      WRITE (6,39) HEAD
      WRITE (6,3A) TML,TMJ,TMN,TKE,TEJ,TEJCUT,TMJCUT
      &MMACH=RVMAX/CO
      WRITE(6,41) TECUT1,TMCUT1,TECUT2,TMCUT2,TECUT3,TMCUT3,
      1TECUT4,TMCUT4,TECUT5,TMCUT5,AMMACH
      WRITE (6,35) MN,2(MN),UUKMAX,TMASS
      NPOS=0
      IF (IJOHN.GT.1) GO TO 1
      GO TO 2
  98765 WRITE (6,40)
      WRITE (6,23) I,TW,RP(J),RPHI(I),CT,BETA(I)
      IERROR=1
      STOP
  C
  C   FORMATS
  C
  23 FORMAT (14.2X,1P12E10.3)           MAIN452B
  24 FORMAT (2H1I,5X,2H Z,8X,2HTZ,BX,3HEPS,7X,2H E,6X,3HPH1,7X,6HBT,6M) MAIN453B
      )X,4HDPHI,6X,4HRPHI,6X,4H V,6X,4H R,6X,4H TAU,6X,4H C/) MAIN453A
  25 FORMAT (2H1I,6X,1HZ,8X,3H VJ,8X,2HVN,7X,3H RV,7X,3HDMJ,7X,3HDMN,7XMAIN454B
      1,3HDEL,7X,3HDM,7X,4HDMJK,9X,3HTMJ/) MAIN454A
  26 FORMAT (8E10.4)                   MAIN455B
  27 FORMAT (1H1//' INITIAL POSITION')  MAIN456
  28 FORMAT ( //'/50X,'INPUT PARAMETERS'//,5X,'ALPHA = ',F6.3,7X,'K COMAIN457
      INSTANT = ',F6.3,7X,'THICKNESS OF LINER = ',F6.3,7X,' DENSITY = ', MAIN4574
      2F6.3//5X,A10.5X,' THICKNESS = ',F6.3,7X,' DENSITY = ',F6.3,5X,'FACMAIN4575
      3STOP = ',F6.4//5X,'LINER HEIGHT = ',F10.4,7X,'LINEF RADIUS = ',F10.4MAIN4576
      4,//5X,' INCREMENT OF Z (DZ) = ',F10.4,7X,' INCREMENT OF TIME (DTZ)MAIN4577
      5 ',F10.4,7X,'NUMBER OF ELEMENTS (N) = ',I4,//50X,'DETONATION'//) MAIN4578
  29 FORMAT(5X,'EXPLOSIVE = ',5X,A10,3X,'DETTONATION VELOCITY(D) = ', MAIN4579
      1F10.5,5X,'EXPLOSIVE DENSITY = ',F6.3//5X,'POINT OF DETONATION FROM MAIN4580
      2CONE APEX(DPOINT) = ',F10.4,7X,'DET. RADIUS (RDPT) = ',F10.4//50X,MAIN4581
      3'TARGET INPUTS'//5X,'TARGET DENSITY = ',F7.3,7X,'STAND-OFF DISTANCMAIN4582
      4E = ',F7.3,7X,'CK CONSTANT(BHN) = ',F10.6//50X'MISC. INPUTS'//5X, MAIN4583
      5A10,'PLOTS')                                MAIN4584
  30 FORMAT(///////////,30X,' SUMMARY OF RESULTS'//,1 LINER MASS = 'MAIN4585
      1,F10.4,' GM ',5X,'JET MASS = ',F10.4,' GH ',5X,'SLUG MASS = ',MAIN4586
      2F10.4,' GM ',//', TOTAL KINETIC ENERGY = ',F10.4,' ERGS*1.0E12'//,MAIN4587
      3 TOTAL JET KINETIC ENERGY = ',F10.4,' ERGS*1.0E12'//, TOTAL JET KIMAIN4588
      4NETIC ENERGY ABOVE JET VELOCITY .25 CM/MSEC = ',F10.4,' ERGS*1.0E1MAIN4589
      52'//, TOTAL JET MASS ABOVE JET VELOCITY .25 CM/MSFC = ',F10.4,' GMMAIN4590
      6 ')//)                                     MAIN4590
  31 FORMAT (//7(2H I,6X,2H Z,7X))             MAIN4591
  32 FORMAT (//7(3H I,6X,2H R,7X))             MAIN4591
  33 FORMAT (//7(3H I,6X,2HPI,7X))            MAIN4592
  34 FORMAT (7(14.4X,F7.4,3X))              MAIN4592
  35 FORMAT (' JET TIP AT I = ',I5,' RELATIVE POSITION Z/H = ',F10.8//MAIN4593
      1' MEASURED JET TIP VELOCITY = ',F10.8,' MM/MICROSEC'//, MEASURED MMAIN4594
      2ASS OF JET TIP = ',F10.4,' GM ',/1H1)          MAIN4594
  36 FORMAT (7E10.3,215)                      MAIN4595
  37 FORMAT (I1,8A10)                         MAIN4596
  38 FORMAT (I1,30X,8A10)                      MAIN4597
  39 FORMAT (I1H1,30X,8A10)                    MAIN4598
  40 FORMAT ('ERROR')
  41 FORMAT (' KINETIC ENERGY ABOVE .5 CM/MSEC = ',F10.4,
      1' AND JET MASS = ',F10.4)                  MAIN500
  42 ' KINETIC ENERGY ABOVE .4 CM/MSEC = ',F10.4, MAIN501
      1' AND JET MASS = ',F10.4/ MAIN502
  43 ' KINETIC ENERGY ABOVE .3 CM/MSEC = ',F10.4, MAIN503
  44 ' AND JET MASS = ',F10.4/ MAIN504
  45 ' KINETIC ENERGY ABOVE .2 CM/MSEC = ',F10.4, MAIN505
  46 ' AND JET MASS = ',F10.4/ MAIN506
  47 ' KINETIC ENERGY ABOVE .1 CM/MSEC = ',F10.4, MAIN507
  48 ' AND JET MASS = ',F10.4/ MAIN508
  49 ' KINETIC ENERGY ABOVE .05 CM/MSEC = ',F10.4, MAIN509
  50 ' AND JET MASS = ',F10.4/ MAIN510
  51 ' MAXIMUM RELATIVE MACH NUMBER = ',F10.4/) MAIN511-
  END

```

```

SUBROUTINE PENTRAT (N,Z,P,TZ,DMU,BETA,TAU,C,VJ,RV,VJO,DMASS,MN) * 511* 1
 1 HEAD,PSO,PPT,NCD,EPSI,DAI) PENTT 2
C COMPUTE PENETRATION,RADIUS OF JET,RADIUS OF THE HOLE. PENTT 3
C
C DIMENSION HEAD(8) PENTT 4
C DIMENSION EPSI(100), DAI(100) PENTT 5
C DIMENSION PPT(50), PSO(50), PVJT(50) PENTT 6
C DIMENSION Z(100), TZ(100), DMU(100), BETA(100), TAU(100), C(100), PENTT 7
C 1 VJ(100), R(100), RV(100) PENTT 8
C
C COMMON PENTT9
C
C COMMON ALHAD, EPS, RHOJ, RHOC, RF, RFH10, UTZ, SU, CK, DA, H, U, PENTT10
C 1 PT, DEGTOR PENTT11
C COMMON AMU(100), THETA(100), F(100), DF(100), T(100), DT(100), PENTT12
C 1 G(100), P(100), A(100), DELA(100), DVJ(100), ZDET(100), PENTT13
C 2 RSG(100), RC(100), T1, UMIN PENTT14
C
C PENETRATION PHASE PENTT15
VJO=0.0 PENTT16
DC 11 I=MN,N PENTT17
EPS=EPSI(1) PENTT18
DA=DAI(I) PENTT19
IF (I.LE.MN) VJ(I)=VJ(MN) PENTT20
IF (I.EQ.1) RETURN PENTT21
IF (VJO.GT.0.0) GO TO 4 PENTT22
VJO=VJ(MN) PENTT23
JC1=1 PENTT24
AKAY=SQRT (RHOJ/RHOC) PENTT25
AK1=AKAY+1. PENTT26
AK3=(3.+AKAY)/(2.*AKAY) PENTT27
AKOK1=AKAY/AK1 PENTT28
A1OK1=1./AK1 PENTT29
HHN=320. PENTT30
IF (UMIN.GT.1.0) BHNEUMIN PENTT31
IF (CK.EQ.0.) CK=(2250.+4.20*BHN)*1.0E-5 PENTT32
IF (UMIN.GT.1.0) UMIN=(CK*1.0E5-1350.)/20400. PENTT33
T1=T1*(.751-.28)/(VJO-.28) PENTT34
C
C M=MN PENTT35
A(I)=0. PENTT36
DELA(I)=0. PENTT37
DF(I)=0. PENTT38
F(I)=0. PENTT39
DVJ(I)=0. PENTT40
SUMMU=0. PENTT41
K=I-1 PENTT42
T2(K)=TZ(K)-TZ(I) PENTT42A
DMASS=DMU(K) PENTT42B
IF (VJ(K).LE.0.0) VJ(K)=1.0E-02 PENTT42C
AMU(K)=VJ/I*T(J(K)) PENTT42D
THETA(K)=1.0*TAU(K) PENTT42E
F(K)=THETA(K)/AMU(K)-C(K)/VJO PENTT42F
DF(K)=F(K) PENTT42G
SUMMU=AMU(K)**(-AKAY)*DF(K)+SUMMU PENTT42H
T(K)=AMU(K)**(1.+AKAY)*(T0-(1.+AKAY)*SUMMU) PENTT42I
DT(K)=T(K)-T0 PENTT42J
G(K)=VJO*(T(K)/AMU(K)-F(K)) PENTT42K
G
PENTT42L

```

```

A(K)=Z(K)-R(K)*COT(BETA(K)/2.)
DELA(K)=A(K)
VJ(K)=VJ(2)
NCD=]
IF (SO.EQ.0.) NCD=25
DO 3 J=1,NCD
IF (NCD.GT.1) SO=FLOAT(J)*RF*2.
Z0=H+SO
TO=Z0/VJO
IF (Z0.GE.VJO*T1) GO TO 1
PT=AK1*(VJO*T1)**AKOK1*Z0**A1OK-SQRT(AKAY*AK1*UMIN*T1)*(VJO*T1)*
1 *AKOK1*Z0**A1OK)-20
VJT=(AK1*(VJO*T1)**AKOK1*Z0**A1OK-(Z0+PT))/(AKAY*T1)
GO TO 2
1 CONTINUE
PT=AKAY*(VJO*T1)-SQRT(UMIN*T1)*(VJO*T1+Z0/AKAY))
VJT=VJO-PT/(AKAY*T1)
2 CONTINUE
PSO(J)=FLOAT(J)
PPT(J)=PT
PPT(J)=PPT(J)*10.
PVJT(J)=VJT
3 CONTINUE
C IF PLOTTING PENATRATION- STANDOFF CURVE USE 2. CD TO PLOT HOLE #PENTT64
IF (NCD.GT.1) NCD=3
IF(NCD.GT.1) SO=FLOAT(NCD)*RF*2.
IF (NCD.GT.1) PT=PPT(NCD)*.1
IF (NCD.GT.1) VJT=PVJT(NCD)*.1
Z0=SO+H
TO=Z0/VJO
RETURN
4 CONTINUE
TZ(I)=T2(I)-T2(1)
DMASS=DMU(I)
IF (VJ(I).LE.0.0) VJ(I)=1.0E-02
AMU(I)=VJO/VJ(I)
IF (AMU(I).LT.0.) RETURN
THETA(I)=TZ(I)+TAU(I)
F(I)=THETA(I)/AMU(I)-C(I)/VJO
DF(I)=F(I)-F(I-1)
SUMMU=AMU(I)**(-AKAY)*DF(I)+SUMMU
T(I)=AMU(I)**(1.+AKAY)*(TO+(1.+AKAY)*SUMMU)
DT(I)=T(I)-TO
G(I)=VJO*(T(I)/AMU(I)-F(I))
A(I)=Z(I)-R(I)*COT(BETA(I)/2.)
DELA(I)=A(I)-A(I-1)
DVJ(I)=VJ(I)-VJ(I-1)
DZ0DT(I)=(T(I)-TZ(I))*DVJ(I)/DTZ-VJ(I)+DELA(I)/DTZ
DZ0DT(I)=VJ(I)-((T(I)-TZ(I))*DVJ(I)/DTZ+DELA(I)/DTZ)
IF (T(I).GT.T1) GO TO 6
IF (Z0.GE.VJO*T1) GO TO 5
C CALCULATE DEPTH OF PENETRATION
C
P(I)=Z0*((T(I)/TO)**AKOK1-1.0)
RSQ(I)=2.*R(I)*EPS*DA*DMASS/DZ0DT(I)
RSQ(I)=SQRT(ABS(PSQ(I)))

```

PENTT42M  
PENTT42N  
PENTT43  
PENTT44  
PENTT45  
PENTT46  
PENTT47  
PENTT48  
PENTT49  
PENTT50  
PENTT51  
PENTT52  
PENTT53  
PENTT54  
PENTT55  
PENTT56  
PENTT57  
PENTT58  
PENTT59  
PENTT60  
PENTT61  
PENTT63  
PENTT64A  
PENTT65  
PENTT66  
PENTT67  
PENTT68  
PENTT69  
PENTT70  
PENTT71  
PENTT72  
PENTT75  
PENTT76  
PENTT77  
PENTT78  
PENTT79  
PENTT79A  
PENTT80  
PENTT81  
PENTT82  
PENTT83  
PENTT84  
PENTT85  
PENTT86  
PENTT87  
PENTT88  
PENTT89  
PENTT90  
PENTT91  
PENTT92  
PENTT93  
PENTT94  
.NTT95  
.CWT96  
PENTT97

```

C          CALCULATE RADIUS OF THE JET          PENTT98
C          RC(I)=SQRT(RHOJ/(2.*AKAY*CK))*SQRT(T1/T0)*VJO*(Z0/(Z0+P(I)))**AK3  PENTT94
C          1 *RSQ(I)                                PENT100
C          GO TO 9                                PENT101
C          5 CONTINUE                                PENT102
C          P(I)=VJO*(T(I)-T0)*T1/(T1+T(I)/AKAY)  PENT103
C          VJP=VJO*(T1+T0/AKAY)/(T1+T(I)/AKAY)  PENT104
C          DVJP=VJP-VJO
C          DZDFT(I)=(T1-T(I))*DVJP-VJP+DELA(I)  PENT105
C          DZDFT(I)=-DZDFT(I)                      PENT106
C          RSO(I)=2.*R(I)*EPS*DA*DMASS/DZDFT(I)  PENT107
C          PSQ(I)=SQRT(RSO(I))                      PENT108
C          RC(I)=SQRT(RHOJ/(2.*AKAY*CK))*RSQ(I)*VJO*(1.-P(I)/(AKAY*VJO*T1))  PENT109
C          VJPO=VJP                                     PENT110
C          GO TO 10                                 PENT111
C          6 CONTINUE                                PENT112
C          IF (P(I).LT.PT) GO TO 8                  PENT113
C          IF (JC1.NE.1) GO TO 7                  PENT114
C          JC1=2                                    PENT115
C          TP=T(I)                                  PENT116
C          7 CONTINUE                                PENT117
C          IF (T(I).GT.TP) RETURN                  PENT118
C          8 CONTINUE                                PENT119
C          DZDFT(I)=(T1-TZ(I))*DVJ(I)/DTZ-VJ(I)+DELA(I)/DTZ  PENT120
C          P(I)=(AK1*(T1/T0)**AK0K1*T(I))/(T(I)+AKAY*T1)-1.0*Z0  PENT121
C          PSQ(I)=2.*R(I)*EPS*DA*DMASS/DZDFT(I)  PENT122
C          RSO(I)=SQRT(ABS(RSQ(I)))                PENT123
C          RC(I)=SQRT(RHOJ/(2.*AKAY*CK))*(VJO/AKAY)*(AK1*(Z0/(VJO*T1))**A10K  PENT124
C          1 -(Z0+P(I))/(VJO*T1))*RSQ(I)          PENT125
C          9 CONTINUE                                PENT126
C          VJPO=VJ(I-1)                            PENT127
C          10 CONTINUE                               PENT128
C          11 CONTINUE                               PENT129
C          WRITE (6,31) HEAD                         PENT130
C          WRITE (6,22)
C          WRITE (6,29) T1,T0,Z0,PT,VUT,VJO,AKAY,UMIN,CK  PENT131
C          N1=1
C          N2=N
C          IF (N.GE.57) N2=55
C          WRITE (6,30)
C          12 CONTINUE                               PENT132
C          WRITE (6,23)
C          WRITE (6,27)
C          II=0
C          DO 13 I=N1,N2
C          WRITE (6,23) I,AMU(I),THETA(I),F(I),DF(I),T(I),DT(I),G(I),RSQ(I),  PENT133
C          1 A(I),DELA(I),DVJ(I),DZDFT(I)          PENT134
C          13 CONTINUE                               PENT135
C          IF (N.LE.N2) GO TO 14
C          N1=N2+1
C          N2=N
C          GO TO 12
C          14 CONTINUE                               PENT136
C          DO 15 I=MN,N
C          15 CONTINUE                               PENT137

```

```

N1=1          PENT155
N2=N          PENT156
IF (N.GE.50) N2=50    PENT157
WRITE (6,31) HEAD    PENT158W
SO=SO/(2.*RF)        PENT159
WRITE (6,28) SO       PENT160W
WRITE (6,23)          PENT161W
WRITE (6,25)          PENT162W
16 CONTINUE        PENT163
IF (N1.GT.25) WRITE (6,26) PENT164W
DO 19 I=N1,N2        PENT165
IF (P(I).GT.PT) GO TO 20    PENT166
IF (P(I).EQ.0.0) II=II+1    PENT167
IF (I.GT.25) GO TO 17    PENT168
WRITE (6,24) I,P(I),RC(I),PPT(I),PSO(I) PENT169W
GO TO 18          PENT170
17 CONTINUE        PENT171
WRITE (6,24) I,P(I),RC(I) PENT172W
18 CONTINUE        PENT173
19 CONTINUE        PENT174
IF (N.LE.N2) GO TO 20    PENT175
N1=N2+1          PENT176
N2=N          PENT177
GO TO 16          PENT178
20 CONTINUE        PENT179
II=II+1          PENT180
DO 21 I=1,II        PENT181
RC(I)=RC(II)        PENT182
21 CONTINUE        PENT183
RETURN          PENT184
C          PENT185
C          PENETRATION FORMATS          PENT186
C          PENT187
22 FORMAT(40X,'INITIAL CONDITIONS FOR PENETRATION//') PENT188
23 FORMAT (I4.2X,1P12E10.3)          PENT189
24 FORMAT (I3.7X.2(F10.5,10X,F10.5,20X))          PENT190
25 FORMAT (3H I,12X,'P(CM)''15X,'PC(CM)''23X,'PT(MM)''15X,'SO(CD)'//) PENT191
26 FORMAT (1H1.3H I,13X,'P'!18X,'RC')          PENT192
27 FORMAT (2H I,6X,2HMU,BX,5HTHETA,5X,2H F,FX,3H DF,7X,2H T,BX,2HDT,8PENT193
IX,2H G,BX,3HPSQ,BX,1HA,8X,4HDELA,7X,2HDV,6X,4HDZDT/)          PENT194
28 FORMAT (10X,'HOLE PROFILE      SD = ',F6.2,3H CD,25X,'PENETRATION STANPENT195
1DOFF//')          PENT195A
29 FORMAT(5X,'T1 = ',F10.4,5X,'T0 = ',F10.4,5X,' Z0 = ',F10.4,//4X, PENT196
1' PT = ',F10.4,5X,'VJT = ',F10.4,5X,' VJD = ',F10.4//4X,' AKAY = ' PENT197
2,F10.6,5X,' UMIN = ',F10.5,5X,' CK = ',F10.5//)          PENT198
30 FORMAT(1H1,' PENETRATION PHASE//')          PENT199
31 FORMAT (1H1,30X,8A10//)          PENT200
END          PENT201-

```

```

C      SUBROUTINE CALAI (I,Z,R,DPOINT,RDPT,JOHNI,AI)          * 701* 2
C      SURROUNTRUE WILL CALCULATE INCLINATION ANGLE (AI), DETONATION
C      COMPONENT OF THE COLLAPSE VELOCITY (DA). AND WILL CALL CALPHI
C      SURROUTINE WHICH WILL CALCULATE 1./PHIO (RPHIO) GIVEN (AI).
C
C      DIMENSION Z(100), R(100)
C      COMMON ALRAD, EPS, RHOJ, RHOC, RF, RPHIO, DTZ, SO, CK, DA, H, D,
C      PT, DEGTOR
C      ALPHA=ALRAD*DEGTOR
C      THETA=ATAN((R(I)-RDPT)/(DPOINT+Z(I)))
C      THETA=THETA*DEGTOR
C      AI=90.-(ALPHA-THETA)
C      IF (AI.LT.0.) AI=180.-(ALPHA-THETA)
C      CALL CALPHI (AI)
C      AI=AI/DEGTOR
C      DA=D/SIN(AI)
C      RETURN
C      END
C
C      CALAI 2
C      CALAI 3
C      CALAI 4
C      CALAI 5
C      CALAI 6
C      CALAI 7
C      CALAI 8
C      CALAI 9
C      CALAI10
C      CALAI11
C      CALAI12
C      CALAI13
C      CALAI14
C      CALAI15
C      CALAI16
C      CALAI17
C      CALAI18
C      CALAI19-

```

## SUBROUTINE CALPHI (AI)

```

C GIVEN AN INCLINATION ANGLE (AI) INTERPOLATE INTO TABLES AND FIND
C AN ANGLE PHIO, THEN CALCULATE 1./PHIO (RPHIO) AND RETURN.
C
C DIMENSION TPHI(37), TAI(37)
C COMMON ALRAD, EPS, RHOJ, RHOC, RF, RPHIO, DTZ, SD, CK, DA, H, D,
C PT, DEGTOR
C DATA TPHI /0.0, .08, .25, .59, 1.02, 1.43, 1.78, 2.03, 2.47, 2.86,CALPI 90
C 1 3.30, 3.70, 4.14, 4.51, 5.08, 5.65, 5.98, 6.37, 6.70, 7.01, 7.22,CALPI100
C 2 7.42, 7.58, 7.73, 7.90, 8.06, 8.17, 8.23, 8.28, 8.30, 8.24, 8.18,CALPI110
C 3 8.08, 7.99, 7.85, 7.75, 7.56/CALPI120
C DATA TAI /0.0, .02, .05, .15, .23, .32, .42, .48, .60, .72, .84,CALPI130
C 194, 1.06, 1.14, 1.29, 1.44, 1.54, 1.67, 1.79, 1.92, 2.03, 2.16, 2.CALPI140
C 228, 2.41, 2.61, 2.79, 3.01, 3.14, 3.25, 3.38, 3.57, 3.72, 3.84, 4.CALPI150
C 300, 4.16, 4.29, 4.47/CALPI160
C TAI SCALE FACTOR 100 DEG = 5.01 COUNTS (SFI=5.01/100.)
C TPHI SCALE FACTOR 40 DEG = 8.08 COUNTS (SFPHI=8.08/40.)
C SFI=.0501
C SFPHI=.207
C X=SFI*AI
C DO 1 J=1,37
C IF (TAI(J).GT.X) GO TO 2
C 1 CONTINUE
C 2 CONTINUE
C DXI=X-TAI(J-1)
C RDX=DXI/(TAI(J)-TAI(J-1))
C Y=RDX*(TPHI(J)-TPHI(J-1))+TPHI(J-1)
C IF (PHIO.LE..0001) PHIO=0.
C PHIO=Y/SFPHI
C RPHIO=1.0/PHIO
C RPHIO=RPHIO*DEGTOR
C RETURN
C END
C * 720* 3
C CALPI 2
C CALPI 3
C CALPI 4
C CALPI 5
C CALPI 6
C CALPI 7
C CALPI 8
C CALPI 9
C CALPI100
C CALPI110
C CALPI120
C CALPI130
C CALPI140
C CALPI150
C CALPI160
C CALPI17
C CALPI18
C CALPI19
C CALPI20
C CALPI21
C CALPI22
C CALPI23
C CALPI24
C CALPI25
C CALPI26
C CALPI27
C CALPI28
C CALPI29
C CALPI30
C CALPI31
C CALPI32
C CALPI33
C CALPI34-

```

```

SUBROUTINE VELGR (IK,UJK,DMJK,IS)
DIMENSION UJK(200), DMJK(200)
E=0.
IJK=IK-1
1 KP=]
C      COMPRESSION OF THE JET
DO 2 M=IS,IJK
IF (UJK(M).GE.UJK(M+1)) GO TO 2
IF (ABS(UJK(M)-UJK(M+1)).LE.1.E-5) GO TO 2
T1=DMJK(M)*UJK(M)+DMJK(M+1)*UJK(M+1)
T2=E*DMJK(M+1)*(UJK(M)-UJK(M+1))
DEM=1.0/(DMJK(M)+DMJK(M+1))
UJK(M)=(T1-T2)*DEM
UJK(M+1)=(T1+T2)*DEM
KP=0
2 CONTINUE
IF (KP.EQ.0) GO TO 1
RETURN
END

```

•	754	4
VELGR	2	
VELGR	3	
VELGR	4	
VELGP	5	
VELGR	6	
VELGH	7	
VELGP	8	
VELGP	9	
VELGP	10	
VELGP	11	
VELGR	12	
VELGH	13	
VELGR	14	
VELGR	15	
VELGR	16	
VELGH	17	
VELGR	18	
VELGP	19-	

```

SURROUNTING PLOTS (N,UJK,DPOINT,RDPT,HEAD,PSO,PHT,NCD,NPLT,ISTART) * 773* 5
DIMENSION PSO(50), PPT(50), S(50) PLOTS 2
DIMENSION B(5000), HEAD(R) PLOTS 3
DIMENSION UJK(200), DMJK(200) PLOTS 4
DIMENSION RD(4), CV(4), AB(4), TC(4), PC(4), DMNJ(4), VVC(4) PLOTS 5
DIMENSION Z(100), T2(100), TAU(100), E(100), PHI(100), DPHI(100), VN(100), DMJ(100) PLOTS 6
1 BETA(100), GAMMA(100), R(100), C(100), VJ(100), VN(100), DMJ(100) PLOTS 7
2 , DMN(100), DEJ(100), DEN(100), RPHI(100), V(100) PLOTS 8
DIMENSION F(4), G(4) PLOTS 9
COMMON ALRAD, EPS, RHOJ, RHOC, RF, RPHIO, DTZ, SD, CK, DA, H, D, PLOTS10
1 PT, DEGTOR PLOTS11
COMMON /LPLOT/ Z, T2, TAU, E, PHI, DPHI, BETA, GAMMA, R, C, VJ, VN, PLOTS12
1 DMJ, DMN, DEJ, DEN, RPHI, V PLOTS13
DATA DMNJ(1), DMNJ(2) /10HRELATIVE M, 4HASS>/ PLOTS14D
DATA RD(1), RD(2), RD(3) /10HRELATIVE D, 10HINSTANCE FR, 10HOM CONEPLOTS15D
1 AP/ PLOTS16D
DATA RD(4) /3HEX>/ PLOTS17D
DATA CV(), CV(2), CV(3) /10HCOLLAPSE V, 10HELOCITY IN, 10H CM/MICPLOTS18D
1KOS/ PLOTS19D
DATA CV(4) /3HEC>/ PLOTS20D
DATA AB(1), AB(2), AB(3) /10HANGLE BETA, 10H (DEGREES), 1H>/ PLOTS21D
DATA TC(1), TC(2), TC(3) /10HTIME OF CO, 10HLLAPSE (MI), 10HCRU SEC PLOTS22D
1) > / PLOTS23D
DATA PC(1), PC(2), PC(3) /10HPOINT OF C, 10HOLLAPSE (M, 3HM)>/ PLOTS24D
DATA VVC(1), VVC(2), VVC(3) /10H V, VJ (MM, 10M/MICROSEC), 1H>/ PLOTS25D
DATA TJET /4HJET>/ PLOTS26D
DATA TSLUG /5HSLUG>/ PLOTS27D
XPAGE=14 PLOTS28
CALL PLTCCR (XPAGE,1,B(1),B(5000)) PLOTS29
1IR=1-START PLOTS30
YMAX=12. PLOTS31
CALL PLOTS1 (3.0,3.0,1.0,YMAX,.1,.50,RD,VVC,16,10,4) PLOTS32
CALL PLTCCD (1.0,Z(1),V(1),II) PLOTS33
CALL PLTCCD (1.0,Z(1),VJ(1),II) PLOTS34
CALL PLTCCD (4.0,Z(1),UJK(1),II) PLOTS35
CALL PLCCSP (XS,YS,UFAC) PLOTS36
XX=.25 PLOTS37
YY=VJ(35)+.04*.5 PLOTS38
YY=V(35)+.04*.5 PLOTS39
PLOTS40
DO EXPEHMINTAL DATA POINTS FOR THE 105MM UNCONFINED SHAPED CHARGE. PLOTS41
CALL PLTEXP(N) PLOTS42
PLOTS43
PLOTS44
PLOTS45
PLOTS46*
PLOTS47
PLOTS48*
PLOTS49
PLOTS50*
PLOTS51
PLOTS52*
PLOTS53
PLOTS54*
PLOTS54A
PLOTS54B
PLOTS54C
C
C
C
C
CPOINT=DPOINT*10.
ENCODE (21,2,S(1) )DPOINT
RDPT=RDPT*10.
ENCODE (17,3,S(4) )RDPT
ALPHA=ALRAD*DEGTOR
ENCODE (20,4,S(8) )ALPHA
RF=RF*10.
ENCODE (1H,5,S(12) )RF
EPS=EPS*10.
ENCODE (19,6,S(16) )EPS
YY=YMAX+.2*YS
XMAX=1.0
XX=.5*XMAX-.2*XS*.7.

```

```

XX=0.0          PLOT554D
CALL PLTCCT(.2,HEAD(1),0.,1.,XX,YY)    PLOT554E
YY=.85*YMAX    PLOT555
XX=.6          PLOT556
CALL PLTCCT (.1,S(1)+0.,1.,XX,YY)      PLOT557
YY=.80*YMAX    PLOT558
CALL PLTCCT (.1,S(4)+0.,1.,XX,YY)      PLOT559
XA=.5-.1*XS*10.   PLOT55A
YA=-1.1*YS     PLOT560
CALL PLTCCT (.1,S(8)+0.,1.,XA,YA)      PLOT561
XA=.5-.1*XS*9.   PLOT562
YA=-1.3*YS     PLOT563
CALL PLTCCT (.1,S(12)+0.,1.,XA,YA)     PLOT564
YA=-1.5*YS     PLOT565
CALL PLTCCT (.1,S(16)+0.,1.,XA,YA)     PLOT566
C THIS NEXT STATEMENT RYPASSES SOME PLOTTING ROUTINES PLOT567
C IF (NPLT.GT.0) GO TO 1                PLOT568
CALL PLOTS1 (3.+16.+1.+160...1,20.,RD,PC,16,11+4) PLOT569
CALL PLTCCD (1+0,Z(ISTART),C(ISTART)+II)      PLOT570
CALL PLTCCP          PLOT571
CALL PLOTS1 (3.0+3.0,1.0+1.0...1,RD,DMNJ,16,10+4) PLOT572
XX=.35          PLOT573
YY=DMN(35)-.1  PLOT574
CALL PLTCCT (.2,TSLUG,0.,1.,XX,YY)      PLOT575
YY=DMJ(35)-.1  PLOT576
CALL PLTCCT (.2,TJET,0.,1.,XX,YY)      PLOT577
CALL PLTCCD (1+0,Z(ISTART),DMJ(ISTART),II)    PLOT578
CALL PLTCCD (1+0,Z(ISTART),DMN(ISTART),II)    PLOT579
CALL PLOTS1 (3.0+16.,1.0+180...1,20.,RD,AB,16,10+4) PLOT580
CALL PLTCCD (1+0,Z(ISTART),HETA(ISTART),II)    PLOT581
1 CONTINUE          PLOT582
CALL PLTCCP          PLOT583
C THIS NEXT STATMENT PART OF PLOTTING BYPASS PLOT584
C DO PENETRATION PLOTS( HOLE PROFILES). PLOT585
CALL PLOTOPEN (N,S,PST,PFT,NCU,HEAD)      PLOT586
RETURN          PLOT587
C
2 FORMAT (9H (L-H) = ,FB,4,4H MN>) PLOT588
3 FORMAT (5H RD = ,FB,4,4H MM>)      PLOT589
4 FORMAT (9H ALPHA = ,F6,2+5H DEG>)    PLOT590
5 FORMAT (6H RF = ,FB,4,4H MM>)      PLOT591
6 FORMAT (7H EPS = ,FB,5,4H MM>)      PLOT592
END          PLOT593

```

```

SUBROUTINE PLOTS1 (XBAR,YBAR,XMAX,YMAX,DY,PTX,PTY,NNCX,NNCY)
 1 NCD
  DIMENSION PTX(4), PTY(4)
  CNY=NNCY
  CNX=NNCX
  YS=YMAX/5.
  XS=XMAX/7.
  CALL PLTCCS (XBAR,YBAR,XMIN,YMIN,XS,YS)
  HT=.15
  YY=-.8*YS
  XX=.5*XMAX-HT*CNX*XS
  CALL PLTCCT (HT,PTX(1),0.,1.,XX,YY)
  XX=-.8*XS
  YY=.5*YMAX-HT*CNY*YS
  CALL PLTCCT (HT,PTY(1),1.,0.,XX,YY)
  CALL PLTCCA (DX,DY,XMIN,XMAX,YMIN,YMAX,.4)
  CALL LABELA (DX,DY,XMIN,XMAX,YMIN,YMAX,1.0,1,0)
  RETURN
END
* A71* 6
PLOT1 2
PLOT1 3
PLOT1 4
PLOT1 5
PLOT1 6
PLOT1 7
PLOT1 8
PLOT1 9
PLOT110
PLOT111
PLOT112
PLOT113
PLOT114
PLOT115
PLOT116
PLOT117
PLOT118
PLOT119-

```

```

SUBROUTINE PLOTPEN (N,S,PSU,PPT,NCD,HEAD) * 840* 7
DIMENSION TSO(4), TPT(4), HEAD(8)
DIMENSION S(50), PSO(50), PPT(50)
DIMENSION HOL(2), HCN(100), PEN(3), PENT(3), RAD(2)
COMMON ALRAD, EPS, RHOJ, RHOC, RF, RPHI0, DTZ, SU, CK, DA, M, D,
1 PT, DEGTOR
COMMON AMU(100), THETA(100), F(100), DF(100), T(100), DT(100),
1 G(100), H(100), A(100), DELA(100), DVJ(100), DZDET(100),
2 RSG(100), RC(100), T1, UMIN
DATA HOL(1), HOL(2) /10HWHOLE PROF1, 3HLE>/
DATA PEN(1), PEN(2), PEN(3) /10HRADIUS=VS-, 10HDEPTH OF P, AMEN,(MPLOTN110
)M>/
DATA PENT(1), PENT(2), PENT(3) /10HTIME=VS-DE, 10HPTM OF PEN, GM-(PLOTN130
)CM>/
DATA RAD(1), RAD(2) /10HRADIUS (MM, 2H)>/
DATA TSU(1), TSU(2) /10HSTANOFF -, 5H(CD)>/
DATA TPT(1), TPT(2) /10HPENETRATIO, 7HN (MM)>/
HM=0.
DO 1 I=1,N
IF (P(I).GE.PT) GO TO 2
P(I)=P(I)
RCN(I)=RC(I)
IF (RC(I).GT.RM) RM=RC(I)
1 CONTINUE
P(N)=P(N)
2 CONTINUE
N=1
PM=P(N)
XMAX=10.
XMIN=-XMAX
YMIN=-PM
IF (PM.LT.100.) YMIN=-100.
IF (PM.LT.60.) YMIN=-60.
YMAX=0.
YS=(YMAX-YMIN)/R.
XS=YS
XRAF=3.0
YBAR=15.0
CALL PLTCOS (XBAH,YBAR,XMIN,YMIN,XS,YS)
XA=-.2*X$*.5*12.
YA=YMAX*.3*YS
CALL PLTCCT (.20,HOL(1),0.,1.,XA,YA)
XA=-.1*X$*.5.
YA=YMIN*.5*YS
CALL PLTCCT (.1,RAD(1),0.,1.,XA,YA)
XA=-.1*X$*.9.
YA=YMIN-.75*YS
CALL PLTCCT (.1,S(1),0.,1.,XA,YA)
XA=-.1*X$*.7.
YA=YMIN-YS
CALL PLTCCT (.1,S(4),0.,1.,XA,YA)
ENCODE (1A,5,T(1)) 50
XA=-.1*X$*.8.
YA=YS*.1.2
CALL PLTCCT (.1,T(1),0.,1.,XA,YA)
XA=XMIN-.8*X$*
YA=.5*YMIN-.1*YS*.5*1R.

```

```

CALL PLTCCT (.1,HEAD(2),1..0.,XA,YA)          PL01N58
XA=-.2*X5*15.                                 PL01N59A
YA=YS*1.4                                     PL01N59H
CALL PLTCCT (.2,HEAD(1),0..1.,XA,YA)          PL01N59C
DX=1.                                         PL01N59
DY=1.                                         PL01N60
CALL PLTCCA (DX,DY,XMIN,XMAX,YMIN,YMAX,4)    PL01N61
DY=2.*DY                                       PL01N62
DX=5.0                                       PL01N63
XMIN=-XMAX                                    PL01N64
XMAX=0.                                       PL01N65
CALL LABELA (DX,DY,XMIN,XMAX,YMIN,YMAX,-10.0,-10.0) PL01N66
DY=0.                                         PL01N67
XMAX=-XMIN                                    PL01N68
XMIN=0.                                       PL01N69
CALL LABELA (DX,DY,XMIN,XMAX,YMIN,YMAX,10.0,0.0) PL01N70
RC(N)=0.                                       PL01N71
P(N)=PM                                       PL01N72
CALL PLTCCD (1.0,RC(1),P(1),N)                PL01N73
RCN(N)=0.                                      PL01N74
CALL PLTCCD (1.0,RCN(1),P(1),N)               PL01N75
XA=-.1*X5*10.                                 PL01N76
YA=,P*YS                                     PL01N77
CALL PLTCCT (.1,S(8),0..1.,XA,YA)             PL01N78
XA=-.1*X5*9.                                 PL01N79
YA=YS                                       PL01N80
CALL PLTCCT (.1,S(12),0..1.,XA,YA)            PL01N81
YA=,E*YS                                     PL01N82
CALL PLTCCT (.1,S(16),0..1.,XA,YA)            PL01N83
IF (NCD,GT,1) GO TO 3                         PL01N84
CALL PLTCCP                                     PL01N85
RETURN                                         PL01N86
3 CONTINUE                                     PL01N87
XMAX=P50(NCD)                                PL01N88
YMAX=0.                                       PL01N89
DO 4 I=1,NCD                                  PL01N90
IF (PPT(I).GT.YMAX) YMAX=PPT(I)              PL01N91
4 CONTINUE                                     PL01N92
YMAX=.01*YMAX                                PL01N93
YMAX=AINT(YMAX)+1.0                          PL01N94
YMAX=YMAX*100.                                PL01N95
DY=.2*YMAX                                    PL01N96
CALL PLOTS1 (3.0,3.0,XMAX,YMAX,1.,DY,T50,TPT,7,8,2) PL01N97
CALL PLCCSP (XS,YS,UFAC)                      PL01N98
XA=.5*XMAX-.2*X5*7.                          PL01N98A
XA=0.                                         PL01N98B
YA=YMAX+.2*YS                                PL01N98C
CALL PLTCCT (.2,HEAD(1),0..1.,XA,YA)          PL01N98D
YA=-1.1*YS                                     PL01N99
XA=.5*XMAX-.1*X5*10.                         PL01N100
CALL PLTCCT (.1,S(8),0..1.,XA,YA)             PL01N101
XA=.5*XMAX-.1*X5*9.                          PL01N102
YA=-1.3*YS                                     PL01N103
CALL PLTCCT (.1,S(12),0..1.,XA,YA)            PL01N104
YA=-1.5*YS                                     PL01N105
CALL PLTCCT (.1,S(16),0..1.,XA,YA)            PL01N106
CALL PLTCCD (1.0,P50(1),PPT(1),NCD)          PL01N107
CALL PLTCCP                                     PL01N108
RETURN                                         PL01N109
5 FORMAT (6H 50 = .F6.2,4H CD>)             PL01N110
END                                           PL01N111
                                              PL01N112-

```

```

SUBROUTINE PLTEXP (N)
  DIMENSION PEXX(60), PEXVJ(60), PEXVO(60), PEXV(4), TEXP(3). *1002* 8
 1  PEXPX(4) PLTEP 2
  DIMENSION BASC(3) PLTEP 3
  COMMON ALHAD, EPS, RHOJ, HHOC, RF, RPHIO, DTZ, SO, CK, DA, M, U PLTEP 4
  DATA TEXP(1), TEXP(2), TEXP(3) /10HEXPERIMENT/ 10HAL DATA + 2M>PLTEP 5
 1/ PLTEP 7U
  DATA (PEXX(I),I=1,9) /4.0, 4.5, 5.0, 5.5, 6.0, 6.5, 7.0, 7.5, 8.0/PLTEP 8D
  DATA (PEXVJ(I),I=1,9) /7.01, 6.68, 6.35, 6.03, 5.62, 5.01, 4.17, 3PLTEP 9D
 1.19, 2.25/ PLTEP10U
 1.87D, 1.724, 1.509/ PLTEP11D
  DATA (PEXPX(I),I=1,3) /5.68, 6.94, 8.21/ PLTEP12D
  DATA (PEXV(I),I=1,3) /2.1, 1.78, 1.42/ PLTEP13D
  M=10 PLTEP14D
  ICOUNT=ICOUNT+1 PLTEP15
  IF (ICOUNT.LE.1) GO TO 1 PLTEP16
  READ (5,5) M,(PEXX(I),PEXVJ(I),I=1,M) PLTEP17
  M=M+1 PLTEP18H
  PEXX(M)=.875 PLTEP19
  PEYVJ(M)=9.13 PLTEP20
  GO TO 4 PLTEP21
 1 CONTINUE PLTEP22
  PEXX(10)=.875 PLTEP23
  PEYVJ(10)=9.13 PLTEP24
  PEXPX(4)=.910 PLTEP25
  PEXV(4)=9.13 PLTEP26
  FAC=.5*.7506 PLTEP27
  DO 2 I=1,9 PLTEP28
  PEXX(I)=PEXX(I)+FAC PLTEP29
  PEXX(I)=PEXX(I)/M PLTEP30
 2 CONTINUE PLTEP31
  DO 3 I=1,3 PLTEP32
  PEXPX(I)=PEXPX(I)*FAC PLTEP33
  PEXPX(I)=PEXPX(I)/M PLTEP34
 3 CONTINUE PLTEP35
  CALL PLTCCD (2,5,PEXX(1),PEXVO(1),9) PLTEP36
  CALL PLTCCD (2,4,PEXPX(1),PEXV(1),4) PLTEP37
 4 CONTINUE PLTEP38
  YY=5, PLTEP39
  XX=.6 PLTEP40
  CALL PLTCCT (.1,TEXP(1),0.,1.,XX,YY) PLTEP41
  YY=8, CALL PLTCCT (.1,BASC(1),0.,1.,XX,YY) PLTEP42
  CALL PLTCCD (2,5,PEXX(1),PEXVJ(1),M) PLTEP43
  RETURN PLTEP44
  C PLTEP45
  C PLTEP46
 5 FORMAT (I5/(HE10,1)) PLTEP47
  END PLTEP48
                                         PLTEP49-

```

SAMPLE INPUT

CARD NO. 1

HEADING CARD

1 105-MM SHAPED CHARGE SAMPLE CASE

CARD NO. 2

ALPHA 21.	FPS .269	RHOJ 8.9	LINER PARAMETERS HF 4.3185	H 0.	CONF TKS 0.	RHO CONF. 0.	NPLT 0	NPOS 0
--------------	-------------	-------------	----------------------------------	---------	----------------	-----------------	-----------	-----------

CARD NO. 3

RHOC 7.8	SO 0.	CK 0.	TARGET PARAMETERS BHN 300.	T1 112.	UPPOINT 3.9899	WDPT 0.	NEXP 1	N 100
-------------	----------	----------	----------------------------------	------------	-------------------	------------	-----------	----------

105-MM SHAPED CHARGE SAMPLE CASE

INPUT PARAMETERS

ALPHA = 21.000 K CONSTANT = .780 THICKNESS OF LINER = .269 DENSITY = 9.900  
UNCONFINED THICKNESS = 0.000 DENSITY = 0.300 FACTOR = 1.0000  
LINER HEIGHT = 11.250 LINER RADIUS = 4.3185  
INCREMENT OF Z (DZ) = .1125 INCREMENT OF TIME (DTZ) = .1410 NUMBER OF ELEMENTS (NE) = 100  
DETONATION

EXPLOSIVE = CUBE ? DETONATION VELOCITY(V) = .7980 EXPLOSIVE DENSITY = 1.720  
POINT OF DETONATION FROM CONE APEX (DPOINT) = 3.9800 EFF. RADIUS (RDPT) = 0.0000

TARGET INPUTS

TARGET INTENSITY = 7.000 STAND-OFF DISTANCE = 9.000 CR CONSTANT(BHN) = 300.000000  
MISC. INPUTS

SKIP PLOTS

INITIAL POSITION

	$\tau\tau$	$\epsilon_{PS}$	$E$	$\phi_{HI}$	$\phi_{PHI}$	$\beta_{TA}$	$\beta_{HI}$	$\nu$	$\kappa$	$\tau\tau$	$C$
1	0.	3.000E+00	2.400E-01	0.	3.000E+00	0.	0.	0.	0.	0.	0.
2	1.460E-02	5.141E+00	4.301E-02	4.274E+00	1.683E+01	1.683E+01	1.3A3E+01	3.404E+00	0.	4.319E-02	1.989E-01
3	2.000E-02	5.284E+00	4.511E-02	4.233E+00	1.625E+01	1.625E+01	5.49E-01	3.527E+00	0.	6.637E-02	4.124E-01
4	3.000E-02	5.427E+00	1.791E-01	4.191E+00	1.569E+01	1.569E+01	5.565E-01	3.651E+00	0.	1.296E-01	6.407E-01
5	4.000E-02	5.572E+00	1.736E-01	4.149E+00	1.518E+01	1.518E+01	5.776E+00	3.776E+00	0.	1.776E-01	8.439E-01
6	5.000E-02	5.717E+00	2.123E-01	4.107E+00	1.420E+01	1.420E+01	6.994E-01	3.904E+00	0.	2.159E-01	1.143E+00
7	6.000E-02	6.019E+00	2.541E-01	4.066E+00	1.420E+01	1.420E+01	7.313E-01	4.034E+00	0.	2.591E-01	1.417E+00
8	7.000E-02	6.303E+00	2.812E-01	4.024E+00	1.407E+01	1.407E+01	7.671E-01	4.072E+00	0.	2.023E-01	1.672E+00
9	8.000E-02	6.155E+00	2.812E-01	3.933E+00	1.454E+01	1.454E+01	7.912E-01	4.123E+00	0.	2.397E-01	1.06E+00
10	9.000E-02	6.303E+00	3.042E-01	3.942E+00	1.495E+01	1.495E+01	8.171E-01	4.171E+00	0.	2.167E-01	1.223E+00
11	1.000E-01	6.450E+00	2.801E-01	3.900E+00	1.531E+01	1.531E+01	8.529E-01	3.932E+00	0.	2.013E-01	1.857E+00
12	1.100E-01	6.594E+00	2.774E-01	3.859E+00	1.541E+01	1.541E+01	8.83E-01	3.698E+00	0.	2.253E-01	1.406E+00
13	1.200E-01	6.748E+00	2.791E-01	3.816E+00	1.586E+01	1.586E+01	9.694E-01	3.607E+00	0.	2.289E-01	1.588E+00
14	1.300E-01	6.895E+00	2.768E-01	3.777E+00	1.612E+01	1.612E+01	1.02E+01	3.554E+00	0.	2.316E-01	1.637E+00
15	1.400E-01	7.041E+00	2.744E+00	3.736E+00	1.649E+01	1.649E+01	1.07E+01	3.509E+00	0.	2.345E-01	1.912E+00
16	1.500E-01	7.193E+00	2.774E+00	3.695E+00	1.652E+01	1.652E+01	1.15E+01	3.469E+00	0.	2.368E-01	1.313E+00
17	1.600E-01	7.342E+00	2.775E+00	3.653E+00	1.664E+01	1.664E+01	1.14E+01	3.435E+00	0.	2.388E-01	1.319E+00
18	1.700E-01	7.492E+00	2.771E+00	3.612E+00	1.683E+01	1.683E+01	1.13E+01	3.405E+00	0.	2.406E-01	1.449E+00
19	1.800E-01	7.641E+00	2.764E+00	3.571E+00	1.694E+01	1.694E+01	1.12E+01	3.359E+00	0.	2.421E-01	1.326E+00
20	1.900E-01	7.790E+00	2.752E+00	3.532E+00	1.707E+01	1.707E+01	1.10E+01	3.329E+00	0.	2.435E-01	1.664E+00
21	2.000E-01	7.941E+00	2.662E+00	3.468E+00	1.717E+01	1.717E+01	1.09E+01	3.274E+00	0.	2.446E-01	2.740E+00
22	2.100E-01	8.091E+00	2.759E+00	3.444E+00	1.726E+01	1.726E+01	1.079E+01	3.220E+00	0.	2.456E-01	2.878E+00
23	2.200E-01	8.242E+00	2.742E+00	3.405E+00	1.733E+01	1.733E+01	1.063E+01	3.264E+00	0.	2.465E-01	3.015E+00
24	2.300E-01	8.392E+00	2.734E+00	3.363E+00	1.740E+01	1.740E+01	1.042E+01	3.293E+00	0.	2.472E-01	3.154E+00
25	2.400E-01	8.542E+00	2.752E+00	3.321E+00	1.755E+01	1.755E+01	1.021E+01	3.283E+00	0.	2.477E-01	3.292E+00
26	2.500E-01	8.693E+00	2.750E+00	3.279E+00	1.750E+01	1.750E+01	1.002E+01	3.274E+00	0.	2.482E-01	3.430E+00
27	2.600E-01	8.843E+00	2.748E+00	3.238E+00	1.753E+01	1.753E+01	9.91E+00	3.268E+00	0.	2.495E-01	3.567E+00
28	2.700E-01	8.994E+00	2.757E+00	3.195E+00	1.733E+01	1.733E+01	9.959E+00	3.256E+00	0.	2.507E+00	3.705E+00
29	2.800E-01	9.145E+00	2.744E+00	3.154E+00	1.758E+01	1.758E+01	9.936E+00	3.255E+00	0.	2.468E-01	3.842E+00
30	2.900E-01	9.296E+00	2.742E+00	3.112E+00	1.760E+01	1.760E+01	9.912E+00	3.253E+00	0.	2.489E-01	3.929E+00
31	3.000E-01	9.447E+00	2.742E+00	3.074E+00	1.765E+01	1.765E+01	9.886E+00	3.255E+00	0.	2.498E-01	4.117E+00
32	3.100E-01	9.597E+00	2.739E+00	3.027E+00	1.760E+01	1.760E+01	9.861E+00	3.255E+00	0.	2.486E-01	4.205E+00
33	3.200E-01	9.748E+00	2.736E+00	2.985E+00	1.764E+01	1.764E+01	9.840E+00	3.255E+00	0.	2.484E-01	4.391E+00
34	3.300E-01	9.899E+00	2.736E+00	2.943E+00	1.759E+01	1.759E+01	9.811E+00	3.258E+00	0.	2.481E+00	4.528E+00
35	3.400E-01	1.005E+01	2.735E+00	2.900E+00	1.757E+01	1.757E+01	9.791E+00	3.262E+00	0.	2.454E-01	5.592E+00
36	3.500E-01	1.020E+01	2.733E+00	2.858E+00	1.754E+01	1.754E+01	9.768E+00	3.266E+00	0.	2.477E-01	6.655E+00
37	3.600E-01	1.035E+01	2.727E+00	2.815E+00	1.750E+01	1.750E+01	9.745E+00	3.266E+00	0.	2.488E-01	7.799E+00
38	3.700E-01	1.050E+01	2.731E+00	2.772E+00	1.746E+01	1.746E+01	9.722E+00	3.266E+00	0.	2.495E+00	8.920E+00
39	3.800E-01	1.065E+01	2.730E+00	2.730E+00	1.743E+01	1.743E+01	9.700E+00	3.266E+00	0.	2.502E+00	9.900E+00
40	3.900E-01	1.081E+01	2.728E+00	2.687E+00	1.739E+01	1.739E+01	9.678E+00	3.266E+00	0.	2.447E+00	1.000E+00
41	4.000E-01	1.096E+01	2.724E+00	2.644E+00	1.734E+01	1.734E+01	9.655E+00	3.266E+00	0.	2.439E+00	1.042E+00
42	4.100E-01	1.111E+01	2.722E+00	2.601E+00	1.731E+01	1.731E+01	9.631E+00	3.266E+00	0.	2.421E+00	1.075E+00
43	4.200E-01	1.126E+01	2.725E+00	2.558E+00	1.722E+01	1.722E+01	9.607E+00	3.272E+00	0.	2.421E+00	1.105E+00
44	4.300E-01	1.141E+01	2.724E+00	2.515E+00	1.715E+01	1.715E+01	9.584E+00	3.286E+00	0.	2.411E+00	1.135E+00
45	4.400E-01	1.156E+01	2.724E+00	2.472E+00	1.708E+01	1.708E+01	9.565E+00	3.295E+00	0.	2.400E+00	1.164E+00
46	4.500E-01	1.171E+01	2.723E+00	2.429E+00	1.700E+01	1.700E+01	9.545E+00	3.305E+00	0.	2.373E+00	1.193E+00
47	4.600E-01	1.187E+01	2.722E+00	2.384E+00	1.693E+01	1.693E+01	9.525E+00	3.305E+00	0.	2.343E+00	1.222E+00
48	4.700E-01	1.202E+01	2.721E+00	2.343E+00	1.684E+01	1.684E+01	9.505E+00	3.305E+00	0.	2.313E+00	1.251E+00
49	4.800E-01	1.217E+01	2.720E+00	2.300E+00	1.675E+01	1.675E+01	9.485E+00	3.305E+00	0.	2.283E+00	1.280E+00
50	4.900E-01	1.232E+01	2.719E+00	2.256E+00	1.666E+01	1.666E+01	9.465E+00	3.305E+00	0.	2.253E+00	1.309E+00
51	5.000E-01	1.247E+01	2.719E+00	2.212E+00	1.656E+01	1.656E+01	9.445E+00	3.305E+00	0.	2.223E+00	1.338E+00
52	5.100E-01	1.262E+01	2.718E+00	2.176E+00	1.646E+01	1.646E+01	9.425E+00	3.305E+00	0.	2.192E+00	1.367E+00
53	5.200E-01	1.277E+01	2.717E+00	2.132E+00	1.636E+01	1.636E+01	9.405E+00	3.305E+00	0.	2.162E+00	1.396E+00
54	5.300E-01	1.292E+01	2.717E+00	2.083E+00	1.623E+01	1.623E+01	9.385E+00	3.305E+00	0.	2.132E+00	1.425E+00
55	5.400E-01	1.308E+01	2.716E+00	2.034E+00	1.611E+01	1.611E+01	9.365E+00	3.305E+00	0.	2.102E+00	1.454E+00
56	5.500E-01	1.323E+01	2.715E+00	1.985E+00	1.601E+01	1.601E+01	9.345E+00	3.305E+00	0.	2.072E+00	1.483E+00
57	5.600E-01	1.339E+01	2.715E+00	1.936E+00	1.591E+01	1.591E+01	9.325E+00	3.305E+00	0.	2.042E+00	1.512E+00

7	TZ	EPS	E	PHI	PHTA	DPHI	V	W	TAU	C
5.700E-01	1.353E+01	2.714E-01	1.908E+00	1.572E+01	4.812E+01	1.355F-01	3.645E+00	2.202E+01	2.462E+00	7.769E+01
5.800E-01	1.368E+01	2.714E-01	1.465E+00	1.558E+01	4.873E+01	2.140E+01	3.674E+00	2.142E+01	2.505E+00	7.901E+00
5.900E-01	1.393E+01	2.713E-01	1.821E+00	1.543E+01	4.937E+01	1.467E+01	3.713E+00	2.161E+01	2.548E+00	8.034E+00
6.000E-01	1.394E+01	2.713E-01	1.778E+00	1.528E+01	5.005E+01	1.524E+01	3.759E+00	2.117E+01	2.634E+00	8.165E+00
6.100E-01	1.414E+01	2.712E-01	1.733E+00	1.512E+01	5.077E+01	1.584E+01	3.789E+00	2.117E+01	2.677E+00	8.296E+01
6.200E-01	1.429E+01	2.712E-01	1.694E+00	1.496E+01	5.153E+01	1.645E+01	3.831E+00	2.094E+01	2.677E+00	8.427E+01
6.300E-01	1.444E+01	2.711E-01	1.665E+00	1.478E+01	5.234E+01	1.707E+01	3.875E+00	2.070E+01	2.721E+00	8.558E+01
6.400E-01	1.454E+01	2.711E-01	1.601E+00	1.461E+01	5.319E+01	1.772E+01	3.922E+00	2.045E+01	2.764E+00	8.688E+01
6.500E-01	1.474E+01	2.711E-01	1.557E+00	1.442E+01	5.409E+01	1.839E+01	3.972E+00	2.019E+01	2.807E+00	8.816E+01
6.600E-01	1.489E+01	2.710E-01	1.513E+00	1.423E+01	5.505E+01	1.909E+01	4.026E+00	1.992E+01	2.850E+00	8.948E+01
6.700E-01	1.504E+01	2.710E-01	1.469E+00	1.404E+01	5.604E+01	1.976E+01	4.082E+00	1.964E+01	2.893E+00	9.077E+01
6.800E-01	1.520E+01	2.709E-01	1.425E+00	1.383E+01	5.711E+01	2.050E+01	4.143E+00	1.935E+01	2.937E+00	9.206E+01
6.900E-01	1.535E+01	2.709E-01	1.381E+00	1.342E+01	5.825E+01	2.127E+01	4.207E+00	1.905E+01	2.980E+00	9.334E+01
7.000E-01	1.550E+01	2.709E-01	1.337E+00	1.340E+01	5.946E+01	2.206E+01	4.277E+00	1.874E+01	3.023E+00	9.462E+01
7.100E-01	1.565E+01	2.708E-01	1.293E+00	1.317E+01	6.074E+01	2.289E+01	4.351E+00	1.842E+01	3.066E+00	9.589E+01
7.200E-01	1.580E+01	2.708E-01	1.249E+00	1.293E+01	6.210E+01	2.376E+01	4.431E+00	1.809E+01	3.109E+00	9.716E+01
7.300E-01	1.595E+01	2.707E-01	1.204E+00	1.268E+01	6.353E+01	2.466E+01	4.517E+00	1.774E+01	3.153E+00	9.843E+01
7.400E-01	1.610E+01	2.707E-01	1.160E+00	1.243E+01	6.503E+01	2.559E+01	4.610E+00	1.739E+01	3.196E+00	9.968E+01
7.500E-01	1.626E+01	2.707E-01	1.116E+00	1.216E+01	6.662E+01	2.657E+01	4.711E+00	1.701E+01	3.239E+00	1.009E+01
7.600E-01	1.641E+01	2.705E-01	1.071E+00	1.189E+01	6.829E+01	2.760E+01	4.820E+00	1.663E+01	3.282E+00	1.022E+01
7.700E-01	1.656E+01	2.705E-01	1.026E+00	1.160E+01	7.003E+01	2.867E+01	4.939E+00	1.626E+01	3.325E+00	1.034E+01
7.800E-01	1.671E+01	2.705E-01	9.866E-01	1.130E+01	7.186E+01	2.986E+01	5.079E+00	1.581E+01	3.368E+00	1.047E+01
7.900E-01	1.686E+01	2.705E-01	9.392E-01	1.099E+01	7.376E+01	3.108E+01	5.233E+00	1.537E+01	3.412E+00	1.059E+01
7.100E-01	1.701E+01	2.704E-01	8.937E-01	1.067E+01	7.572E+01	3.222E+01	5.370E+00	1.492E+01	3.455L+00	1.071E+01
7.200E-01	1.716E+01	2.704E-01	8.493E-01	1.033E+01	7.775E+01	3.353E+01	5.546E+00	1.445E+01	3.498E+00	1.083E+01
7.300E-01	1.731E+01	2.704E-01	8.048E-01	9.965E+00	7.984E+01	3.491E+01	5.738E+00	1.403E+01	3.541E+00	1.095E+01
7.400E-01	1.747E+01	2.705E-01	7.602E-01	9.622E+00	8.197E+01	3.637E+01	5.955E+00	1.366E+01	3.594E+00	1.107E+01
7.500E-01	1.762E+01	2.705E-01	7.157E-01	9.262E+00	8.413E+01	3.791E+01	6.199E+00	1.293E+01	3.628E+00	1.119E+01
7.600E-01	1.771E+01	2.705E-01	6.937E-01	8.847E+00	8.631E+01	3.953E+01	6.476E+00	1.223E+01	3.671E+00	1.131E+01
7.700E-01	1.782E+01	2.705E-01	6.711E-01	8.479E+00	8.849E+01	4.126E+01	6.793E+00	1.180E+01	3.714E+00	1.142E+01
7.800E-01	1.807E+01	2.704E+01	6.265E-01	8.032E+00	9.066E+01	4.310E+01	7.159E+00	1.119E+01	3.757E+00	1.154E+01
7.900E-01	1.822E+01	2.704E+01	5.373E+00	7.539E+00	9.258E+01	4.525E+01	7.586E+00	1.056E+01	3.800E+00	1.165E+01
8.000E-01	1.837E+01	2.703E+01	4.998E+00	7.022E+00	9.489E+01	4.712E+01	8.095E+00	1.017E+01	3.843E+00	1.177E+01
8.100E-01	1.853E+01	2.703E+01	4.579E+00	6.588E+00	9.693E+01	4.912E+01	8.595E+00	9.725E+00	3.885E+00	1.185E+01
8.200E-01	1.868E+01	2.703E+01	4.032E+00	6.071E+00	9.88E+01	5.117E+01	9.437E+00	9.180E+00	3.930E+00	1.199E+01
8.300E-01	1.883E+01	2.703E+01	3.595E+00	5.529E+00	1.007E+01	5.425E+01	1.036E+01	7.733E+00	3.973E+00	1.210E+01
8.400E-01	1.898E+01	2.702E+01	3.139E+00	4.959E+00	1.025E+01	5.698E+01	1.155E+01	6.936E+00	4.016E+00	1.221E+01
8.500E-01	1.913E+01	2.702E+01	2.692E+00	4.592E+00	1.041E+01	6.712E+01	1.298E+01	6.098E+00	4.059E+00	1.231E+01
8.600E-01	1.928E+01	2.702E+01	2.273E+00	4.279E+00	1.056E+01	7.242E+01	1.427E+01	5.216E+00	4.103E+00	1.242E+01
8.700E-01	1.943E+01	2.702E+01	1.856E+00	3.908E+00	1.071E+01	7.794E+01	1.536E+01	6.308E+00	4.166E+00	1.252E+01
8.800E-01	1.958E+01	2.702E+01	1.432E+00	3.645E+00	1.086E+01	8.371E+01	1.645E+01	7.404E+00	4.226E+00	1.262E+01
8.900E-01	1.974E+01	2.701E+01	1.093E+00	3.396E+00	1.101E+01	8.971E+01	1.754E+01	8.537E+00	4.286E+00	1.272E+01
9.000E-01	1.989E+01	2.701E+01	7.703E+00	3.138E+00	1.117E+01	9.671E+01	1.864E+01	9.694E+00	4.346E+00	1.281E+01

			V <sub>I</sub>	R <sub>V</sub>	B-V <sub>J</sub>	B-V <sub>K</sub>	B-V <sub>N</sub>	C-E <sub>L</sub>	D-B <sub>L</sub>	D-B <sub>M</sub>	D-B <sub>J</sub>	D-B <sub>K</sub>	I-B <sub>J</sub>	
1	7		0.	0.	0.	0.	0.	0.	0.	0.	0.	0.	0.	0.
2	6	6.000E-02	6.421E-01	3.650E-02	3.033E-01	9.446E-02	0.014E-01	1.150E-02	5.480E-01	5.401E-02	5.401E-02	5.401E-02	5.401E-02	0.
3	7	2.000E-02	6.495E-02	2.401E-02	2.401E-01	1.262E-01	6.738E-01	1.397E-02	6.263E-01	7.405E-02	1.331E-01	7.405E-02	1.331E-01	0.
4	8	3.000E-02	6.037E-01	3.602E-02	2.564E-01	2.455E-01	8.735E-01	1.654E-02	7.045E-01	8.914E-02	2.222E-01	8.914E-02	2.222E-01	0.
5	9	4.000E-02	6.160E-01	3.215E-02	2.919E-01	2.675E-01	8.733E-01	1.97E-02	7.828E-01	9.917E-02	3.214E-01	9.917E-02	3.214E-01	0.
6	10	5.000E-02	6.254E-01	3.000E-02	2.969E-01	2.670E-01	8.733E-01	2.186E-02	6.611E-01	1.091E-01	4.305E-01	1.091E-01	4.305E-01	0.
7	11	6.000E-02	6.316E-01	2.836E-02	2.969E-01	2.670E-01	8.733E-01	2.186E-02	6.611E-01	1.091E-01	4.305E-01	1.091E-01	4.305E-01	0.
8	12	7.000E-02	6.421E-01	3.650E-02	3.033E-01	2.653E-01	8.733E-01	2.454E-02	6.394E-01	1.186E-01	5.493E-01	1.186E-01	5.493E-01	0.
9	13	8.000E-02	6.495E-01	3.559E-02	3.051E-01	2.624E-01	8.738E-01	2.734E-02	6.018E+00	1.264E-01	6.777E-01	1.264E-01	6.777E-01	0.
10	14	9.000E-02	6.537E-01	3.456E-02	3.084E-01	2.594E-01	8.741E-01	3.012E-02	5.096E+00	1.380E-01	8.157E-01	1.380E-01	8.157E-01	0.
11	15	1.000E-01	6.616E-01	3.215E-02	2.919E-01	2.555E-01	8.745E-01	3.291E-02	4.174E+00	1.474E-01	9.631E-01	1.474E-01	9.631E-01	0.
12	16	1.100E-01	6.694E-01	3.036E-02	2.969E-01	2.510E-01	8.750E-01	3.571E-02	4.253E+00	1.565E-01	1.120E+00	1.565E-01	1.120E+00	0.
13	17	1.200E-01	6.749E-01	3.453E-02	3.147E-01	2.514E-01	8.751E-01	3.851E-02	4.331E+00	1.656E-01	1.285E+00	1.656E-01	1.285E+00	0.
14	18	1.300E-01	6.794E-01	3.915E-02	3.175E-01	2.544E-01	8.756E-01	4.124E-02	4.431E+00	1.744E-01	1.460E+00	1.744E-01	1.460E+00	0.
15	19	1.400E-01	6.845E-01	3.992E-02	3.206E-01	2.582E-01	8.762E-01	4.130E-02	4.409E+00	1.831E-01	1.643E+00	1.831E-01	1.643E+00	0.
20	21	1.500E-01	6.897E-01	4.065E-02	3.224E-01	2.623E-01	8.769E-01	4.409E-02	4.487E+00	1.931E-01	1.834E+00	1.931E-01	1.834E+00	0.
22	23	1.600E-01	6.937E-01	4.137E-02	3.247E-01	2.662E-01	8.777E-01	4.685E-02	4.566E+00	2.036E-01	1.934E+00	2.036E-01	1.934E+00	0.
24	25	1.700E-01	6.977E-01	4.194E-02	3.264E-01	2.702E-01	8.786E-01	4.946E-02	4.644E+00	2.134E-01	2.034E+00	2.134E-01	2.034E+00	0.
26	27	1.800E-01	7.017E-01	4.257E-02	3.284E-01	2.742E-01	8.795E-01	5.232E-02	4.722E+00	2.232E-01	2.124E+00	2.232E-01	2.124E+00	0.
28	29	1.900E-01	7.066E-01	4.272E-02	3.298E-01	2.785E-01	8.805E-01	5.500E-02	4.800E+00	2.314E-01	2.456E+00	2.314E-01	2.456E+00	0.
30	31	2.000E-01	7.105E-01	4.409E-02	3.332E-01	2.824E-01	8.815E-01	5.765E-02	4.879E+00	2.220E-01	2.678E+00	2.220E-01	2.678E+00	0.
32	33	2.100E-01	7.145E-01	4.469E-02	3.351E-01	2.864E-01	8.825E-01	6.026E-02	5.957E+00	2.291E-01	2.907E+00	2.291E-01	2.907E+00	0.
34	35	2.200E-01	7.191E-01	4.527E-02	3.364E-01	2.904E-01	8.835E-01	6.286E-02	6.035E+00	2.359E-01	3.143E+00	2.359E-01	3.143E+00	0.
36	37	2.300E-01	7.235E-01	4.554E-02	3.367E-01	2.945E-01	8.845E-01	6.537E-02	6.114E+00	2.424E-01	3.386E+00	2.424E-01	3.386E+00	0.
38	39	2.400E-01	7.274E-01	4.646E-02	3.411E-01	2.984E-01	8.855E-01	6.876E-02	6.192E+00	2.494E-01	4.981E+00	2.494E-01	4.981E+00	0.
40	41	2.500E-01	7.315E-01	4.694E-02	3.423E-01	3.012E-01	8.871E-01	7.036E-02	7.270E+00	2.544E-01	5.189E+00	2.544E-01	5.189E+00	0.
42	43	2.600E-01	7.356E-01	4.749E-02	3.441E-01	3.051E-01	8.879E-01	7.268E-02	7.348E+00	2.602E-01	5.499E+00	2.602E-01	5.499E+00	0.
44	45	2.700E-01	7.391E-01	4.800E-02	3.458E-01	3.083E-01	8.887E-01	7.502E-02	7.427E+00	2.652E-01	4.614E+00	2.652E-01	4.614E+00	0.
46	47	2.800E-01	7.424E-01	4.739E-02	3.434E-01	3.107E-01	8.893E-01	7.729E-02	7.505E+00	2.774E-01	4.691E+00	2.774E-01	4.691E+00	0.
48	49	2.900E-01	7.464E-01	4.673E-02	3.411E-01	3.134E-01	8.898E-01	7.951E-02	7.563E+00	2.919E-01	4.934E+00	2.919E-01	4.934E+00	0.
50	51	3.000E-01	7.505E-01	4.542E-02	3.311E-01	3.164E-01	8.903E-01	8.142E-02	8.192E+00	3.149E-01	5.254E+00	3.149E-01	5.254E+00	0.
52	53	3.100E-01	7.545E-01	4.411E-02	3.222E-01	3.195E-01	8.908E-01	8.312E-02	8.362E+00	3.313E-01	5.499E+00	3.313E-01	5.499E+00	0.
54	55	3.200E-01	7.585E-01	4.451E-02	3.191E-01	3.164E-01	8.913E-01	8.477E-02	8.418E+00	3.295E-01	5.929E+00	3.295E-01	5.929E+00	0.
56	57	3.300E-01	7.625E-01	4.370E-02	3.305E-01	3.161E-01	8.918E-01	8.729E-02	8.896E+00	3.434E-01	6.272E+00	3.434E-01	6.272E+00	0.
58	59	3.400E-01	7.664E-01	4.290E-02	3.279E-01	3.141E-01	8.923E-01	9.031E-02	9.275E+00	3.574E-01	6.630E+00	3.574E-01	6.630E+00	0.
60	61	3.500E-01	7.704E-01	4.206E-02	3.250E-01	3.121E-01	8.928E-01	9.321E-02	9.662E+00	3.705E-01	7.001E+00	3.705E-01	7.001E+00	0.
62	63	3.600E-01	7.744E-01	4.126E-02	3.222E-01	3.102E-01	8.933E-01	9.617E-02	9.862E+00	3.876E-01	7.348E+00	3.876E-01	7.348E+00	0.
64	65	3.700E-01	7.785E-01	4.046E-02	3.192E-01	3.083E-01	8.938E-01	9.917E-02	10.031E+00	4.053E-01	7.749E+00	4.053E-01	7.749E+00	0.
66	67	3.800E-01	8.115E-01	3.964E-02	3.162E-01	3.064E-01	8.943E-01	1.027E-02	10.231E+00	4.254E-01	8.149E+00	4.254E-01	8.149E+00	0.
68	69	3.900E-01	8.445E-01	3.884E-02	3.132E-01	3.045E-01	8.958E-01	1.057E-02	10.422E+00	4.454E-01	8.546E+00	4.454E-01	8.546E+00	0.
70	71	4.000E-01	8.775E-01	3.804E-02	3.102E-01	3.026E-01	8.973E-01	1.087E-02	10.613E+00	4.654E-01	8.944E+00	4.654E-01	8.944E+00	0.
72	73	4.100E-01	9.105E-01	3.724E-02	3.072E-01	3.008E-01	8.988E-01	1.117E-02	10.804E+00	4.854E-01	9.345E+00	4.854E-01	9.345E+00	0.
74	75	4.200E-01	9.435E-01	3.644E-02	3.042E-01	3.000E-01	9.003E-01	1.147E-02	11.005E+00	5.054E-01	9.746E+00	5.054E-01	9.746E+00	0.
76	77	4.300E-01	9.765E-01	3.564E-02	3.012E-01	2.992E-01	9.018E-01	1.177E-02	11.206E+00	5.253E-01	1.016E+00	5.253E-01	1.016E+00	0.
78	79	4.400E-01	1.009E-01	3.484E-02	2.982E-01	2.982E-01	9.033E-01	1.207E-02	11.407E+00	5.454E-01	1.055E+00	5.454E-01	1.055E+00	0.
80	81	4.500E-01	1.042E-01	3.404E-02	2.952E-01	2.952E-01	9.048E-01	1.237E-02	11.608E+00	5.654E-01	1.094E+00	5.654E-01	1.094E+00	0.
82	83	4.600E-01	1.075E-01	3.324E-02	2.922E-01	2.922E-01	9.063E-01	1.267E-02	11.809E+00	5.854E-01	1.133E+00	5.854E-01	1.133E+00	0.
84	85	4.700E-01	1.108E-01	3.244E-02	2.892E-01	2.892E-01	9.078E-01	1.297E-02	12.009E+00	6.054E-01	1.171E+00	6.054E-01	1.171E+00	0.
86	87	4.800E-01	1.141E-01	3.164E-02	2.862E-01	2.862E-01	9.093E-01	1.327E-02	12.209E+00	6.254E-01	1.211E+00	6.254E-01	1.211E+00	0.
88	89	4.900E-01	1.174E-01	3.084E-02	2.832E-01	2.832E-01	9.108E-01	1.357E-02	12.409E+00	6.454E-01	1.251E+00	6.454E-01	1.251E+00	0.
90	91	5.000E-01	1.207E-01	3.004E-02	2.802E-01	2.802E-01	9.123E-01	1.387E-02	12.609E+00	6.654E-01	1.291E+00	6.654E-01	1.291E+00	0.
92	93	5.100E-01	1.240E-01	2.924E-02	2.772E-01	2.772E-01	9.138E-01	1.417E-02	12.809E+00	6.854E-01	1.331E+00	6.854E-01	1.331E+00	0.
94	95	5.200E-01	1.273E-01	2.844E-02	2.742E-01	2.742E-01	9.153E-01	1.447E-02	13.009E+00	7.054E-01	1.371E+00	7.054E-01	1.371E+00	0.
96	97	5.300E-01	1.306E-01	2.764E-02	2.712E-01	2.712E-01	9.168E-01	1.477E-02	13.209E+00	7.254E-01	1.411E+00	7.254E-01	1.411E+00	0.
98	99	5.400E-01	1.339E-01	2.684E-02	2.684E-01	2.684E-01	9.183E-01	1.507E-02	13.409E+00	7.454E-01	1.455E+00	7.454E-01	1.455E+00	0.
100	101	5.500E-01	1.372E-01	2.604E-02	2.604E-01	2.604E-01	9.198E-							

	VJ	VN	KV	DWJ	DVN	DEL	DPL	UPJK	TPJ	
7	5.700E-01	5.38E-01	2.617E-02	2.590E-01	1.662E-01	6.338E-01	1.042E-01	4.462E+00	7.417E-01	1.640E+01
~8	5.500E-01	5.273E-01	1.847E-02	2.544E-01	1.702E-01	8.298E-01	1.041E-01	4.540E+00	7.72AE-01	1.758E+01
~9	5.300E-01	5.162E-01	1.671E-02	2.497E-01	1.744E-01	7.256E-01	1.079E-01	4.619E+00	8.057E-01	1.634E+01
~10	5.000E-01	5.048E-01	1.488E-02	2.449E-01	1.790E-01	8.210E-01	1.070E-01	4.697E+00	8.440E+00	1.922E+01
~11	4.900E-01	4.931E-01	1.298E-02	2.449E-01	1.839E-01	8.162E-01	1.070E-01	4.775E+00	8.777E-01	2.010E+01
~12	4.800E-01	4.812E-01	1.100E-02	2.351E-01	1.990E-01	8.110E-01	1.064E-01	4.853E+00	9.171E-01	2.102E+01
~13	4.700E-01	4.690E-01	1.950E-03	2.300E-01	1.945E-01	8.055E-01	1.056E-01	4.932E+00	9.592E-01	2.198E+01
~14	4.600E-01	4.565E-01	4.821E-03	2.249E-01	2.004E-01	7.996E-01	1.047E-01	5.010E+00	1.004E+00	2.298E+01
~15	4.500E-01	4.439E-01	4.612E-03	2.196E-01	2.068E-01	7.932E-01	1.037E-01	5.088E+00	1.052E+00	2.403E+01
~16	4.400E-01	4.310E-01	2.320E-03	2.146E-01	2.136E-01	7.864E-01	1.025E-01	5.167E+00	1.103E+00	2.514E+01
~17	4.300E-01	4.181E-01	1.977E-03	2.091E-01	2.207E-01	7.793E-01	1.012E-01	5.245E+00	1.158E+00	2.629E+01
~18	4.200E-01	4.049E-01	1.464E-03	2.037E-01	2.228E-01	7.715E-01	9.969E-02	5.323E+00	1.216E+00	2.751E+01
~19	4.100E-01	3.914E-01	1.516E-03	1.942E-01	2.369E-01	7.631E-01	9.806E-02	5.401E+00	1.280E+00	2.879E+01
~20	4.000E-01	3.777E-01	1.7656E-03	1.927E-01	2.459E-01	7.541E-01	9.627E-02	5.480E+00	1.348E+00	3.014E+01
~21	3.900E-01	3.640E-01	1.758E-03	1.877E-01	2.459E-01	7.444E-01	9.433E-02	5.558E+00	1.421E+00	3.156E+01
~22	3.800E-01	3.501E-01	1.710E-03	1.838E-02	2.556E-01	7.346E-01	9.223E-02	5.636E+00	1.499E+00	3.306E+01
~23	3.700E-01	3.361E-01	1.609E-02	1.816E-01	2.660E-01	7.207E-01	9.023E-02	5.715E+00	1.573E+00	3.464E+01
~24	3.600E-01	3.220E-01	1.505E-02	1.766E-01	2.771E-01	7.122E-01	8.997E-02	5.793E+00	1.674E+00	3.631E+01
~25	3.500E-01	3.080E-01	1.402E-02	1.716E-01	2.890E-01	7.110E-01	8.755E-02	5.871E+00	1.771E+00	3.809E+01
~26	3.400E-01	2.939E-01	1.209E-02	1.650E-01	3.016E-01	6.984E-01	8.497E-02	5.949E+00	1.874E+00	3.996E+01
~27	3.300E-01	2.799E-01	1.777E-02	1.518E-02	1.550E-01	3.1-0E-01	6.851E-01	8.224E-02	5.949E+00	1.974E+00
~28	3.200E-01	2.659E-01	1.314E-02	1.518E-02	1.816E-01	3.293E-01	6.707E-01	7.934E-02	6.028E+00	1.999E+00
~29	3.100E-01	2.520E-01	1.464E-02	1.487E-01	3.447E-01	6.557E-01	6.762E-02	6.106E+00	2.102E+00	4.405E+01
~30	3.000E-01	2.382E-01	1.346E-02	1.433E-01	3.660E-01	6.399E-01	7.309E-02	6.184E+00	2.227E+00	4.627E+01
~31	2.900E-01	2.246E-01	1.209E-02	1.390E-01	3.767E-01	6.233E-01	6.976E-02	6.263E+00	2.359E+00	4.863E+01
~32	2.800E-01	2.112E-01	1.4-0E-02	1.322E-01	3.939E-01	6.061E-01	6.624E-02	6.341E+00	2.498E+00	5.113E+01
~33	2.700E-01	1.980E-01	1.666E-02	1.223E-01	5.115E-01	5.822E-01	6.242E-02	6.419E+00	5.377E+00	5.377E+01
~34	2.600E-01	1.851E-01	1.4-0E-02	1.172E-01	4.689E-01	5.511E-01	5.893E-02	6.497E+00	5.657E+00	5.657E+01
~35	2.500E-01	1.723E-01	1.516E-02	1.120E-01	4.678E-01	5.322E-01	5.494E-02	6.576E+00	5.952E+00	5.952E+01
~36	2.400E-01	1.598E-01	1.5-0E-02	1.064E-01	4.668E-01	5.132E-01	4.685E-02	6.732E+00	6.233E+00	6.233E+01
~37	2.300E-01	1.476E-01	1.4-0E-02	1.015E-01	5.058E-01	4.942E-01	4.262E-02	6.819E+00	6.494E+00	6.494E+01
~38	2.200E-01	1.356E-01	1.4-0E-02	9.603E-02	5.244E-01	4.756E-01	3.844E-02	6.849E+00	3.613E+00	7.297E+01
~39	2.100E-01	1.239E-01	1.5-0E-02	9.044E-02	5.427E-01	4.573E-01	3.418E-02	6.967E+00	3.781E+00	7.675E+01
~40	2.000E-01	1.123E-01	1.5-0E-02	8.461E-02	5.603E-01	4.397E-01	2.991E-02	7.045E+00	3.947E+00	8.070E+01
~41	1.900E-01	1.010E-01	1.5-0E-02	7.850E-02	5.772E-01	4.228E-01	2.569E-02	7.124E+00	4.112E+00	8.481E+01
~42	1.800E-01	9.78E-01	1.5-0E-02	7.204E-02	5.932E-01	4.068E-01	2.153E-02	7.202E+00	4.344E+00	8.935E+01
~43	1.700E-01	8.80E-01	1.5-0E-02	6.516E-02	6.516E-02	3.918E-01	1.751E-02	7.280E+00	4.424E+00	9.351E+01
~44	1.600E-01	7.870E-01	1.6-0E-02	5.792E-02	5.792E-02	3.779E-01	1.368E-02	7.358E+00	4.577E+00	9.808E+01
~45	1.500E-01	6.770E-01	1.7-0E-02	5.021E-02	5.021E-02	3.573E-01	1.012E-02	7.437E+00	4.721E+00	1.028E+02
~46	1.400E-01	5.671E-02	1.7-0E-02	4.140E-02	4.140E-02	3.1537E-01	6.901E-03	7.515E-00	4.957E-00	1.077E+02
~47	1.300E-01	4.200E-01	1.7-0E-02	3.272E-02	3.272E-02	2.709E-01	5.151E-03	7.622E-00	5.151E-00	1.126E+02
~48	1.200E-01	3.460E-01	1.7-0E-02	2.323E-02	2.323E-02	2.157E-01	4.663E-03	7.733E-00	5.313E-00	1.178E+02
~49	1.100E-01	2.333E-01	1.7-0E-02	1.274E-02	1.274E-02	1.634E-01	3.346E-03	7.844E-00	5.614E-00	1.230E+02
~50	1.000E-01	1.183E-01	1.7-0E-02	1.157E-02	1.157E-02	1.157E-01	2.270E-03	7.950E-00	5.921E-00	1.230E+02

105-mm SHAPED CHARGE SAMPLE CASE

INITIAL CONDITIONS FOR PENETRATION

R1 =	112.0090	T0 =	53.0039	Z0 =	37.1611
E1 =	36.0434	VJT =	.6316	VJN =	.7011
ARRAY =	1.6221PR	WIN =	.10548	CK =	.03510



54	1.254E+00	2.0335E+01	5.429E+00	1.106E-01	1.631E+02	5.014E+01	5.381E+01	1.559E+01	7.246E-01	4.056E-02	-6.793E+00
55	1.277E+00	2.042E+01	5.604E+00	1.246E-01	1.349E+02	5.398E+01	5.498E+01	1.546E+01	6.515E-01	4.094E-01	6.994E-02
56	1.303E+00	2.124E+01	5.265E+00	1.093E-01	1.104E+02	5.792E+01	5.601E+01	1.532E+01	6.063E-01	4.027E-01	6.622E+00
57	1.336E+00	2.174E+01	5.111E+00	1.154E-01	1.135E+02	6.229E+01	5.722E+01	1.542E+01	5.722E+01	4.493E-02	1.089E-02
58	1.356E+00	2.228E+01	4.942E+00	1.011E-01	1.605E+02	6.703E+01	5.849E+01	1.561E+01	5.722E+01	4.116E-02	7.970E+00
59	1.358E+00	2.274E+01	4.942E+00	1.011E-01	1.228E+02	7.214E+01	5.985E+01	1.531E+01	6.142E+00	4.055E-01	1.142E-02
60	1.358E+00	2.274E+01	4.756E+00	1.053E-01	1.252E+02	7.214E+01	5.985E+01	1.531E+01	6.142E+00	4.055E-01	1.142E-02
61	1.358E+00	2.274E+01	4.756E+00	1.053E-01	1.308E+02	7.779E+01	6.130E+01	1.603E+01	6.130E+00	1.110E-01	1.168E-02
62	1.422E+00	2.130E+01	4.555E+00	9.02E-02	1.782E+02	7.779E+01	6.130E+01	1.603E+01	6.244E+00	1.251E+00	1.251E+00
63	1.457E+00	2.343L+01	4.337E+00	9.02E-02	1.364E+02	8.393E+01	6.242E+01	1.626E+01	6.242E+00	1.168E-01	1.193E-02
64	1.469E+00	2.434E+01	4.102E+00	9.23E-02	1.437E+02	9.066E+01	6.458E+01	1.652E+01	1.521E+00	1.227E-01	1.218E-02
65	1.588E+00	2.444E+01	3.850E+00	9.23E-02	1.522E+02	1.511E+01	1.679E+01	1.679E+01	1.679E+00	1.287E-01	1.242E-02
66	1.579E+00	2.552E+01	3.540E+00	9.40E-02	1.592E+02	1.542E+01	1.709E+01	1.814E+01	1.349E+00	1.265E-01	1.265E-02
67	1.627E+00	2.412E+01	3.293E+00	9.73E-01	1.683E+02	1.153E+02	1.740E+01	1.740E+01	1.456E+00	1.412E+01	1.289E-02
68	1.677E+00	2.477E+01	3.092E+00	9.89E-01	1.782E+02	1.251E+02	1.739E+01	1.785E+01	1.449E+00	1.251E+01	1.168E-02
69	1.737E+00	2.737E+01	2.672E+00	1.003E-01	1.673E+02	1.363E+02	1.866E+01	1.866E+01	1.326E+00	1.326E+01	1.193E-02
70	1.794E+00	2.404E+01	2.332E+00	1.003E-01	2.017E+02	1.487E+02	1.732E+01	1.651E+01	2.415E+00	1.607E+01	1.348E-02
71	1.856E+00	2.871E+01	1.974E+00	1.039E-01	2.157E+02	1.627E+02	1.732E+01	1.651E+01	2.415E+00	1.607E+01	1.348E-02
72	1.922E+00	2.463E+01	1.548E+00	1.039E-01	2.315E+02	1.784E+02	1.812E+01	1.740E+01	2.456E+00	1.412E+01	1.289E-02
73	2.004E+00	3.017E+01	2.207E+00	1.039E-01	2.492E+02	1.962E+02	1.962E+01	1.945E+01	2.492E+00	1.796E+01	1.399E-02
74	2.096E+00	3.059E+01	2.059E+00	1.039E-01	2.692E+02	2.164E+02	2.164E+01	2.050E+01	3.121E+00	1.856E+01	1.398E-02
75	2.177E+00	3.177E+01	2.765E+00	1.039E-01	2.923E+02	2.363E+02	2.363E+01	2.098E+01	3.121E+00	1.913E+01	1.404E-02
76	2.274E+00	3.264E+01	2.166E+00	1.039E-01	3.186E+02	2.656E+02	2.656E+01	2.176E+01	3.509E+00	2.156E+01	1.404E-02
77	2.374E+00	3.452E+01	2.452E+00	1.039E-01	3.647E+02	3.196E+02	3.196E+01	2.497E+01	3.710E+00	2.372E+01	1.404E-02
78	2.467E+00	3.454E+01	2.454E+00	1.039E-01	4.238E+02	3.708E+02	3.137E+02	2.404E+01	4.127E+00	2.062E+01	1.404E-02
79	2.746E+00	3.646E+01	3.027E+00	1.039E-01	4.707E+02	4.177E+02	1.200E+02	4.30E+00	2.134E+00	2.134E+01	1.404E-02
80	2.747E+00	3.764E+01	3.264E+00	1.039E-01	5.186E+02	3.186E+02	2.656E+02	4.818E+01	2.176E+00	2.569E+01	1.404E-02
81	3.121E+00	3.613E+01	2.912E+00	1.039E-01	5.494E+02	2.957E+02	2.957E+02	5.02E+01	3.232E+00	2.0562E+01	1.404E-02
82	3.317E+00	4.052E+01	3.411E+00	1.039E-01	6.635E+02	3.305E+02	1.060E+02	1.060E+02	3.322E+00	2.179E+00	1.349E-02
83	3.546E+00	4.205E+01	3.913E+00	1.039E-01	7.587E+02	7.057E+02	1.530E+02	1.530E+02	2.404E+00	2.101E+01	1.349E-02
84	3.749E+00	4.374E+01	4.154E+00	1.039E-01	8.711E+02	4.177E+02	1.200E+02	4.919E+01	4.30E+00	2.134E+01	1.349E-02
85	4.042E+00	4.561E+01	4.561E+00	1.039E-01	9.727E+02	4.024E+02	1.177E+02	4.274E+02	3.013E+01	2.185E+01	1.349E-02
86	4.346E+00	4.772E+01	4.92E+00	1.039E-01	10.66E+02	4.024E+02	1.177E+02	4.274E+02	3.013E+01	2.185E+01	1.349E-02
87	4.715E+00	5.135E+01	5.135E+00	1.039E-01	11.72E+02	4.562E+02	1.177E+02	4.274E+02	3.013E+01	2.185E+01	1.349E-02
88	3.317E+00	4.052E+01	3.411E+00	1.039E-01	6.635E+02	6.141E+02	1.318E+02	1.318E+02	3.074E+00	2.185E+01	1.349E-02
89	3.546E+00	4.205E+01	3.913E+00	1.039E-01	7.587E+02	7.057E+02	1.530E+02	1.530E+02	3.074E+00	2.185E+01	1.349E-02
90	3.749E+00	4.374E+01	4.154E+00	1.039E-01	8.711E+02	4.160E+02	1.177E+02	4.274E+02	3.013E+01	2.185E+01	1.349E-02
91	4.042E+00	4.561E+01	4.561E+00	1.039E-01	9.727E+02	4.024E+02	1.177E+02	4.274E+02	3.013E+01	2.185E+01	1.349E-02
92	4.346E+00	4.772E+01	4.92E+00	1.039E-01	10.66E+02	4.562E+02	1.177E+02	4.274E+02	3.013E+01	2.185E+01	1.349E-02
93	7.010E+00	6.994E+01	7.010E+00	1.039E-01	11.72E+02	5.374E+02	1.318E+02	1.318E+02	3.074E+00	2.185E+01	1.349E-02
94	8.909E+00	7.711E+01	8.017E+00	1.039E-01	12.71E+02	6.141E+02	1.318E+02	1.318E+02	3.074E+00	2.185E+01	1.349E-02
95	1.026E+01	9.465E+01	9.465E+00	1.039E-01	13.64E+02	6.490E+02	1.318E+02	1.318E+02	3.074E+00	2.185E+01	1.349E-02
96	1.226E+01	1.072E+01	1.072E+00	1.039E-01	14.71E+02	6.814E+02	1.318E+02	1.318E+02	3.074E+00	2.185E+01	1.349E-02
97	1.534E+01	1.192E+01	1.192E+00	1.039E-01	15.78E+02	7.138E+02	1.318E+02	1.318E+02	3.074E+00	2.185E+01	1.349E-02
98	2.028E+01	1.415E+01	1.415E+00	1.039E-01	16.81E+02	7.462E+02	1.318E+02	1.318E+02	3.074E+00	2.185E+01	1.349E-02
99	3.005E+01	2.154E+01	2.154E+00	1.039E-01	17.84E+02	7.804E+02	1.318E+02	1.318E+02	3.074E+00	2.185E+01	1.349E-02
100	4.322E+01	4.037E+01	4.037E+00	1.039E-01	18.87E+02	8.146E+02	1.318E+02	1.318E+02	3.074E+00	2.185E+01	1.349E-02

## 105-MM SHAPED CHARGE SAMPLE CASE

HOLE PROFILE		SO = 3.00 CD	PENETRATION STANDOFF	
I	P(CM)	HC(CM)	PT(MM)	SO(CD)
1	0.00000	0.00000	311.70736	1.00000
2	0.00000	0.00000	354.96580	2.00000
3	0.00000	0.00000	380.93877	3.00000
4	0.00000	0.00000	395.21635	4.00000
5	0.00000	0.00000	400.88556	5.00000
6	0.00000	0.00000	399.86846	6.00000
7	0.00000	0.00000	393.45955	7.00000
8	0.00000	0.00000	382.67360	8.00000
9	0.00000	0.00000	370.83340	9.00000
10	0.00000	0.00000	359.28549	10.00000
11	0.00000	0.00000	348.00923	11.00000
12	0.00000	0.00000	336.48630	12.00000
13	0.00000	0.00000	326.20037	13.00000
14	0.00000	0.00000	315.63678	14.00000
15	0.00000	0.00000	305.28231	15.00000
16	0.00000	0.00000	295.12501	16.00000
17	0.00000	0.00000	285.15404	17.00000
18	0.00000	0.00000	275.35450	18.00000
19	0.00000	0.00000	265.73275	19.00000
20	0.00000	0.00000	256.26429	20.00000
21	0.00000	0.00000	246.94767	21.00000
22	0.00000	0.00000	237.77546	22.00000
23	0.00000	0.00000	228.74115	23.00000
24	0.00000	0.00000	219.43869	24.00000
25	0.00000	0.00000	211.06247	25.00000
26	0.00000	0.00000		
27	0.00000	0.00000		
28	0.00000	0.00000		
29	0.00000	0.00000		
30	0.00000	0.00000		
31	0.00000	0.00000		
32	0.00000	0.00000		
33	0.00000	0.00000		
34	0.00000	0.00000		
35	0.00000	0.00000		
36	0.00000	0.00000		
37	0.00000	0.00000		
38	4.08966	.15347		
39	4.34083	2.09919		
40	4.79126	1.46420		
41	5.25781	1.43460		
42	5.74158	1.40390		
43	6.24376	1.37219		
44	6.76463	1.33959		
45	7.30875	1.30593		
46	7.87454	1.27163		
47	8.46474	1.23655		
48	9.04121	1.20080		
49	9.72599	1.16446		
50	10.40131	1.12760		

I	P	PC
1	11.10963	1.09029
2	11.85363	1.05261
3	12.63628	1.01462
4	13.46083	.97641
5	14.33090	.93804
6	15.25045	.89958
7	16.22349	.86112
8	17.25609	.82272
9	18.34664	.80865
10	19.48506	.80245
11	20.67288	.79583
12	21.91220	.78874
13	23.20498	.78114
14	24.55304	.77303
15	25.95794	.76432
16	27.42096	.75498
17	28.94292	.74494
18	30.50486	.73845
19	32.14110	.72330
20	33.84023	.70978
21	35.59544	.69633
22	37.40375	.68182

105-MM SHAPED CHARGE SAMPLE CASE

SUMMARY OF RESULTS

INFR MASS = 385.8492 GM JET MASS = 122.9672 GM SLUG MASS = 262.8820 GM

TOTAL KINETIC ENERGY = 6.3894 ERGS\*1.0E12

TOTAL JET KINETIC ENERGY = 6.2273 ERGS\*1.0E12

TOTAL JET KINETIC ENERGY ABOVE JET VELOCITY .25 CM/MSEC = 5.6405 ERGS\*1.0E12

TOTAL JET MASS ABOVE JET VELOCITY .25 CM/MSEC = 46.2734 GM

KINETIC ENERGY ABOVE .5 CM/MSEC =	3.8664	AND JET MASS =	19.7223
KINETIC ENERGY ABOVE .4 CM/MSEC =	4.4964	AND JET MASS =	27.5096
KINETIC ENERGY ABOVE .3 CM/MSEC =	5.3368	AND JET MASS =	38.0850
KINETIC ENERGY ABOVE .2 CM/MSEC =	5.8294	AND JET MASS =	53.7738
KINETIC ENERGY ABOVE .1 CM/MSEC =	6.1685	AND JET MASS =	84.4073

MAXIMUM RELATIVE MACH NUMBER = .8821

JET TIP AT I = 38 RELATIVE POSITION Z/H = .37000000

MEASURED JET TIP VELOCITY = 7.01100675 MM/MICROSEC

MEASURED MASS OF JET TIP = 6.1533 GM

DISTRIBUTION LIST

<u>No. of Copies</u>	<u>Organization</u>	<u>No. of Copies</u>	<u>Organization</u>
12	Commander Defense Technical Info Center ATTN: DDC-DDA Cameron Station Alexandria, VA 22314	1	Director US Army ARRADCOM Benet Weapons Laboratory ATTN: DRDAR-LCB-TL Watervliet, NY 12189
1	Assistant Secretary of the Army (R&D) ATTN: Asst for Research Washington, DC 20310	1	Iowa Army Ammo Plant ATTN: J. Polson Burlington, IA 52601
2	HQDA (DAMA-ZA; DAMA-AR) Washington, DC 20310	1	Commander US Army Aviation Research and Development Command ATTN: DRSAV-E P. O. Box 209 St. Louis, MO 63166
1	Commander US Army Materiel Development and Readiness Command ATTN: DRCDMD-ST 5001 Eisenhower Avenue Alexandria, VA 22333	1	Director US Army Air Mobility Research and Development Laboratory Ames Research Center Moffett Field, CA 94035
2	Commander US Army Armament Research and Development Command ATTN: DRDAR-TSS Dover, NJ 07801	1	Commander US Army Communications Rsch and Development Command ATTN: DRDCO-PPA-SA Fort Monmouth, NJ 07703
4	Commander US Army Armament Research and Development Command ATTN: DARPA-FR-E Mr. T. Stevens Mr. G. Randers-Pehrson Mr. J. Hershkowitz Mr. J. Pearson Dover, NJ 07801	1	Commander US Army Electronics Rsch and Development Command Technical Support Activity ATTN: DELSD-L Fort Monmouth, NJ 07703
1	Commander US Army Armament Materiel Readiness Command ATTN: DRSAR-LEP-L, Tech Lib Rock Island, IL 61299	1	Commander US Army Missile Command ATTN: DRSMI-R Redstone Arsenal, AL 35809
		1	Commander US Army Missile Command ATTN: DRSMI-YDL Redstone Arsenal, AL 35809

DISTRIBUTION LIST

<u>No. of Copies</u>	<u>Organization</u>	<u>No. of Copies</u>	<u>Organization</u>
1	Commander US Army Missile Command ATTN: Mr. W. Zecher Redstone Arsenal, AL 35809	3	Commander Naval Surface Weapons Center ATTN: DG-50 Mr. S. Griscavage DX-21, Lib Br. Dahlgren, VA 22448
1	Commander US Army Missile Command ATTN: Mr. B. Cobb Redstone Arsenal, AL 35809	2	Commander Naval Surface Weapons Center ATTN: Code 730, Lib Silver Spring, MD 20910
1	Commander US Army Tank Automotive Research & Development Cmd ATTN: DRDTA-UL Warren, MI 48090	1	Commander Naval Weapons Center ATTN: Code 3835 China Lake, CA 93555
2	Commander US Army Materials and Mechanics Research Center ATTN: DRXMR-RF, J. Mescall Tech Lib Watertown, MA 02172	2	Commander Naval Weapons Center ATTN: Code 3431, Tech Lib Code 3835, R. Sewell China Lake, CA 93555
1	Director US Army TRADOC Systems Analysis Activity ATTN: ATAA-SL, Tech Lib White Sands Missile Range NM 88002	1	Commander Naval Research Laboratory Washington, DC 20375
2	Chief of Naval Research Department of the Navy ATTN: Code 427 Code 470 Washington, DC 20325	1	USAF/AFRDDA Washington, DC 20311
2	Commander Naval Air Systems Command ATTN: Code AIR-310 Code AIR-350 Washington, DC 20360	1	AFSC/SDW Andrews AFB Washington, DC 20311
1	Commander Naval Ordnance Systems Command ATTN: Code ORD-0332 Washington, DC 20360	1	US Air Force Academy ATTN: Code PJS-41 (NC) Tech Lib Colorado Springs, CO 80840
		1	AFATL/DLJW (J. Foster) Eglin AFB, FL 32542
		1	AFWL (SUL, LT Tennant) Kirtland AFB, NM 87116

DISTRIBUTION LIST

<u>No. of Copies</u>	<u>Organization</u>	<u>No. of Copies</u>	<u>Organization</u>
1	Director Lawrence Livermore Laboratory ATTN: Dr. J. Kury P. O. Box 808 Livermore, CA 94550	2	Firestone Tire & Rubber Defense Rsch & Products Div. ATTN: Mr. E. Clark Mr. R. Berus 1200 Firestone Parkway Akron, OH 44317
1	Director Lawrence Livermore Laboratory ATTN: Dr. M. Wilkins P. O. Box 808 Livermore, CA 94550	1	General Dynamic Pomona Div ATTN: J. Cuadros Mail Zone 4-75 P. O. Box 2507 Pomona, CA 91766
1	Director Lawrence Livermore Laboratory ATTN: Dr. E. Lee P. O. Box 808 Livermore, CA 94550	1	Honeywell, Inc. Government and Aeronautical Products Division ATTN: C. R. Hargreaves 600 Second Street Hopkins, MN 55343
1	Director Lawrence Livermore Laboratory ATTN: Dr. H. Hornig P. O. Box 808 Livermore, CA 94550	2	Physics International Corp. ATTN: Dr. L. Behrmann Dr. R. Brown 2700 Merced Street San Leandro, CA 94577
1	Director Lawrence Livermore Laboratory ATTN: Tech Lib P. O. Box 808 Livermore, CA 94550	2	Rockwell International Missile Systems Division ATTN: O. Kiphart H. Cox 4300 East 5th Avenue P. O. Box 1259 Columbus, OH 43216
1	Battelle Columbus Labs ATTN: Mr. Joseph E. Backofen 505 King Avenue Columbus, OH 43201	1	Sandia Laboratories ATTN: Dr. W. Herrmann Albuquerque, NM 87115
2	Dyna East Corporation ATTN: P. C. Chou J. Carleone 227 Hemlock Road Wynnewood, PA 19096	1	Shock Hydrodynamics ATTN: Dr. L. Zernow 4710-4716 Vineland Avenue North Hollywood, CA 91602

DISTRIBUTION LIST

<u>No. of Copies</u>	<u>Organization</u>
1	Systems, Science & Software ATTN: Dr. R. Sedgwick P. O. Box 1620 La Jolla, CA 92037
1	Drexel Institute of Technology Wave Propagation Rsch Center ATTN: Prof. P. Chou Philadelphia, PA 19104
4	University of California Los Alamos Scientific Lab ATTN: Dr. J. Walsh Dr. R. Karpp Dr. B. Craig P. O. Box 1663 Los Alamos, NM 87544
1	University of Denver Denver Research Institute ATTN: Mr. R. F. Recht 2390 S. University Boulevard Denver, CO 80210

Abe Jean Proving Ground

Dir, USAMSAA  
ATTN: DRXSY-D  
DRXSY-MP, H. Cohen  
J. Kramar  
B. Oehrli  
R. Bell, RAMD  
Cdr, USATECOM  
ATTN: DRSTE-T0-F  
Dir, USACSL, Bldg. E3516  
ATTN: DRDAK-CLB-PA

### USER EVALUATION OF REPORT

Please take a few minutes to answer the questions below; tear out this sheet, fold as indicated, staple or tape closed, and place in the mail. Your comments will provide us with information for improving future reports.

1. BRL Report Number \_\_\_\_\_
2. Does this report satisfy a need? (Comment on purpose, related project, or other area of interest for which report will be used.)  
\_\_\_\_\_  
\_\_\_\_\_  
\_\_\_\_\_
3. How, specifically, is the report being used? (Information source, design data or procedure, management procedure, source of ideas, etc.)  
\_\_\_\_\_  
\_\_\_\_\_  
\_\_\_\_\_
4. Has the information in this report led to any quantitative savings as far as man-hours/contract dollars saved, operating costs avoided, efficiencies achieved, etc.? If so, please elaborate.  
\_\_\_\_\_  
\_\_\_\_\_  
\_\_\_\_\_
5. General Comments (Indicate what you think should be changed to make this report and future reports of this type more responsive to your needs, more usable, improve readability, etc.)  
\_\_\_\_\_  
\_\_\_\_\_  
\_\_\_\_\_
6. If you would like to be contacted by the personnel who prepared this report to raise specific questions or discuss the topic, please fill in the following information.

Name: \_\_\_\_\_

Telephone Number: \_\_\_\_\_

Organization Address:  
\_\_\_\_\_  
\_\_\_\_\_  
\_\_\_\_\_